

UNIVERSIDADE DE LISBOA  
FACULDADE DE CIÊNCIAS  
DEPARTAMENTO DE FÍSICA



# **EEG SOURCE ANALYSIS DURING CIRCULAR RHYTHMIC HUMAN ARM MOVEMENTS**

**Inês Filipa Dias de Almeida**

**MESTRADO INTEGRADO EM ENGENHARIA BIOMÉDICA E BIOFÍSICA**

Perfil de Engenharia Clínica e Instrumentação Médica

Dissertação orientada por:

Univ.-Prof. Dipl.-Ing. Dr. techn. Gernot R. Müller-Putz,  
Institute of Neural Engineering, Graz University of Technology

e

Prof. Alexandre Andrade,  
Faculdade de Ciências da Universidade de Lisboa

2017





## *Acknowledgements*

This thesis would not have been possible without the help, support and guidance of many people.

First of all, I must acknowledge Professor Gernot Müller-Putz who gave me the opportunity to work under his supervision, for the time spent guiding me and for the useful critiques to the project.

I must also acknowledge Professor Alexandre Andrade for the valuable tips and for the support during my thesis.

I want to thank Reinmar Kobler and Andreea Sburlea for all the patient guidance and for all the useful discussions. I learned a great deal from you.

I would like to mention the INE group for making my stay so pleasant, in particular, I want to thank Joana Pereira for all the precious tips and encouragement.

I would like to express my very great appreciation to my parents who supported me throughout my studies, both at home and abroad, and Diogo Cunha, my biggest companion during my stay in the other side of Europe, for the patient opinions.

Finally, the support of the Erasmus+ program of the European Union was crucial for my internship abroad.



## *Abstract*

Decoding arm movement trajectory from brain signals would allow motor impaired people to control an arm prosthetic. Studies show that we can estimate a vector that points in the direction of arm movements based on single motor neuron activity - the population vector. This type of recording requires the surgical insertion of electrodes in the cerebral cortex. Although such invasive recordings would offer high spatial resolution, noninvasive recording have the advantage of high temporal resolution and no need for surgery. Researchers have managed to decode movement properties from noninvasive brain signals with similar accuracy as from invasive recordings. But can we find a noninvasive analogous of the population vector, a vector that points in the direction of the arm movement? This was the motivation for this thesis. To approach this question we acquired EEG, EOG and kinematic data from 12 healthy subjects while they performed a rhythmic circular right arm movement. We analyzed the data in the time and frequency domains. In the time domain we explored mainly the data averaged over cycles. We found a pattern that looked as if the potentials in the scalp rotated with the arm. To better visualize this rotation, we fit one dipole per time-stamp in the averaged cycle data of each subject to describe the scalp's potentials. The dipoles rotated along the cycle for all subjects, most of them in the same direction and plane of rotation, with exception for two subjects whose rotation was opposite and three subjects with a slightly different rotation plan. In the frequency domain, we used the Source Power Comodulation algorithm (SPoC), an algorithm that searches for components whose power correlates with a target variable, in our case, the arm kinematics. By applying this algorithm to 20-24 Hz band-pass filtered data, we found two components per subject, each calculated with different kinematic target variables. The results show components that when applied to the non band-pass filtered data, created signals whose power spectrum highly correlated with the given targets (the average of the absolute correlations being 85.5%). The physiological reason for both these phenomena is not entirely understood. To find the analogous of the population vector there is still a long way to go, and we hope this thesis was a first step towards it.

**Keywords:** electroencephalogram, brain, rhythmic arm movements, population vector, movement decoding.



## Resumo

O cérebro controla direta ou indiretamente todas as ações do corpo humano, entre elas o nosso movimento. O movimento é uma capacidade fundamental ao ser humano e, por essa mesma razão, indivíduos que sofram de incapacidades motoras têm uma redução considerável da sua qualidade de vida. Uma interface cérebro-computador (mais conhecida pelo seu nome em inglês *brain-computer interface (BCI)*) é um sistema que permite o controlo de dispositivos externos usando sinais cerebrais. Esta tecnologia é particularmente interessante para pessoas com incapacidade motora uma vez que não necessita de *input* físico e poderia ser usada para controlar uma neuroprótese ou um braço robótico. Existem várias estratégias que possibilitam o controlo destes sistemas, mas para o controlo de uma prótese do braço seria preferível usar uma estratégia natural, que não implicasse uma aprendizagem exaustiva por parte do utilizador. Para esse fim, é necessário decodificar vários parâmetros motores de acordo com a intenção do utilizador, como por exemplo, a direção do braço.

A possibilidade de um dia conseguir decodificar sinais cerebrais para o controlo de dispositivos externos já começa a ganhar forma, mas ainda não é possível a um nível suficientemente eficaz. Usando métodos invasivos de aquisição de sinais cerebrais que requerem cirurgia para implantar elétrodos no córtex cerebral, Georgopoulos *et al.* conseguiram distinguir entre movimentos direcionais (em 8 direções num plano horizontal) em macacos. Nessas experiências criou o conceito de vetor de população (*population vector*) que é um vetor calculado a partir da atividade de neurónios motores que tem a particularidade de apontar na direção do movimento executado. Já no campo dos métodos de aquisição não-invasivos podemos destacar o eletroencefalograma (EEG) e o magnetoencefalograma (MEG) que adquirem sinais elétricos e magnéticos (respetivamente) com sensores colocados fora do crânio. Vários investigadores usaram estes métodos de aquisição para decodificar sinais cerebrais durante tarefas de movimento direcionais usando regressões lineares em sinais de baixa frequência, e modulações em frequência para sinais na gama dos 50-90 Hz (banda de frequência  $\gamma$ ) e em frequência mais baixas para os 10-30 Hz (bandas de frequência  $\alpha$  e  $\beta$ ).

Algo que ainda não foi estudado é a possibilidade de encontrar um análogo ao vetor população usando métodos não-invasivos. Este não teria os mesmos princípios do vetor de Georgopoulos, uma vez que nos é impossível inferir a atividade de neurónios singulares em métodos não-invasivos, mas teria o mesmo objetivo: apontar na direção do movimento executado.

Para explorar este conceito realizámos aquisição de dados EEG, eletrooculograma (EOG) e dados cinéticos do braço direito de 12 sujeitos saudáveis, enquanto estes executavam um movimento rítmico, circular, no sentido dos ponteiros do relógio num plano vertical à sua frente. Durante a aquisição, os sujeitos focaram o seu olhar numa cruz mostrada através de um monitor colocado a sua frente, de forma a minimizar os movimentos oculares. Adicionalmente, uma divisória foi colocada perto do lado direito da face de cada sujeito impedindo os mesmos de observarem o seu braço enquanto realizavam o movimento requisitado, não obtendo assim qualquer *feedback* visual do seu membro superior. Os dados cinéticos foram adquiridos com um sensor *Kinect* para a *Xbox 360* que ao longo da experiência localizou as junções do braço direito dos sujeitos. Os dados cinéticos foram filtrados com um passa-banda 0.3-0.8 Hz e, ao longo dos ciclos do braço, os pontos extremos do braço (*i.e.*, os máximos e mínimos nas coordenadas

vertical e horizontal) foram anotados nos dados para possibilitar a associação dos sinais cerebrais com a trajetória do braço em cada ciclo. Para cada sujeito os canais EEG ruidosos foram interpolados, os dados foram referenciados à média comum de todos os canais, e os sinais foram filtrados numa banda de frequência 0.25-100 Hz e com um filtro tapa banda nos 50 e nos 100 Hz, este último para rejeitar o ruído de fundo. Os sinais de EEG e EOG foram separados em épocas conforme a posição do braço, sendo que cada época passou então a consistir num ciclo do braço completo que começa no ponto mais alto da coordenada vertical. Cada época foi depois temporalmente distorcida para que todas tivessem a mesma duração. As épocas com artefactos foram rejeitadas da análise usando métodos automáticos de rejeição. *Independent Component Analysis* (ICA) foi utilizada para identificar e posteriormente rejeitar componentes independentes referentes a movimentos musculares e oculares. Por fim, os dados foram explorados em ambos os domínios de tempo e frequência.

No domínio do tempo, estudámos mais especificamente a média das épocas de EEG e EOG durante os ciclos do braço. Uma vez que sinais não-invasivos são muito sujeitos a ruído, a média elimina artefactos singulares e acentua os sinais que aparecem constantemente nos dados. Os sinais do ciclo médio mostraram um padrão interessante para todos os sujeitos; um comportamento rotacional ao longo da rotação do braço direito. Para acompanhar a rotação dos potenciais, procurámos por um dipolo que descrevesse a distribuição topográfica a cada ponto do tempo. A rotação dos potenciais do EEG ao longo do ciclo médio foram verificados com a rotação da direção do dipolo ao longo do ciclo. A grande maioria dos sujeitos obteve um dipolo a rodar no mesmo sentido no mesmo plano (segundo a regra da mão direita, com um vetor de rotação a apontar para a zona frontal esquerda do cérebro). Cinco sujeitos foram a exceção, 2 desses cujo dipolo rodava no sentido contrário, e os restantes 3 sujeitos cujo dipolo rodava no mesmo sentido, mas num plano ligeiramente diferente. Em todos os sujeitos o dipolo ajustado rodava, de forma relativamente uniforme.

No domínio da frequência, estudámos em particular a banda de frequência dos 20 aos 24 Hz. Escolheu-se esta banda de frequência pois demonstrou os resultados mais interessantes e já tinha sido utilizada em estudos prévios. Usámos um algoritmo chamado SPoC (*Source Power Comodulation*) que encontra componentes de atividade cerebral cuja amplitude em frequência correlacione com uma variável alvo. Como variável alvo usámos os dados cinéticos do braço direito, e como *input* os dados cerebrais filtrados por um filtro passa-banda (20-24 Hz). Os resultados traduziram-se numa série de componentes cuja amplitude correlacionava ou anti-correlacionava com o movimento do braço, muitas delas com projeções topográficas consistentes com as áreas cerebrais motoras. Encontraram-se algumas semelhanças entre os padrões de ativação das componentes do SPoC dos vários sujeitos, ainda que os resultados variassem entre cada um. Ao projetar as componentes aos dados não-filtrados pelo passa-banda, verificamos que as modelações em frequência de facto correlacionam com as variáveis-alvo como esperado, com uma média da norma das correlações de todos os sujeitos a 85,5%.

No domínio temporal, ainda que recorrendo à média de todos os ciclos (épocas), este é o primeiro estudo que demonstra de forma não-invasiva, a existência de um dipolo com comportamento rotacional ao longo da rotação do braço. Para o seu uso em tecnologias de BCI, é necessário encontrar o mesmo fenómeno em épocas únicas, tornando possível uma classificação em *single-trial* e em tempo real. No

que toca aos resultados no domínio da frequência, a procura por componentes cuja fonte poderia estar envolvida na criação do movimento circular foi também bem-sucedida.

Este estudo abriu portas para uma série de investigações futuras. Para trabalhos posteriores destaco a necessidade de uma análise estatística, de usar mais do que um dipolo para descrever a distribuição de potenciais no domínio temporal, de explorar os dados em cada movimento e não apenas a sua média, e de explorar paradigmas semelhantes durante o movimento do braço esquerdo.

Os resultados desta tese serviram, portanto, como primeiro passo na direção de encontrar o análogo não-invasivo do vetor de população.

**Palavras-chave:** eletroencefalograma, cérebro, movimento rítmico do braço, vector de população, decodificação de movimentos.





# Contents

<b>Acknowledgements</b>	<b>iii</b>
<b>Abstract</b>	<b>v</b>
<b>Resumo</b>	<b>vii</b>
<b>List of Figures</b>	<b>xiii</b>
<b>List of Tables</b>	<b>xvii</b>
<b>List of Abbreviations</b>	<b>xix</b>
<b>1 Introduction</b>	<b>1</b>
1.1 Physiology behind movement . . . . .	1
1.1.1 Movement impairment and solutions . . . . .	3
1.2 Brain-Computer Interfaces . . . . .	4
1.2.1 BCI and their role in motor restauration . . . . .	5
1.2.2 Current BCI strategies and their limitations . . . . .	5
1.3 Brain activity acquisition . . . . .	6
1.3.1 Electroencephalography – a noninvasive method . . . . .	6
1.4 Decoding upper limb trajectory from brain activity . . . . .	8
1.4.1 Using invasive methods – spike activity in single neurons . . . . .	8
1.4.2 Using invasive methods – intracortical potentials . . . . .	9
1.4.3 Using noninvasive methods . . . . .	10
Decoding movement imaginations . . . . .	12
1.5 Context and motivation of the project . . . . .	12
1.6 Overview of this Thesis . . . . .	13
<b>2 Methods</b>	<b>15</b>
2.1 Experimental design . . . . .	15
2.1.1 Behavioral task . . . . .	15
2.1.2 One trial . . . . .	16
2.2 Data acquisition . . . . .	16
2.2.1 Participants . . . . .	16

2.2.2	Montage . . . . .	17
2.2.3	Irregularities during acquisition . . . . .	18
<b>3</b>	<b>Signal Processing</b>	<b>19</b>
3.1	Kinematic data processing . . . . .	19
3.2	Bioelectric signals processing . . . . .	20
3.2.1	Artifact epochs removal . . . . .	21
3.2.2	Independent component analysis . . . . .	22
3.3	Data Analysis . . . . .	23
3.3.1	Time domain analysis . . . . .	23
3.3.2	Frequency domain analysis . . . . .	24
	SPoC algorithm . . . . .	26
<b>4</b>	<b>Results</b>	<b>29</b>
4.1	Behavioral analysis . . . . .	29
4.2	Time domain . . . . .	30
4.2.1	Rotating dipoles . . . . .	33
4.3	Frequency domain . . . . .	39
4.3.1	SPoC . . . . .	41
<b>5</b>	<b>Discussion</b>	<b>47</b>
5.1	Behavioral analysis . . . . .	47
5.2	Time domain analysis . . . . .	48
5.3	Frequency domain analysis . . . . .	50
5.4	Limitations of the study . . . . .	52
5.5	Future Work . . . . .	52
5.6	Relevance of the study . . . . .	53
<b>6</b>	<b>Conclusion</b>	<b>55</b>
	<b>Bibliography</b>	<b>57</b>
<b>A</b>	<b>Study Information Sheet</b>	<b>65</b>
<b>B</b>	<b>Frequency domain results - Extra</b>	<b>69</b>
B.1	Frequency results for single subjects . . . . .	69
B.2	SPoC results for other frequency bands . . . . .	69

# List of Figures

1.1	Elements of the brain involved in the creation of a voluntary movement, from initiation to execution. Adapted from [3] . . . . .	2
1.2	Motor areas of the cerebral cortex. Figures adapted from [1]. . . . .	2
1.3	Primary motor cortex areas: On the right we can see a map of the several regions of one hemisphere of the primary motor cortex (highlighted in green in the brain Figure), where the movement is planned. The shoulder/elbow/hand region is highlighted in blue. Adapted from [5] . . . . .	3
1.4	Basic design and operation of a BCI system. Starting from brain data acquisition, the data is processed and translated into commands that are sent for an external device to execute. The feedback from the device enables to user to learn faster how to control the BCI. Adapted from [8] . . . . .	4
1.5	Different electrophysiological brain signal acquisition methods: from most to less invasive, and from highest to lowest resolution. From [35]. . . . .	6
1.6	Electrophysiological origins of the potentials captured by electrodes in the scalp (EEG - left) and electrodes in the cerebral cortex (LFP - right). The EEG electrodes measure the scalp potentials caused by cortical currents which, in turn, are originated from the potential changes in the neurons from the cortical layers 1 to 4. These currents can be described by a dipole perpendicular to the cortical surface. The LFP electrodes, on the other hand, measure the potential changes caused by neurons of cortical layers 1 to 4 directly from the cortex. From [39]. . . . .	7
1.7	Decoding movement directions with the population vector: A) 2-dimensional horizontal movements in 8 directions performed by behaving monkeys; B) spike activity of one motor neuron (five repetitions) during the 8 directional task; C) estimation of the population vector for the 8 directions. The population vector can be calculated according to the neurons' spike activity. From [41] [42]. . . . .	9
1.8	Noninvasive 3-dimensional decoding of natural arm movements: measured (think blue) and decoded (dashed red) x, y and z position and velocity coordinates of the arm. From [69]. . . . .	11
2.1	Arm movement representation: right-handed clockwise circular motion. . . . .	15

2.2	Experimental design: A) Experiment setup of 12 runs of 7 trials each; B) Single trial sequence diagram. Each trial starts with a blue cross (3-4 seconds) to announce the beginning of the trial. The cross then turns either green ( <b>M</b> ove trial) or red ( <b>R</b> est trial). After 20 seconds of performing one of the tasks, the cross disappears and the subject has 6-8 second break. . . . .	16
2.3	Electrode montage for EEG (white electrodes) and EOG (green). The ground electrode was placed on AFz (black) and the reference on the right mastoid (blue). . . . .	17
2.4	Experimental setup: subjects sat down and performed the movement. Kinect was placed in front of the subjects and recorded the positions of right hand during the experiment. Placed by the side of the subjects' face was a black cardboard that occluded the movement. . . . .	18
3.1	Kinect sensor coordinate system. The movement was performed in the device's XY plane. . . . .	19
3.2	Division of the data into quarter sections, according to the coordinates of the subjects' right-hands. Markers were added in the maxima and minima in the X' and Y' coordinates, dividing the data into 4 sections - quarters. One cycle begins at the highest vertical (Y) point, and ends at the next highest vertical point. . . . .	20
3.3	Data time warping representation: The quarters were time-warped to fit a 0.5 second window. Each epoch, which consists of four quarters or one full cycle, lasted 2 seconds after warping. . . . .	21
3.4	Activation patterns examples of artefactual ICs that were removed (top) and good ICs (bottom). . . . .	23
3.5	Dipole fitting: (A) the head model used (collin27) with the projected electrodes; (B) an example of two ICs with artefactual sources (1 from muscles and 2 from eye movements) rejected by spatial filtering the dipole sources. Dipole/IC 3 is an example of a good source. Both figures refer to subject 1. . . . .	24
3.6	Overview of the pipeline used to process the data. The raw kinematic and EEG data is processed into Rest and Move data, and the Move data is further processed into A) all frequencies data and B) BP filtered data. . . . .	25
3.7	Three-sphere head model created in Brainstorm for dipole fitting. . . . .	26
3.8	SPoC algorithm. SPoC takes the observable space (an original signal $X$ , and a target variable $z$ ) and tries to find a source $S$ whose power modulates with the target. . . . .	27
3.9	SPoC target values: on the left a representation of the quarter-divided arm cycle with four vectors (D1 to D4) representing the average direction of the arm during each quarter. On the right, the four possible sets of SPoC target variables used for quarter epochs Q1, Q2, Q3 and Q4, out of which only the first two (for D1 and D2) were used. . . . .	28
4.1	Subjects' right-hand X and Y coordinates (in cm) during cycles, divided into quarter sections according to the maximums and minimums in these coordinates. . . . .	31
4.2	Boxplots of the level of time warping the quarters suffered per subject (after data processing). . . . .	32

4.3	Subjects' right-elbow X and Y coordinates (in cm) during cycles (dotted blue line) and averaged-cycles (orange thick line). . . . .	32
4.4	Single subject potential distribution in 8 time instants of the averaged arm cycle data, separated by 250 ms. . . . .	34
4.5	Grand average of all subjects' potential distribution during arm cycles. In (A) the scalp projections in the same time instants as in Figure 4.4, in (B) a continuous graph of channels' potential change before, during and after each average cycle, in (C) the channel order to more easily interpret (B) - the channels are ordered from left to right and from front to back. . . . .	35
4.6	Dipole of the grand-average cycles from all subjects. On the left we used a moving dipole method, on the right a regional dipole. Color encodes time from the beginning (blue) to the end (red) of the cycle. . . . .	36
4.7	Single subject dipoles of the average cycles viewed from the top, front and front-right - subjects 1 to 6. . . . .	37
4.8	Single subject dipoles of the average cycles viewed from the top, front and front-left - subjects 7 to 12. . . . .	38
4.9	Centers of the brain estimated dipoles during arm cycles. Each color encodes one subject. All centers are placed in the center region of the brain. . . . .	39
4.10	Estimated dipole over time from the average cycle data (top), of the average cycle data with shuffled quarters (mid) and from the average 2-second epoched rest data (bottom) from data of subject 1. The change in color encodes the change in time from the start of a cycle (dark blue) to the end of the cycle (red). . . . .	40
4.11	Difference between Move and Rest spectra: Grand-average from all subjects. See Figure 4.5c for channel reference. . . . .	41
4.12	SPoC algorithm outputs for frequency band 20-24 Hz, for direction D1 (top) and direction D2 (bottom). For each components we display one scalp plot of the components' activity pattern, the Hilbert power of the activity of each cycle, and the average Hilbert power activity for all cycles (blue line) which is suppose to correlate with the target variable (orange line). . . . .	42
4.13	Frequency modulations of the data with the SPoC components' weights applied - Direction D1. The color scales vary from subject to subject. . . . .	44
4.14	Frequency modulations of the data with the SPoC components' weights applied - Direction D2. The color scales vary from subject to subject. . . . .	45
5.1	Single subject average cycle in 8 distinct time windows equally spaced (250 ms). These correspond to the same single subject average as in Figure 4.4, but with added time delay according to the dipole rotation timing. . . . .	49
5.2	Diagram of the grand-average dipole rotation with arm rotation. . . . .	50
B.1	Single subject frequency spectra difference between the Move and Rest data. In the vertical axis we have the EOG and EEG channels, ordered as in figure 4.5c . . . . .	69

B.2	SPoC algorithm outputs for frequency band 10-13 Hz, for direction D1 (top) and D2 (bottom). For each component we display its activity patterns in a scalp plot, the hilbert power of its source activity, the average hilbert power of its source activity and the target variable. . . . .	70
B.3	SPoC algorithm outputs for frequency band 13-20 Hz. Same description as for figure B.2.	71
B.4	SPoC algorithm outputs for frequency band 24-30 Hz. Same description as for figure B.2.	72

# List of Tables

4.1	Summary information of the processed data. The columns of the first three subjects are highlighted to remind the reader that they had different acquisition conditions. . . . .	29
4.2	Correlations of SPoC's components 20-24 Hz frequency modulations applied to the un-filtered data. In green the values higher than 80% and in blue the values lower than -80%. . . . .	46





# List of Abbreviations

<b>BCI</b>	<b>B</b> rain <b>C</b> omputer <b>I</b> nterface
<b>CAR</b>	<b>C</b> ommon <b>A</b> verage <b>R</b> eference
<b>ECoG</b>	<b>E</b> lectro <b>c</b> orticogragphy
<b>EEG</b>	<b>E</b> lectroencephalography
<b>ERP</b>	<b>E</b> vent <b>R</b> elated <b>P</b> otential
<b>FES</b>	<b>F</b> unctional <b>E</b> lectrical <b>S</b> timulation
<b>ICA</b>	<b>I</b> ndependent <b>C</b> omponent <b>A</b> nalysis
<b>IC</b>	<b>I</b> ndependent <b>C</b> omponent
<b>LFP</b>	<b>L</b> ocal <b>F</b> ield <b>P</b> otentials
<b>MARA</b>	<b>M</b> ultiple <b>A</b> rtifact <b>R</b> ejection <b>A</b> lgorithm
<b>MEG</b>	<b>M</b> agnetoencephalography
<b>MI</b>	<b>M</b> otor <b>I</b> magery
<b>MUA</b>	<b>M</b> ultiple <b>U</b> nit <b>A</b> ctivity
<b>PCA</b>	<b>P</b> rincipal <b>C</b> omponent <b>A</b> nalysis
<b>SMA</b>	<b>S</b> upplementary <b>M</b> otor <b>A</b> rea
<b>SPoC</b>	<b>S</b> ource <b>P</b> ower <b>C</b> omodulation
<b>SUA</b>	<b>S</b> ingle <b>U</b> nit <b>A</b> ctivity
<b>SCI</b>	<b>S</b> pinal <b>C</b> ord <b>I</b> njury



# 1 Introduction

## 1.1 Physiology behind movement

The brain has a crucial role in the human body. The endocrine and the nervous systems control all body functions [1]. The first controls hormone segregation into the circulatory system; the second is composed of specialized cells – neurons – that receive internal and external sensory stimuli and transmit them to effector organs and among themselves. The information the brain sends to the effector organs through the nervous pathways is finely coordinated allowing them to work harmoniously together for the well-being of the individual.

A voluntary motion starts as an electrical signal in the brain, namely in association areas (non-primary areas of the cerebral cortex) and in the limbic system. Several areas of the brain (thalamus, basal ganglia and cerebellum) work together with the primary motor cortex to plan the movement (how broad, how fast, how should each muscle move. . . ), and all this information is sent via neural pathways in the spinal cord to the effector organs - the muscles - where the movement is executed (see Figure 1.1) [2].

The cerebral cortex is the outer layer of the cerebral hemispheres composed of approximately 10 billion neurons and works with the constant association of other structures of the brain to send information to the effector organs, through neural pathways. Different areas of the cerebral cortex are specialized for different functions [1]. On the turn from the 19th to the 20th century, the different areas of the human cerebral cortex were divided according to its histological and functional characteristics. The areas with the highest activity during body movements were the ones anterior to the central and precentral sulci (see Figure 1.2, on the left) which were named motor cortex (divided into pre-, primary and supplementary motor areas). By the mid-20th century, Penfield *et al.* [4], [5] applied small electric stimuli to specific areas of the motor cortex of some of his patients during open brain surgery and wrote down which area of the body responded to each stimuli, thus creating a map of the primary motor cortex (see Figure 1.3).

The motor execution is affected by past information that has been stored in the memory. This is the reason why repeating a movement several times makes it more natural (for instance when learning a musical instrument). The premotor area stores programs of motor activity assembled from past experiences. With the inputs from the sensory cortex, the thalamus, the basal ganglia and memory information, the premotor cortex programs the activity of the primary motor area. The primary motor cortex is the final station for conversion of the design into the execution of the movement [1].

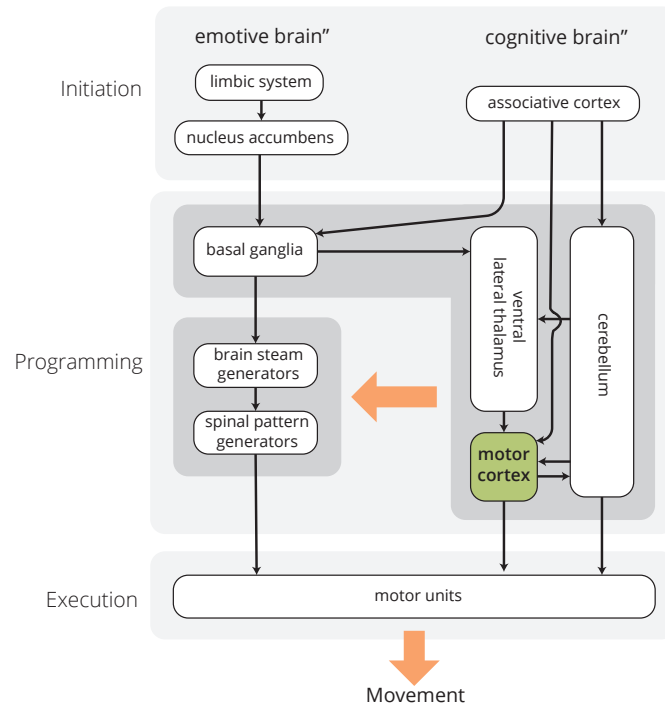


FIGURE 1.1: Elements of the brain involved in the creation of a voluntary movement, from initiation to execution. Adapted from [3]

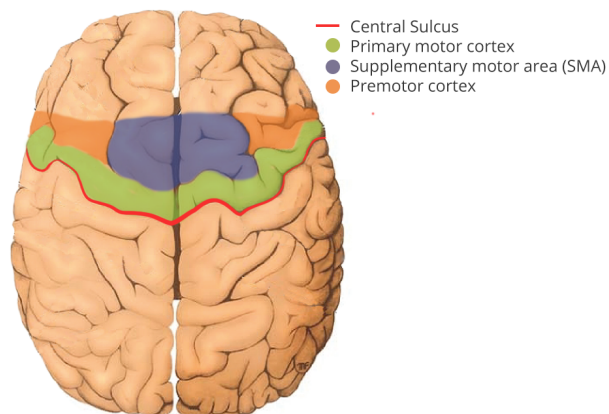


FIGURE 1.2: Motor areas of the cerebral cortex. Figures adapted from [1].

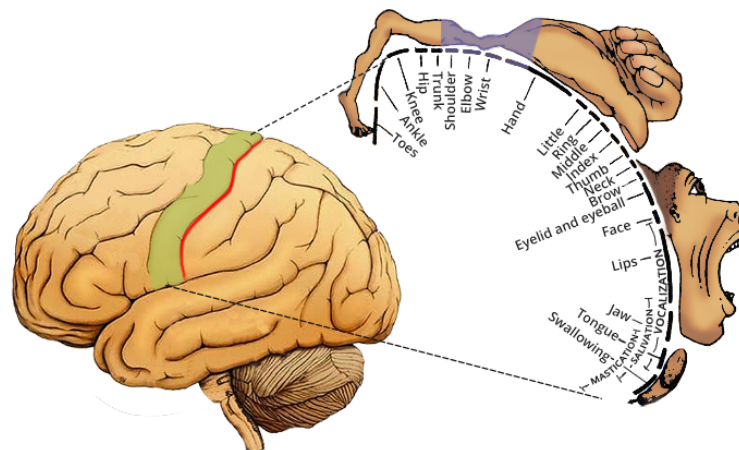


FIGURE 1.3: Primary motor cortex areas: On the right we can see a map of the several regions of one hemisphere of the primary motor cortex (highlighted in green in the brain Figure), where the movement is planned. The shoulder/elbow/hand region is highlighted in blue. Adapted from [5]

Voluntary arm movements can be regarded as discrete (such as reaching movements) or rhythmic (such as walking). A discrete movement can be perceived as part of a rhythmic one, just like a rhythmic movement can be perceived as a series of discrete movements. Nevertheless, there are different brain areas active during each type of movement and, as such, there might be different mechanisms associated to each [6]. Rhythmic movements are automatic and therefore might need less cognitive effort when compared to discrete movements, thus explaining why different parts of the brain are active in each type of motion [6], [7]. There is still a lot of unexplained variables and unknown mechanisms regarding how the brain creates the movement commands.

### 1.1.1 Movement impairment and solutions

Moving is a natural ability of the human being. We need it to run away from a predator, to cultivate the fields or to button our shirts. One single movement involves the cooperation of several elements of the body. The disturbance of one of those elements (brain, neural pathways or muscles) can cause a person to lose the ability to move freely. Brain injury, brainstem stroke, cerebral palsy (brain disorders), spinal cord injury, amyotrophic lateral sclerosis, multiple sclerosis (neural pathways disorders) or muscular dystrophies (muscle disorder) are some examples that can lead to the partial or total loss of voluntary movement ability [8] which can, of course, cause a great nuisance for the patients who may become dependent of a caregiver to perform the most mundane tasks.

Let us focus on spinal-cord injury (SCI) patients. The extent of movement lost due to a SCI depends on where the lesion occurred - the higher in the spinal cord the lesion is, the most movement capability might be lost. Depending on the lesion, there is a range of solutions to be explored. In the case of tetraplegia (partial or total loss of control of all four limbs and torso), the patient can use the remaining

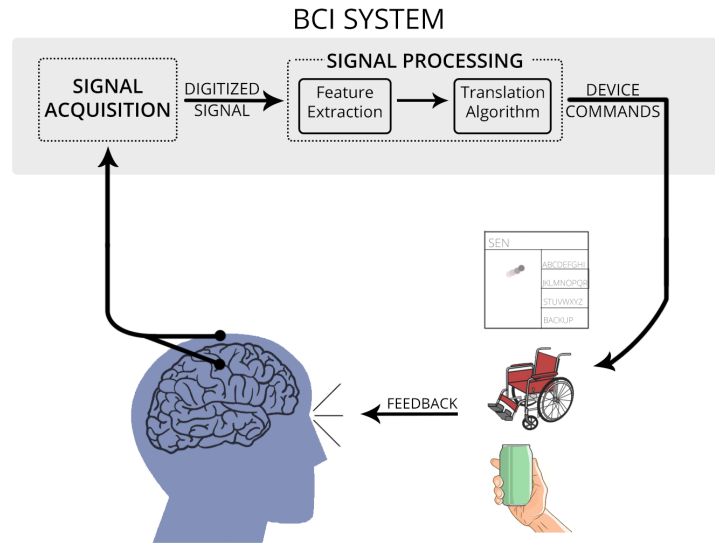


FIGURE 1.4: Basic design and operation of a BCI system. Starting from brain data acquisition, the data is processed and translated into commands that are sent for an external device to execute. The feedback from the device enables to user to learn faster how to control the BCI. Adapted from [8]

of his healthy muscles as a control for assistance devices. In the 90's, a tetraplegic patient (spinal cord injury at C4 level) with remaining shoulder and neck muscle control, used his left shoulder position to control a functional electric stimulation (FES) neuroprosthesis that enabled him to control his right arm to have a drink [9]. In most severe cases where a patient does not have control of shoulder/neck muscles, one can still use eye tracking devices to control, for example, a cursor on a screen [10], [11], or voice recognition systems to control, for example, a wheelchair [12].

Another solution is to use what is called a brain-computer interface (BCI), which is particularly interesting for its non-dependence of any muscles as a control mechanism. Unfortunately, reliable and easy-to-use BCI systems usable in a daily context are still to be developed.

## 1.2 Brain-Computer Interfaces

A BCI is a system that translates brain activity into commands for external devices [8]. BCI systems use brain signals acquired from the user (see section 1.3) and decode the user's command in real-time. The brain signals need to be processed and their main features extracted and translated into commands legible for the external device to perform (Figure 1.4). The feature extraction depends on the type of BCI system used and is discussed below.

### 1.2.1 BCI and their role in motor restauration

There are around 250 000 to 500 000 new cases of SCI patients each year worldwide [13]. While some patients can restore their movement ability through therapy, others lose completely their ability to walk, grasp an object, or talk. BCI systems are particularly interesting for movement-impaired people since they allow for non-muscular communication and control [8]. Several researchers have worked on creating BCI systems for motor rehabilitation. BCIs have been used to control simulated wheelchairs by healthy people [14] and tetraplegic patients [15]; to control a FES neuroprosthesis to restore the hand grasp of a SCI patient [16], [17]; or to control grasp movements on a robotic arm [18]. More recently, researchers have studied hybrid neuroprosthesis which uses as input, as an example, both BCI and a shoulder position sensor to control an FES neuroprosthesis of the elbow and hand of paralyzed patients [19], [20].

### 1.2.2 Current BCI strategies and their limitations

To decode intention from brain signals is a challenging task. The complexity of the brain signals led researchers to come up with approaches that use known identifiable brain responses to certain external stimuli or mental strategies [8]. Specific external events create specific potentials in the users' brain – event related potentials (ERPs). The BCIs based on external stimuli (or ERP-based BCIs) use visual, auditory or tactile stimuli that the user pays attention to. This concept is mostly used for communication purposes, for example, to create several BCI spellers [21]–[24].

Another category of BCIs is based on induced responses of the brain. These do not depend on any external stimulus but rather on self-induced mental tasks. Motor imagery (MI) describes the mental rehearsal of a movement without its execution. This movement rehearsal creates a known and measurable synchronization (or desynchronization) of neuron activity in the motor cortex, which reflects into an increase (or decrease) of power in certain frequency bands. These variations in power can be measured and used as a feature for discriminating between two or more different MIs [25]. With this method, one can distinguish between MI of the right hand *vs.* the left [26], [27], right foot *vs.* left [28], hands *vs.* feet [29], and between different MIs of the same limb [30]. These can be used to select between a limited number of options on a computer screen or, for example, to control a cursor on a computer [31].

To date, only a few ERP-based BCI have been used for a long-period of time outside of the research fields [32], [33]. These rely on shifting attention between external stimuli, which can be unpleasant for users. Induced-response based BCIs have limited number of degrees of freedom and they do not mirror the way one plans a movement. For control of an arm prosthesis, in order to achieve a more natural control and to reduce training time, the movements decoded by the BCI need to be closely related to the user's intention [34].

Directly decoding the movement trajectory of the limbs from brain activity would open doors to a natural control an arm prosthesis. This topic has been target of study for over three decades. The state of

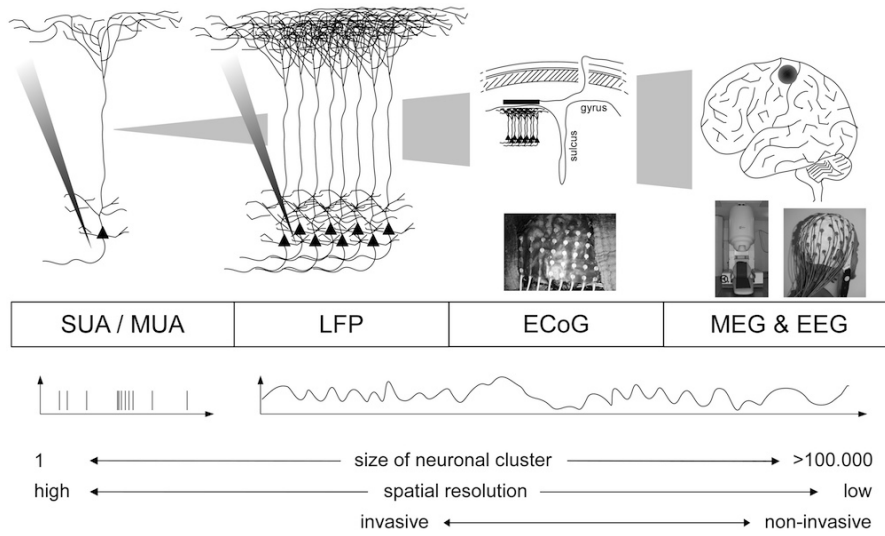


FIGURE 1.5: Different electrophysiological brain signal acquisition methods: from most to less invasive, and from highest to lowest resolution. From [35].

the art of decoding of arm execution and imagination parameters from brain activity will be approached below in section 1.4.

### 1.3 Brain activity acquisition

It is relevant to distinguish at least two groups of brain signal acquisition methods: invasive and noninvasive. The major difference is that the first requires surgical insertion electrodes beneath the cranium, and the second does not require any sort of physical harm to the user. Among the invasive group, one can mention single/multiple unit activity (SUA/MUA) which is referred to spike activity of single/multiple neurons; local field potentials (LFP) which are defined as extracellular potential differences recorded at electrodes inserted into the cortical sheet; and a slightly less invasive method called electrocorticography (ECoG), which records brain activity from the surface of the cerebral cortex. Among the noninvasive group, we should highlight magnetoencephalography (MEG) and electroencephalography (EEG), which record noninvasively external magnetic fields and electric potentials, respectively (see Figure 1.5, from [35]).

#### 1.3.1 Electroencephalography – a noninvasive method

EEG is the brain activity acquisition method most commonly used for BCI control. It is non-expensive, does not require heavy equipment, has a high time resolution and is noninvasive (which would be preferred by people with SCI [36]).



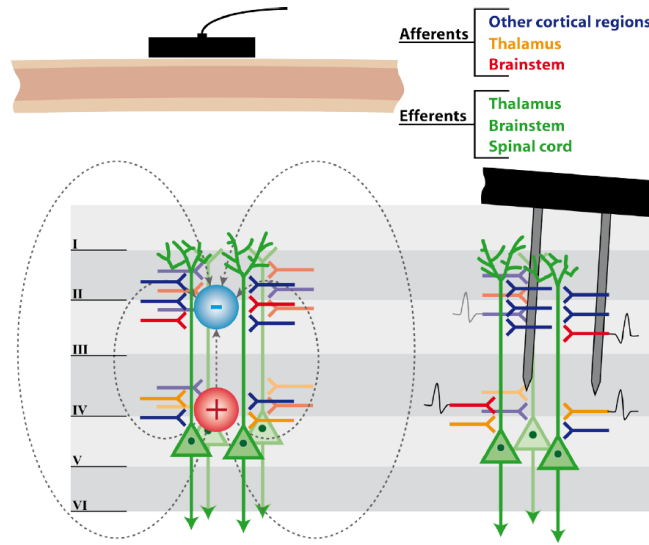


FIGURE 1.6: Electrophysiological origins of the potentials captured by electrodes in the scalp (EEG - left) and electrodes in the cerebral cortex (LFP - right). The EEG electrodes measure the scalp potentials caused by cortical currents which, in turn, are originated from the potential changes in the neurons from the cortical layers 1 to 4. These currents can be described by a dipole perpendicular to the cortical surface. The LFP electrodes, on the other hand, measure the potential changes caused by neurons of cortical layers 1 to 4 directly from the cortex. From [39].

When cortical neurons are activated, local current flows are produced. EEG uses electrodes to measure the electric potential distribution at the scalp, measuring mostly the currents that flow during synchronous excitations of large groups of pyramidal neurons in the cerebral cortex [37]. Cortical pyramidal neurons are excellent dipoles due to their unique anatomical structure parallel to each other and perpendicular to the cortical surface [38]. Because the signals are attenuated by distance and volume conductance caused by the intermediate layers (the meninges, skull, and skin), only synchronous brain activity can be measured at scalp level.

Even though the EEG signals have poorer signal quality and spatial resolution compared to invasive methods, they share origins: the action potential spiking rates of cortical layers 1 to 4 (see Figure 1.6) [39]. This indicates that what is measurable with invasive methods such as LFP and ECoG, is fundamentally the same as what is measurable with EEG despite the modifications caused by volume conduction and limited spatial resolution.

EEG records complex brain signals in a wide spectrum of frequencies. Several frequency bands can be named:  $\delta$  ( $< 4$  Hz),  $\theta$  (4-7 Hz),  $\alpha$  (8-12 Hz),  $\beta$  (13-30 Hz) and  $\gamma$  ( $> 30$  Hz). The change in brain signal power, in respect to a reference period, due to an event is called an event-related synchronization/desynchronization (ERS/ERD) [40]. When a user executes or mentally rehearses a movement, a desynchronization of motor neurons occurs thus creating a measurable decrease of power mostly in the  $\mu$  (roughly same frequency band as  $\alpha$ , but from the motor cortex) and  $\beta$  bands. This power decrease is usually contralateral to the side of the body that moved, *i.e.*, if the user executes or rehearses a movement

with his right arm, there will be a power decrease on the left side of the arm motor cortex area.

## 1.4 Decoding upper limb trajectory from brain activity

One of the possible applications of BCI is to use it as a natural control system for a robotic arm or a neuroprosthesis for reintegration of arm function in movement impaired patients. The specific movement intention is recognized by the BCI and the prosthesis or the robotic arm executes the movement [34]. The control of such devices should be natural and familiar to the end users, thus less training would be necessary for an efficient control. As stated in section 1.1, several structures of the brain contribute to the execution of one movement but most voluntary movement planning culminate in the motor cortex where the information is sent to the effector organs via neural pathways. This means that parameters of movement execution, such as arm movement direction, are encoded in the motor area of the cerebral cortex and it might be possible to decode such parameters and use them to replicate movement artificially.

### 1.4.1 Using invasive methods – spike activity in single neurons

Georgopoulos *et al.* [41]–[44] recorded single neurons in the arm area of the motor cortex of primates while they performed directional center-out tasks with their arms. The monkeys were instructed to move a frictionless manipulandum to one of 8 directions in a 2-dimensional (2D) almost horizontal plane [41], [42] and to one of 8 vertices in a 3-dimensional (3D) box [43], [44]. They inferred that the spike activity in single neurons changed with an orderly fashion with the direction of movement and that, for one given cell, the spike activity was highest with movements in a particular direction (the cell's preferred direction) and decreased gradually with movements made in directions away from the preferred one. In Figure 1.7 - B we see the spike activity of one neuron from the motor cortex of a monkey, recorded five times for each of the eight directions of movement in Figure 1.7 – A. This neuron's preferred direction was around 135° and 180°, where the spike activity is most frequent. Considering each neuron in the arm motor cortex as a vector that points to its preferred direction with amplitude proportional to its spike activity, the sum of all vectors at a given instant will point in the direction of the arm movement performed and it is called population vector (in Figure 1.7 – C, for 8 directional movements, direction of arm movement is the dotted grey line, and the population vector is the thick blue line). This also applies to movements in 3 dimensions.

In 1990, Caminiti *et al.* [45] showed that when movements in similar directions were performed in different spatial areas (and therefore, using different sets of muscles), the population vector still pointed in the direction of the movement.

Several other works have corroborated and extended the information of the works of Georgopoulos. Regarding 2D environments, Kurata *et al.* [46] studied wrist movements; Koike *et al.* [47] decoded left vs. right reaching movements; Fu *et al.* [48] decoded different range arm movements in 8 directions; and Mulliken *et al.* [49] decoded arm movements in 8 directions, in a study in which monkeys controlled a

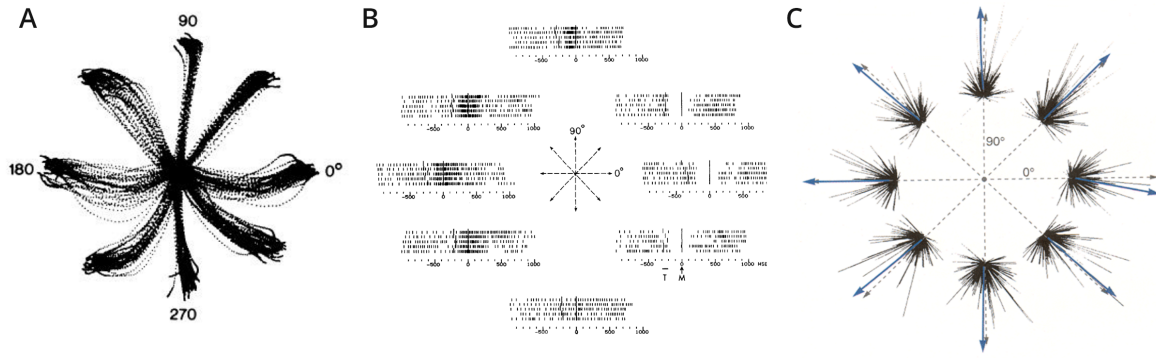


FIGURE 1.7: Decoding movement directions with the population vector: A) 2-dimensional horizontal movements in 8 directions performed by behaving monkeys; B) spike activity of one motor neuron (five repetitions) during the 8 directional task; C) estimation of the population vector for the 8 directions. The population vector can be calculated according to the neurons' spike activity. From [41] [42].

cursor in real-time using brain signals. In a study by Taylor *et al.* [50], monkeys controlled a real-time neuroprosthesis in a 3D environment with machine learning techniques and data over several days. In the same study, the authors stated that the effectiveness of control was enhanced by visual feedback and training.

More recent studies have proved that similar concepts can also be applied to humans. Hochberg *et al.* [51], Truccollo *et al.* [52] and Kim *et al.* [53] conducted studies where tetraplegic patients controlled a cursor on a screen by imagining limb motions. These studies also argue that movement parameters remain encoded in the motor cortex years after spinal cord injury. Chadwick *et al.* [54] studied the continuous control of a simulated arm (with 2 degrees-of-freedom – shoulder and elbow joints in the horizontal plane) by a tetraplegic patient. They successfully trained a decoder that allowed the subject to perform simulated arm movements.

### 1.4.2 Using invasive methods – intracortical potentials

Cortical currents can be measured on the surface of the cerebral cortex - ECoG, or by penetrating this surface - LFP.

Using LFPs, some research groups have attempted to decode direction of arm movement in behaving monkeys in center-out tasks with information from time domain [55] and frequency domain [56]. The first used machine learning algorithms and the second found out that the  $\delta$  band frequency ( $<4$  Hz) has the highest influence in movement direction decoding, followed by high  $\gamma$  (63-200 Hz), and finally  $\theta$  and  $\alpha$  (6-13Hz).

Using ECoG, Toro *et al.* [57] found information related to the kinematics of complex movements encoded in the  $\mu$  frequency band (8-12 Hz) in ECoG signals of the motor-sensory cortex. Ball *et al.* [58] studied the role of other frequency bands in decoding, and they stressed the  $<2$  Hz and 52-125

Hz as the frequency bands most related to movement trajectory, and stated that from 6 to 50 Hz there is “little or no significant directional information”. Nakanishi *et al.* [59] drew similar conclusions: they decoded movements from frequencies below 4 Hz which resulted in the highest correlation to the executed movement, and the band 50-90 Hz had the next highest correlation. Schalk *et al.* [60] and Pistohl *et al.* [61] decoded circular and complex arm movements (respectively) from ECoG signals of epileptic patients. They managed to decode movements from low-frequency components ( $<10$  Hz) using linear regression methods. Spüler *et al.* [62] explored the brain signals of paralyzed patients during different hand movements from 5-150 Hz and Yanagisawa *et al.* [63] for frequencies  $<8$  Hz and 25-40 Hz.

Overall, LFP and ECoG studies have reported the possibility to decode movement from low-frequency signals ( $<10$ Hz) and in frequency modulations mostly in the  $\gamma$  frequency band ( $>50$  Hz) but also 25-40 Hz.

### 1.4.3 Using noninvasive methods

Even though brain signals acquired from noninvasive methods have unarguably lower spatial resolution than other similar but invasive methods, several works have proven that upper limb trajectory features can be decoded in noninvasive brain signals. Among noninvasive methods, a direct comparison under identical conditions between EEG and MEG revealed that the decoding accuracy did not effectively differ [35].

In 2005, Georgopoulos *et al.* [64] used a linear decoding algorithm to decode movement trajectory from a pentagon-drawing task, using MEG signals. He used a linear regression method to reconstruct the pentagon, demonstrating that noninvasive brain signals might have enough trajectory information. In 2008, Waldert *et al.* [35] managed to classify between four wrist directions in a center-out task using a linear classification algorithm with both EEG and MEG brain signals. They found that most information seemed to be encoded in the low frequency ( $<7$  Hz), but little was encoded in the  $\beta$  band (10-30 Hz) and high- $\gamma$  (62-87 Hz).

Bradberry *et al.* used MEG [65], [66] and EEG [67], [68] to decode two-dimensional and three-dimensional movement trajectory. They used a linear decoding algorithm applied to low-frequency signals. Ofner *et al.* [69] created a new paradigm based on Bradberry’s [68] that allowed for decoding of broad natural arm movements without the need for external targets. With the new paradigm, they managed to decode continuous movements from low-frequency brain signals (band-pass filter at 0.5 Hz and 2 Hz) using a linear regression algorithm (results in Figure 1.8, with the decoded position and velocity coordinates in dotted red line, and the measured movement in blue).

Other studies that corroborate the fact that it is possible to decode movement trajectory from noninvasive brain signals include: Hammon *et al.* [70] classified reaching tasks in different directions; Yeom *et al.* [71] decoded arm velocity in a 3D center-out task, using a linear regression algorithm in the frequency band 0,5-8 Hz from MEG signals in healthy subjects (the frequency bands of 9–22, 25–40 and 57–97

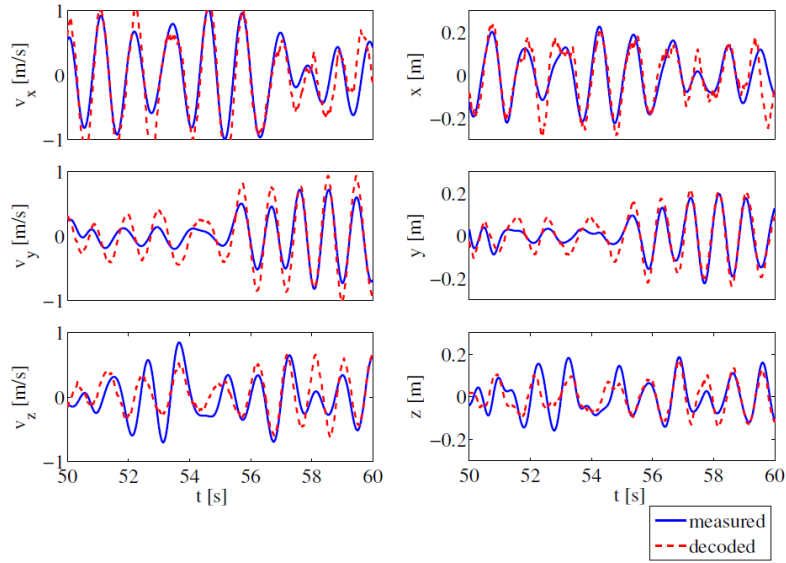


FIGURE 1.8: Noninvasive 3-dimensional decoding of natural arm movements: measured (think blue) and decoded (dashed red) x, y and z position and velocity coordinates of the arm. From [69].

Hz did not appear to encode movement velocities); McFarland *et al.* [72] decoded 3D movements using EEG data filtered into several frequency bands (ranging from 10 to 31 Hz), and concluded that the frequency band that led to maximum accuracy was different for each subject; Choi [73] reconstructed EMG signals from EEG during reaching tasks, and later estimated the shoulder and elbow angles; Lv *et al.* [74] used a drawing task and Robinson *et al.* [75] a horizontal center-out task to decode movements in a 2D plane with movements in four directions; and Kim *et al.* [76] decoded movements during predefined continuous trajectories.

Some studies argue that even though  $\mu$  (8-12 Hz) and  $\beta$  (12-30 Hz) bands are associated with movement intent they have little information regarding movement trajectory [35], [58], [59], [71]. It is, however, possible that some of these studies' results were misinterpreted due to the properties of linear regression methods [77]. Korik *et al.* [78] state that spatio-temporal power pattern of various frequency bands (including  $\mu$  and  $\beta$ ) hold significant information regarding movement parameters.

Some works have looked into hand and finger movement decoding, to recreate grasping movements [79]–[81]. Wang *et al.* [82] and Toda *et al.* [83] decoded wrist and finger movement directions, respectively, in a 2D center-out task from MEG signals in healthy subjects. Seeber *et al.* [84] studied frequency modulations during fast and slow finger flexion movements, and found a clear relationship to the movement phase in the mid- $\beta$  (18–24 Hz) and high- $\beta$  (24–30 Hz) frequency range. Overall, most studies give evidence that most trajectory information is encoded in the  $\delta$  frequency band (<4 Hz) of the motor cortex, some state that there are frequency modulations in high- $\gamma$  (60-90 Hz) and some argue that  $\mu$  (8-12 Hz) and  $\beta$  (12-30 Hz) bands are overlooked and might encode important trajectory information.

All the studies mentioned above give further proof that noninvasive brain signals might carry information to decode movement trajectory and that it might be eventually possible to use noninvasive BCI systems for natural control of prosthesis. More detailed reviews on this topic can be found in Jerbi *et al.* [85] and Müller-Putz *et al.* [34].

### **Decoding movement imaginations**

Research on movement execution decoding is important to get a better insight on how the brain encodes movement information. But to be used by motor-impaired people, the decoding of arm trajectory imagination is the goal. This task is more demanding since there is no direct visual and sensory feedback from the imagined movements.

Studies by Pfurtscheller *et al.* [26] showed that during execution and imagination of a movement similar areas show power changes. This provides evidence that directional movement imagination should be possible to be decoded just as movement execution.

Vučković *et al.* studied imagination of four same wrist movements [86] and of flexion/extension of the left and right wrists. Gu *et al.* [87] studied fast *vs.* slow wrist extensions in paralyzed ALS patients. Regarding broader arm movements, Bradberry *et al.* [88] attempted to continuously decode imagination of moving the target in four directions. Their single-trial accuracy was very satisfactory (>70%), although other researchers pointed out how the results may have been overestimated [89], [90]. Later, Ofner *et al.* [91] distinguished between imaginations of horizontal and vertical arm movements, and Kim *et al.* [76] studied and succeeded in decoding both execution and imagination of a defined arm trajectory with similar accuracy. All the studies mentioned in this subsection used EEG for brain signal acquisition.

## **1.5 Context and motivation of the project**

Being able to efficiently decode brain activity would be a major step for neuroscience. Among its applications, one can focus on motor rehabilitation. The idea that patients with motor impairment may learn to control a robotic arm with nothing but their thoughts still sounds like science fiction, but several efforts have been conducted to reach such goal.

With BCI systems, people are able to control devices without any physical movement. So far, this has been possible mostly using unnatural mental strategies mentioned in section 1.2.2. These BCI systems are not intuitive and require the user to learn the control commands and would not be practical for a daily use. An ideal BCI would be based on more natural strategies like the motion intention *per se*, *i.e.*, the person would imagine an action, e.g. open right hand, and the external device would perceive and act on that thought.

Previous works have advocated that it is possible to decode movement trajectory of the arm from brain activity either from invasive or noninvasive methods. Studies that used recordings from single cells

(invasive) showed that it is possible to calculate a vector that points in the direction of the arm movement at any given time point - the population vector (see section 1.4.1). Other studies have proven possible the decoding of movement trajectory from noninvasive signals (see section 1.4.3).

If it is possible to decode movement parameters from noninvasive brain signals, would it be possible to find a noninvasive analogous population vector? This was the main research question of this thesis and the motivation behind the project. To approach this question, we recorded EEG, EOG and kinematic data from 12 healthy subjects while they performed a rhythmic, broad, repetitive motion with their right arm.

## 1.6 Overview of this Thesis

This thesis reflects the work of a 7-month Master's project during an internship at the Institute of Neural Engineering (INE) of the Graz University of Technology, in Austria. During that time, I worked on planning the experiment, acquiring data and processing the data under the supervision and guidance of researchers of the INE.

Throughout the rest of this thesis, I describe the methodology and results obtained during the project. In section 2 I depict the methods of acquisition, the paradigm and equipment I used for the recordings of 12 healthy subjects, and mention some setbacks and how they were overcome. In section 3 I describe how the data was preprocessed, the artifact rejection methods applied, and finally the analysis methods used. This section is divided into two sub-sections: time-domain analysis, where the methods used for analysis in the time domain are described, and frequency-domain analysis, with the methods we explored to find power modulations. In sections 4 and 5, I show the results obtained in the project and discuss them. The results and discussion are separated into time and frequency-domain. In section 5 I also give my insight on the limitations of the thesis, what could be the future steps in this research and the relevance of this thesis' results. Finally in 6, a brief summary of the thesis and its results is given.





## 2 Methods

### 2.1 Experimental design

#### 2.1.1 Behavioral task

The experiment consisted of 12 runs, each with 7 trials, giving a total of 84 trials (Figure 2.2). Each trial belonged to one of the two conditions: move (M) and rest (R), with a respective ratio of 4:1. In the move trials (M) subjects were asked to perform a movement with their right arm. The movement was a circular clockwise motion in the vertical plane as if the subjects were drawing a circle in front of them (Figure 2.1). It was continuous and allowed for several directions in one plane. The width and the duration of the movement were not fixed, to allow for the movement to be as natural as possible. Beforehand, subjects were properly instructed and had the chance to practice the movement with a uniform velocity. We trained them so that a full cycle would have a duration of 2 seconds (corresponding to a frequency of 0.5 Hz), and the broadness of the movement around the size of their torso. During acquisition, the eyes were staring at a fixation cross in the center of the screen to minimize eye movements.

The movement involved the rotation of both elbow and shoulder joints. Previous studies advocated that the brain activity during movement is more related to the arm direction and not to the joint rotation [92], [93]. This allowed us to tell our subjects to perform the movement as they felt more comfortable, not restraining any joint. Subjects were asked to keep the rest of the body and right hand relaxed, and the wrist joint angle constant, to more easily track the movement with our sensor.

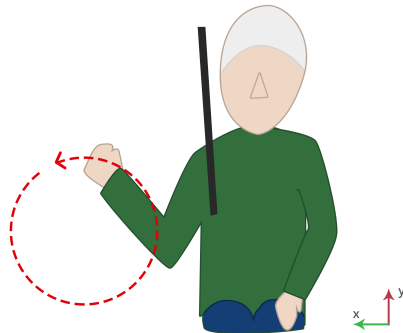


FIGURE 2.1: Arm movement representation: right-handed clockwise circular motion.

In the rest trials (R), the subjects were asked to stay in a rest position, with their body relaxed, both hands on their lap and eyes staring at a fixation cross in the center of the screen, as they did in the move trials (M).

### 2.1.2 One trial

Each trial consisted of a 1) preparation period, 2) task period, and 3) break period (Figure 2.2 - B), and lasted for 31-34 seconds. During the preparation period, a blue cross appeared in the center of the screen. During this period, subjects were asked to remain in a rest position staring at the fixation cross, and to try not to blink. After 3-4 seconds, the cross would turn either green (trial M) or red (trial R), signaling the subjects to perform one of the tasks. After 20 seconds, the cross would disappear, marking the end of the task period. The 6-8 second breaks in the end of each trial were planned for the subjects to blink, relax or adjust their body position.

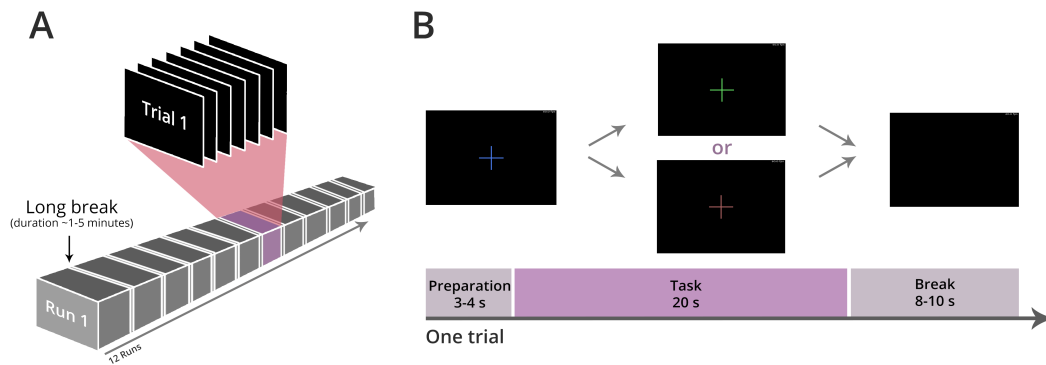


FIGURE 2.2: Experimental design: A) Experiment setup of 12 runs of 7 trials each; B) Single trial sequence diagram. Each trial starts with a blue cross (3-4 seconds) to announce the beginning of the trial. The cross then turns either green (**M**ove trial) or red (**R**est trial). After 20 seconds of performing one of the tasks, the cross disappears and the subject has 6-8 second break.

## 2.2 Data acquisition

### 2.2.1 Participants

Twelve healthy right-handed subjects aged 20-29 (eight males, average age of 24) participated in the study. All had normal or corrected vision, and all consented to be part of the study. Before the experiment, they were presented with the information sheet attached in section A.

During the experiment, EEG, EOG and arm kinematic variables were recorded. The subjects sat on a comfortable chair at 1.5 meters distance from a screen, in a darkened and electrically shielded room.

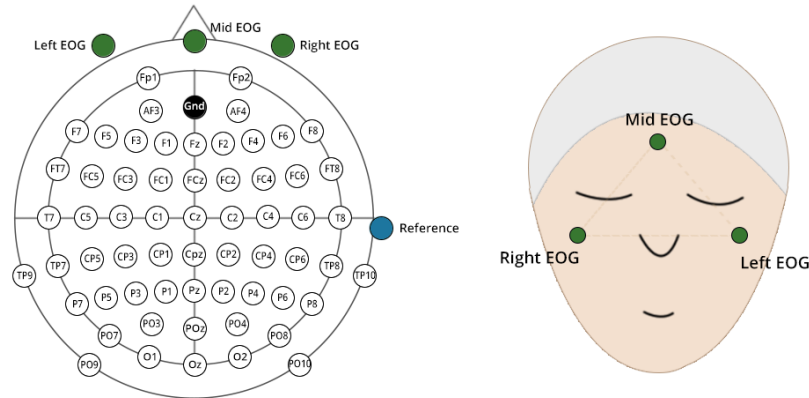


FIGURE 2.3: Electrode montage for EEG (white electrodes) and EOG (green). The ground electrode was placed on AFz (black) and the reference on the right mastoid (blue).

### 2.2.2 Montage

EEG signals were acquired with 64 active Ag/AgCl electrodes arranged according to the International 10–10 system (actiCAP, BrainAmp from Brain Products Munich, Germany). Three out of the 64 electrodes were repositioned for EOG to track eye movements. The EOG electrodes were placed above the nasion and below the outer canthi of the eyes. Signals were sampled at a frequency of 1000Hz, with all impedances kept below 20k $\Omega$ , with the reference placed at the right mastoid and ground on AFz (Figure 2.3). The kinematic data of the right hand was recorded using Kinect Sensor for Microsoft’s Xbox 360 (Microsoft, Redmond, USA). This sensor recorded X, Y and Z positions of the body joints (hand, wrist, elbow, shoulder,...) during the experiment.

For source analysis, the electrode positions were recorded using CMS 20 EP system (Zebris Medical GmbH, Isny, Germany) for each subject.

For time-synchronization of the different data streams, we used the Lab Streaming Layer (LSL) from the Swartz Center for Computational Neuroscience (SCCN) which ensures the unified collection of measurement time series (freely available in GitHub<sup>1</sup>). The paradigm was created using SNAP (Simulation and Neuroscience Application), a Python based software available in GitHub<sup>2</sup>. During the acquisition, SNAP streamed time markers representing the beginning and end of each trial, which were then used to mark time instances in EEG. There is a short time lag between SNAP sending a command and the command being displayed on the screen. To measure this time lag, we used a photodiode to detect when the beginning of the trial was displayed on the screen.

The movement was occluded using a black cardboard (see Figure 2.4). In a pilot acquisition we noticed high activity in the occipital cortex (which is related to visual stimuli) and some abnormal activity in the right-EOG channel, probably due to the arm proximity to the electrode that was placed on the face,

<sup>1</sup>at <https://github.com/sccn/labstreaminglayer>

<sup>2</sup>at <https://github.com/snap-stanford/snap-python>

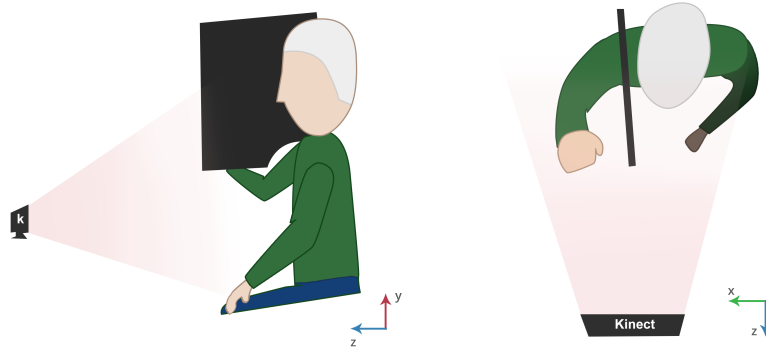


FIGURE 2.4: Experimental setup: subjects sat down and performed the movement. Kinect was placed in front of the subjects and recorded the positions of right hand during the experiment. Placed by the side of the subjects' face was a black cardboard that occluded the movement.

below the right eye. The black cardboard solved both these problems by occluding visual feedback, and forcing the subjects to perform the movement further from the face.

### 2.2.3 Irregularities during acquisition

The first three subjects had different conditions from the rest. Subject 1 did not have the movement occluded and had the ground electrode placed on his right wrist. Subjects 2 and 3 had the movement occluded with cardboard goggles that were rather uncomfortable, and the ground was placed in AFz location (as the other subjects). The first three acquisitions were important to reshape the setup of the experiment for the remaining nine subjects. Their results are also taken into consideration throughout this thesis.

For the first six subjects only 70 trials were recorded in total, in contrast with the later 6 that had 84. A lot of data was rejected during the processing of the first subjects data, and therefore we chose to record more data for the rest of the subjects.

During acquisition, the subjects arm speed was monitored and some trials were cancelled and repeated if the subject was not performing the task correctly. This was only implemented after the first three subjects.

The kinematic data recorded from subjects 9 and 11 was noisy and did not seem to reflect the arm movements in some of the trials. Overall, the hardware used (the Kinect Sensor) had a rather unstable behavior – at times it would not successfully track the body movements.

Finally, subjects 6 and 12 showed an abnormal low-frequency electrical activity in frontal electrodes. We could not find any relation between these artifacts and the subject's behavior (arm movement, eye blinks,...). We think this flaw might have been caused by the Kinect Sensor interfering with the EEG cap. These artifacts were removed, but led to an extra loss of data for both subjects.

## 3 Signal Processing

The data were imported to MATLAB (R2012A) and the data streams were synchronized by adjusting the time-stamps of the SNAP events using the photodiode data (mentioned in section 2.2.2). The kinematic and the EEG data were processed separately. Then the two types of data were analyzed together. An overview of the data processing procedure is illustrated in figure 3.6.

### 3.1 Kinematic data processing

The Kinect Sensor recorded three-dimensional position of the right-hand at each time-point. The coordinates X, Y and Z correspond to horizontal, vertical and depth (Figure 3.1), and the movement was done approximately on the XY vertical plane.

The data were band-pass filtered (infinite impulse response (IIR) Butterworth; fourth-order; zero phase; cut-off frequencies 0.3 and 0.8 Hz) to remove high-frequency noise and emphasize the circular motion (the movement was performed at approximately 0.5 Hz).

For each 20-second M trial data, principal component analysis (PCA) was performed to retain the two main coordinates of the movement, thus creating 2 new X' and Y' coordinates. The maxima and minima of both X' and Y' coordinates were extracted and markers were added to the EEG data at these time-points. The markers on the continuous EEG data discriminate quarter fragments (Figure 3.2).

The quarter-markers from one trial would only be added to the EEG data if:

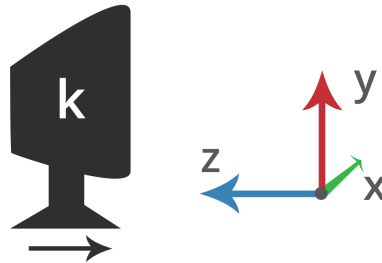


FIGURE 3.1: Kinect sensor coordinate system. The movement was performed in the device's XY plane.

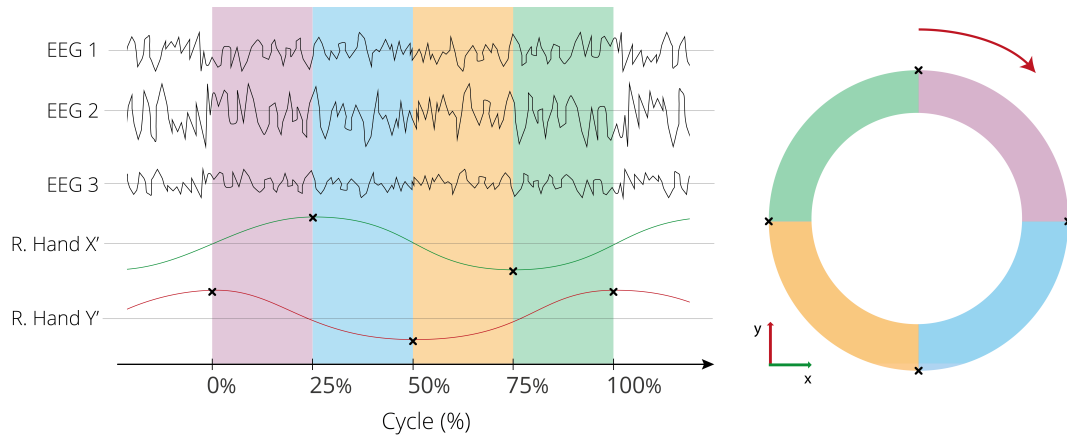


FIGURE 3.2: Division of the data into quarter sections, according to the coordinates of the subjects' right-hands. Markers were added in the maxima and minima in the X' and Y' coordinates, dividing the data into 4 sections - quarters. One cycle begins at the highest vertical (Y) point, and ends at the next highest vertical point.

1. the PCA rotation plane didn't rotate more than  $45^\circ$  (*i.e.*, if the movement was performed around the XY plane);
2. the markers followed a circular order (max. vertical, max. horizontal, min. vertical, min. horizontal, max. vertical,...);
3. the markers were more than 0.25 seconds apart from each other (*i.e.* movement twice faster than expected considering 2-second cycles).

Using this algorithm, whenever a subject performed a considerable non-cyclic movement at the beginning of a task, a full trial would be rejected due to the non-coherent circular order of the quarter-markers. To counteract this, whenever one trial did not meet the requirements above, the algorithm would ignore a few seconds of data in the beginning and end of each trial and repeat one more time (maximum of two repetitions).

### 3.2 Bioelectric signals processing

The data processing and analysis was performed mainly on EEGLAB toolbox for MATLAB (version 14.0.0b) [94]. The data were down sampled to 250 Hz, were visually inspected for bad channels, and those were removed and interpolated (*i.e.* estimated considering the neighbor channels). Usually, only peripheral (less relevant for the task in question) channels were interpolated.

The data were re-referenced to the common average of all channels. This is called a common average reference (CAR) and it leaves the data "reference-free". It also functions as a high-pass spatial filter, enhancing the components with highly focal distributions.

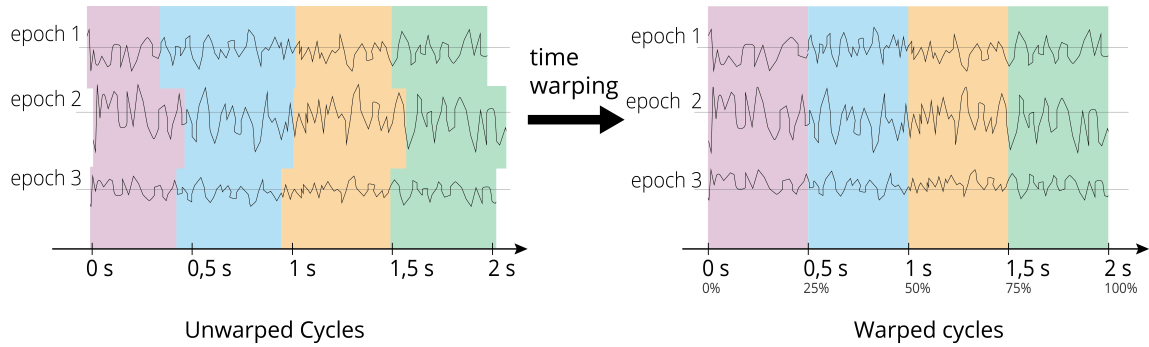


FIGURE 3.3: Data time warping representation: The quarters were time-warped to fit a 0.5 second window. Each epoch, which consists of four quarters or one full cycle, lasted 2 seconds after warping.

The data were bandpass filtered (IIR Butterworth; tenth-order; zero phase; cut-off frequencies 0.25 and 100 Hz) and notch filtered (IIR; notch frequencies 50 and 100 Hz; bandwidth of 2 Hz with attenuation of 1 dB; zero phase) to remove line noise. Although studies state that high-pass filtering below 0.5 Hz does not produce optimal results regarding signal-to-noise ratio and artifact rejection using ICA [95], we chose the lower cutoff frequency at 0.25 Hz because the movement was done in this frequency range.

The data were divided into Move and Rest data. The continuous Move data were epoched into full cycles that started when the hand was at the highest vertical position, and finished at the next highest vertical position. Because the movement speed was not fixed, not all epochs had the same size. To solve this, the quarters were time-warped to fit 0.5 seconds, making each full cycle last 2 seconds (which was the speed subjects were asked to perform the movement) - Figure 3.3. The Rest data were kept in a continuous format, and no artifact removal or component analysis was performed.

When using time-warping, one has to keep in mind that it also warps the frequency identity of the data. For time-domain analysis, it will not relevantly change how the data is processed and analyzed. For frequency-domain analysis, we band-passed filtered the data before the time warping, maintaining therefore the information of the band frequency within the data (see Figure 3.6 for an overview of the data processing pipeline).

#### 3.2.1 Artifact epochs removal

If any of the four quarters in one epoch were warped more than 50%, the whole epoch was rejected. This rejected the cycles whose quarters took more than 0.75 seconds and less than 0.25 seconds.

To reject further artifacts, we used EEGLAB functions for automatic trial rejection. Three criteria were used:

**Threshold** - epochs at any time-point over the threshold ( $70 \mu\text{V}$ ) were marked for rejection;

**Probability** - epochs with time-points over 5 times its standard deviations were marked for rejection;

**Kurtosis** - epochs whose kurtosis was higher than 6 were marked for rejection. Higher kurtosis means most of the variance is the result of infrequent extreme deviations, as opposed to frequent modestly-sized deviations [96].

The last two methods were then computed one more time for better cleaning. In the end, an average of 38% of the cycles (or 175) were removed per subject.

### 3.2.2 Independent component analysis

EEG signals are generated by numerous neural sources and noise components. One can think of the scalp signals as a weighted sum of potentials from independent sources spread over the cerebral cortex. If we consider a source space  $s(t)$  and a noise factor  $n(t)$ , the EEG signals would be reconstructed as in equation 3.1.

$$x(t) = \mathbf{A}s(t) + n(t) \quad (3.1)$$

In equation 3.1,  $\mathbf{A}$  is a mixing matrix that transforms the source space  $s(t)$  into the EEG scalp potentials  $x(t)$ .

Independent component analysis (ICA) is an algorithm that enables the separation of the data into individual components. It searches for a linear representation of the original data, so that its components are non-gaussian and statistically independent [95]. Assuming EEG sources are independent, the independent components (ICs) can be perceived as their sources. ICs can then be represented as in equation 3.2. In this equation,  $x(t)$  represents the original EEG data,  $\hat{s}(t)$  represents the ICs' source activity, and  $\mathbf{W}$  is the unmixing matrix and is given by  $\mathbf{W} = \mathbf{A}^{-1}$ .

$$\hat{s}(t) = \mathbf{W}x(t) \quad (3.2)$$

The matrices  $\mathbf{W}$  and  $\mathbf{A}$  correspond to activation weights and to the activation patterns of the ICs, respectively. The activation patterns can be interpreted as the scalp projections of the activation weights.

Some ICs may be related to artifacts such as eye movements, muscle activity or noise components (see Figure 3.4). These can be identified and removed from the data, to reduce the influence of eye and muscle activity in the data, without removing more epochs.

We computed ICA on the EEG and EOG data using the Infomax algorithm [97]. To identify and reject artefactual components, we used the MARA algorithm [98]. This automatic algorithm calculates several features for each component, and estimates the statistical chance that they come from artefactual sources. MARA was successful in removing most of the artefactual components.

For some subjects, MARA did not remove all eye and muscle related ICs. To remove those, we first searched for the spatial source of each remaining component by fitting a dipole to each. The ICs whose



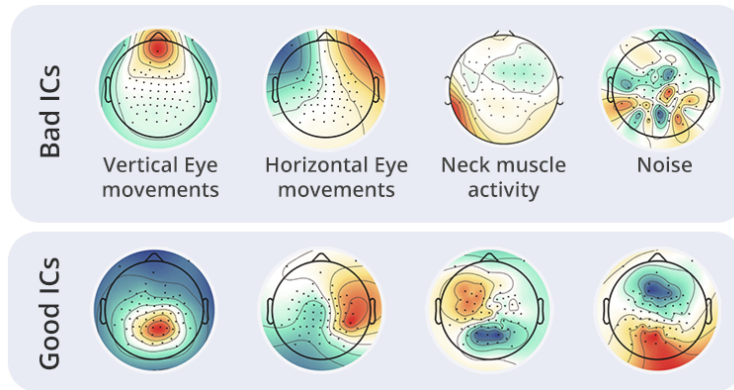


FIGURE 3.4: Activation patterns examples of artefactual ICs that were removed (top) and good ICs (bottom).

source was placed below the thalamus or very frontal (see Figure 3.5b) were considered muscle and eye activity (respectively) and were removed. Dipoles were fit to the components using DIPFIT, a plug-in from EEGLAB that uses Fieldtrip's functions [99]. The function fits a dipole on the head model whose location and direction better describe the scalp's potential distribution or, in the components' case, its activation patterns. The head model used was a Boundary Element Method (BEM) model based on the Colin27 brain template (an average of 27 MRI scans from one individual).

The electrode position acquisition was done manually using Zebris system. This system recorded the 3D coordinates of each electrode. The electrode positions acquired were then adjusted and projected into the head model using the command *MRI Registration* from Brainstorm (version from January 2017) [100]. The new electrode positions were then re-uploaded to EEGLAB (Figure 3.5a).

After removing the artefactual components with MARA and with dipole location, we visually inspected and removed any other artefactual components. A summary of the data processing pipeline is displayed in Figure 3.6 - A.

## 3.3 Data Analysis

The analysis methods were divided into time domain and frequency domain analysis.

### 3.3.1 Time domain analysis

The cleaned data were averaged over cycles, resulting in a 2-second segment of the average EEG during a cycle for each subject. EEG data is very prone to noise from the exterior or from internal processes of the brain that are not of interest for our analysis. Averaging removes the influence of one-time-effects and enhances the potentials that are present in the cycle data.

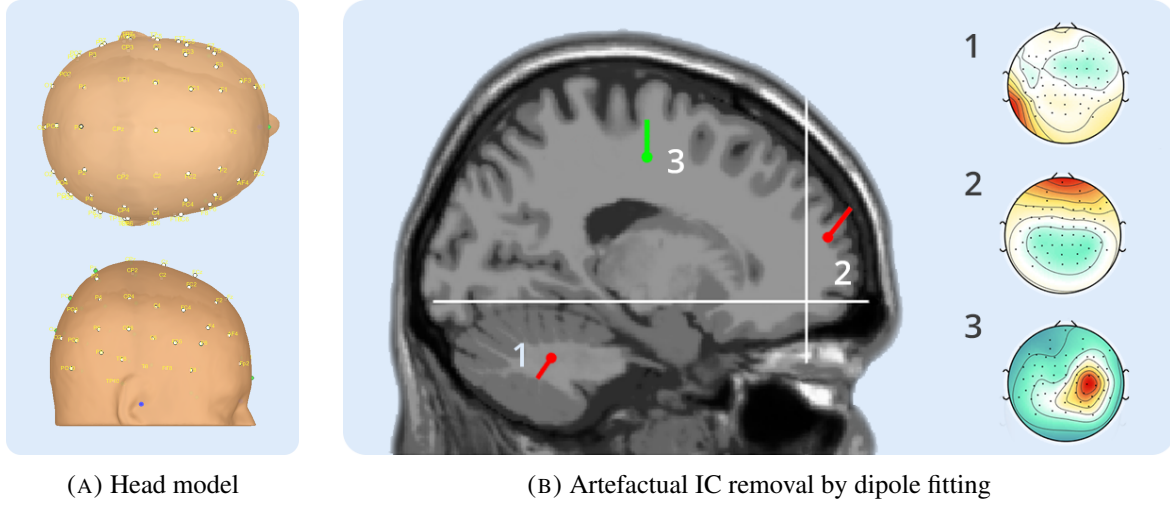


FIGURE 3.5: Dipole fitting: (A) the head model used (collin27) with the projected electrodes; (B) an example of two ICs with artefactual sources (1 from muscles and 2 from eye movements) rejected by spatial filtering the dipole sources. Dipole/IC 3 is an example of a good source. Both figures refer to subject 1.

To search for how the scalp potentials changed during the average cycle of each subject, we down-sampled the data into 50 Hz and fit a dipole per time-stamp (for a total of 100 dipoles over the 2-second data segments). This dipole fitting did not aim to find activity sources in the brain, but rather to see how the scalp projections "rotated" with the arm rotation.

We imported the subjects' data into Brainstorm and created a 3-concentric-sphere head model (Figure 3.7), and computed the noise co-variance matrix using the data from the Rest trials. The same head model was used for all subjects. We fit one dipole per time stamp of the average cycles, creating for each subject a sequence of 100 dipoles. Brainstorm also uses Fieldtrip's dipole fitting functions. In this case we searched for a *regional* dipole - a dipole whose origin remained fixed but direction changed during time, as opposing to a *moving* dipole whose origin also changes. This method was faster, easier to observe how the dipole's direction changes and the origins of the dipoles were not our focus but rather their direction. This algorithm finds the best origin for the whole time scale, and then fits the direction of the dipoles on each time stamp.

### 3.3.2 Frequency domain analysis

To explore the data in the frequency domain we either used 1) the non-warped data (before epoching and artifact rejection), or 2) band-pass filtered the data into frequencies of interest before time warping (see Figure 3.6 - B).

As stated in section 1.1, when a person moves, there is a power decrease in the  $\mu$  (8-13 Hz) and  $\beta$  (13-30 Hz) bands on the motor cortex. We used the Welch method to compute the power spectra of both

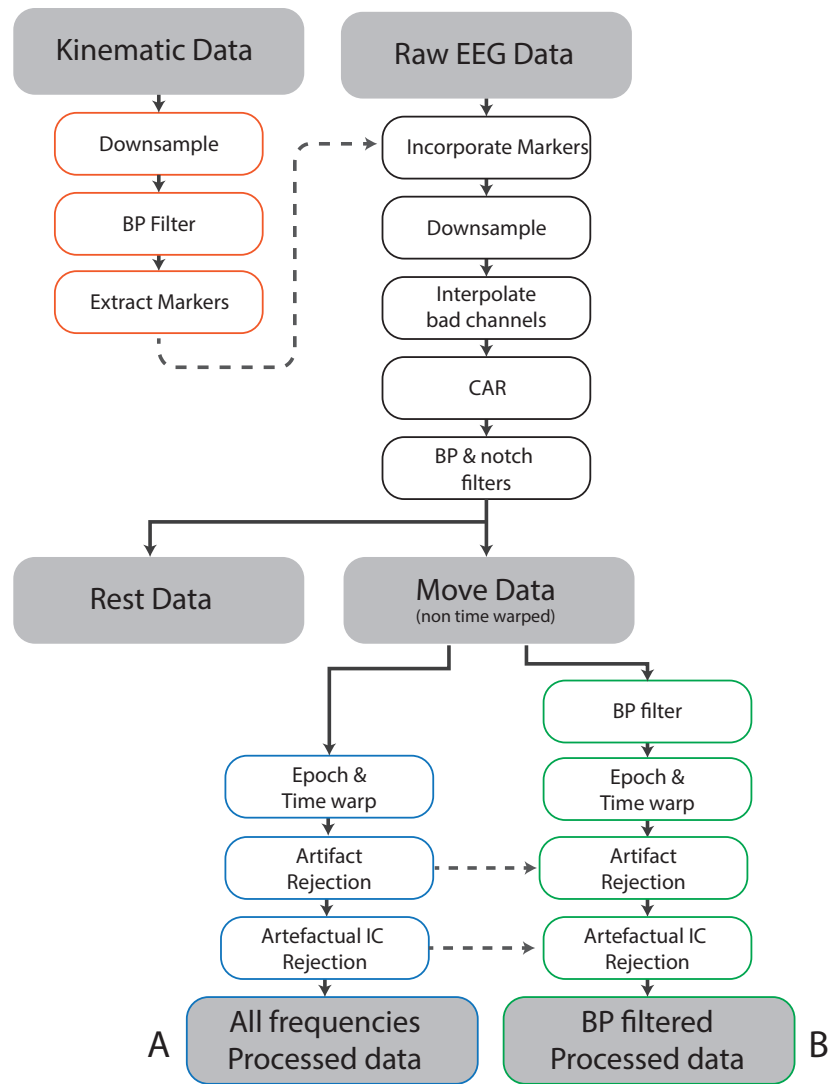


FIGURE 3.6: Overview of the pipeline used to process the data. The raw kinematic and EEG data is processed into Rest and Move data, and the Move data is further processed into A) all frequencies data and B) BP filtered data.

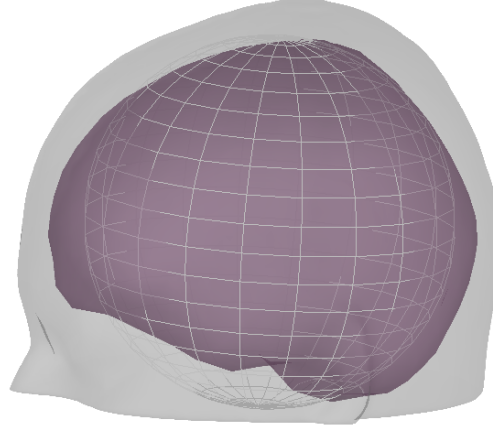


FIGURE 3.7: Three-sphere head model created in Brainstorm for dipole fitting.

Move and Rest (non-warped) data. We then computed the difference between Rest and Move to check for amplitude changes.

Band-pass filtering the data before time-warping allowed us to explore certain frequency bands while still time-warping the data. The filtered data (B) were epoched and time-warped the same way as the unfiltered data (A). The ICA unmixing matrices from data A were copied to data B, and the new source activity was calculated (see equation 3.2). The same epochs and ICs rejected in A were rejected in B, thus enabling a direct comparison between the filtered and unfiltered data. The data were filtered in the following frequency bands: 4-10 Hz, 10-13 Hz, 13-20 Hz, 20-24 Hz and 24-30 Hz. We chose the bands 10-13 Hz ( $\mu$ ) and 20-24 Hz (mid- $\beta$ ) because there is a considerable decrease of power amplitude in the motor cortex in these frequency bands in specific. The others were the most adjacent to these two. To explore the data in these frequency bands and search for power modulations that might correlate with the kinematic data, we used SPoC, an algorithm described below.

### SPoC algorithm

SPoC (or Source Power Comodulation) is an algorithm created by Dähne *et al.* [101] that finds source components whose power correlates with a target variable. The algorithm maximizes function 3.3, where  $z(e)$  is the target variable and  $\tilde{z}(e)$  is the power of the estimated component's activity (given by  $\mathbf{W}^T x(t)$ , where  $\mathbf{W}$  is the unmixing matrix and  $x(t)$  the original data, much like described in equation 3.2) for one epoch  $e$ . The data  $x(t)$  need to be separated into epochs and  $z(e)$  needs to be a scalar per epoch.

$$f_{r2} = \text{Corr}[\tilde{z}(e), z(e)]^2 \quad (3.3)$$

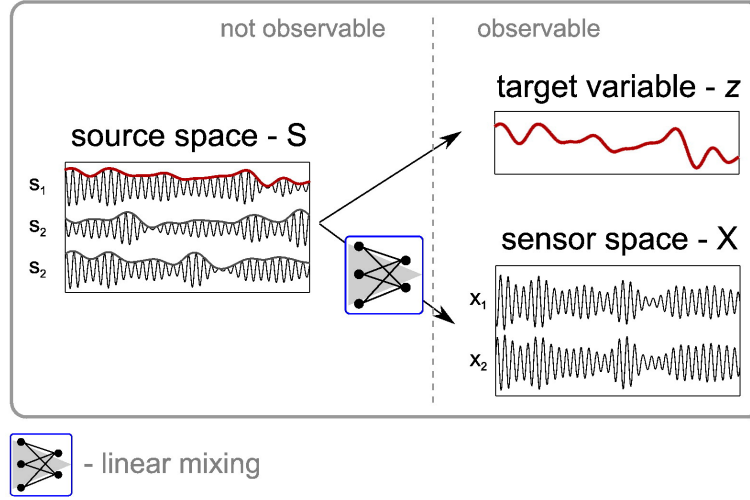


FIGURE 3.8: SPoC algorithm. SPoC takes the observable space (an original signal  $X$ , and a target variable  $z$ ) and tries to find a source  $S$  whose power modulates with the target.

SPoC assumes the original data  $x(t)$  have been band-pass filtered in a frequency band of interest, so that the power of the projected signal can be approximated by its variance within the interval - equation 3.4).

$$\tilde{z}(e) = Var[\mathbf{W}^T x(t)](e) \quad (3.4)$$

Overall, SPoC uses as input the original epoched EEG data  $x(t)$  and a target variable  $z(e)$  (observable data), and gives as output an unmixing matrix  $\mathbf{W}$  and its source activity  $\mathbf{W}x(t)$  that maximizes equation 3.3 (not observable data) - Figure 3.8.

According to literature, the frequency bands most related to movement parameters are high- $\gamma$  (50-90 Hz), but studies have also found modulations in  $\mu$  (8-13 Hz) and  $\beta$  (13-30 Hz). As mentioned in section 3.3.2, we band-pass filtered the data in the following frequency bands: 10-13 Hz, 13-20 Hz, 20-24 Hz, 24-30 Hz. The band-pass filtered processed data (B in Figure 3.6) of the mentioned frequency bands, were used as input  $x(t)$  of SPoC algorithm. As target variable  $z(e)$  we used the kinematic data, so we could find components whose power activity correlated with the circular movement.

The algorithm uses as target a scalar per epoch. Since we wanted to look for changes during the cycle, we re-epoched the data into quarters, and used a target scalar per quarter. Lets assume each quarter (Q1 to Q4) has an average movement direction vector (D1 to D4 in Figure 3.9). As target values we used the equivalent of the inner product of vector D1 with vectors D1 to D4, which results in the sequence 1, 0, -1 and 0. This could be described "how much the arm is going in that direction (D1) during each quarter (Q1 to Q4)".

We created other sets of target variables for D2, D3 and D4 (Figure 3.9 - right). Because SPoC maximizes the squared correlation, directions 3 and 4 are not relevant since they result in the same

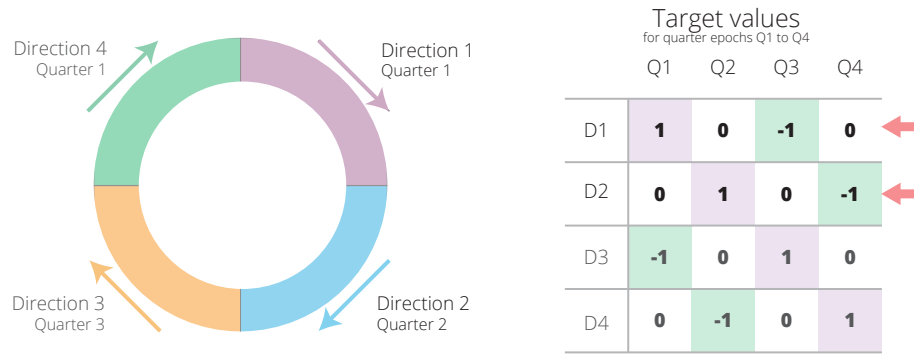


FIGURE 3.9: SPoC target values: on the left a representation of the quarter-divided arm cycle with four vectors (D1 to D4) representing the average direction of the arm during each quarter. On the right, the four possible sets of SPoC target variables used for quarter epochs Q1, Q2, Q3 and Q4, out of which only the first two (for D1 and D2) were used.

components as 1 and 2 (respectively), so in the end only the sequences for direction D1 and D2 were used. SPoC was computed twice for each subject and each frequency band: one time to search for the component whose power correlated with target from D1 (Q1=1, Q2=0, Q3=-1, Q4=0) and another to search for correlation with target from D2 (Q1=0, Q2=1, Q3=0, Q4=-1).

With SPoC we can compute as many components per target variable as we want. We chose one, to get the one most correlated with the kinematic data.

## 4 Results

### 4.1 Behavioral analysis

Displayed in Table 4.1 is the summary information of the data for each subject. It displays how much data was removed and how much remained per subject.

TABLE 4.1: Summary information of the processed data. The columns of the first three subjects are highlighted to remind the reader that they had different acquisition conditions.

	Subject 1	Subject 2	Subject 3	Subject 4	Subject 5	Subject 6	Subject 7	Subject 8	Subject 9	Subject 10	Subject 11	Subject 12	Average
<b>Move trials recorded</b>	54	58	61	56	56	56	68	67	67	67	67	67	62
<b>Rest trials recorded</b>	14	12	15	14	14	14	16	17	17	17	17	17	15
<b>Cycles recorded</b>	447	461	548	467	502	476	467	411	487	571	370	487	471
<b>Percentage cycles removed</b>	26%	21%	55%	31%	42%	30%	30%	40%	64%	27%	62%	25%	38%
<b>Remaining cycles</b>	330	365	245	320	292	329	326	247	173	415	148	366	296
<b>ICs retained</b>	30	22	25	29	16	18	18	25	23	15	23	34	25
<b>Channels Interpolated</b>	T7, T8, Fp1, PO9, PO10	-	PO9, TP9, T7, T8	TP10, TP8, C6	F8	T7, T8	T7, T8, TP9 TP10, PO10	T7, TP9, F7	T7, T8, TP7	T7, T8, FT7, FT8 TP9, TP7, F7Fp2, Fp1, F8	T8, TP8, PO9, F6, O2	T7, T8, FT7, FT8, TP8, TP7, TP10, F6, F5, F7, Fp2, PO9	-

The first three subjects are highlighted because they had different acquisition conditions (see section 2.2.3).

The reason for the different amount of trials recorded for each subject is addressed in section 2.2.3. Subjects 9 and 11 had the most amount of cycle data rejected (above 60%). This was mainly due to the Kinect Sensor not acquiring the hand position properly (see section 2.2.3). Subjects 6 and 12 showed

abnormal artefactual signals in the frontal channels during acquisition (see section 2.2.3). This caused a big amount of channels to be interpolated in subject 12's data. For subject 6 these artifacts were not as frequent and we managed to remove the artefactual trials instead of interpolating the channels. The channels interpolated were peripheral, except for channel C6 in subject 4 and channels F5 and F6 for subject 12.

On average 38% of the data was rejected, leaving us with an average of 296 cycles per subject (or approximately 10 minutes of movement data per subject).

In Figure 4.1 we can observe and compare each subject's X and Y coordinates during the hand cycles, and in Figure 4.2 the time-warping ratios for each quarter group, *i.e.*, how much we had to warp the quarter's data to fit 0.5 seconds, according to the equation 4.1.

$$Warp\ ratio = \frac{\Delta_{expected}}{\Delta_{true}} \quad (4.1)$$

In Figure 4.1 we can notice how subjects 1, 3, 6, 10, 11 and 12 performed the movement slightly broader than the other six subjects. The Figure depicts the horizontal (X) and vertical (Y) coordinates but not depth (Z). Subject 3 performed the movement slightly in depth, while the rest of the subjects performed the movement closer to the XY plane.

In Figure 4.2 we see that for most subjects, the hand velocity during quarters Q1 and Q3 (blue and yellow in the figure) differs from the velocity of quarters Q2 and Q4 (orange and purple). For subjects 5, 6, 7 and 12 quarters Q2 and Q4 take longer on average, while for the rest of the subjects the opposite occurs.

Figure 4.3 displays the right-elbow X and Y positions during the cycles. We can observe how the subjects performed the movement by analyzing the elbow positions during the task. Broader elbow positions means that the arm movement was performed with rotation of the shoulder joint. This is the case for subjects 1, 3, 6, 9, 10 and 12 who have broader elbow positions. Subject's 1 elbow positions are very scattered meaning his movement was not constant.

## 4.2 Time domain

In Figure 4.4, we can observe how the average scalp distribution changed over time for the 12 subjects during their average cycle. The scalp plots were taken at eight equally distant time windows (separated by 250 ms).

All subjects show a rotational-like pattern. The scalp distributions at opposite points of the cycle (1 second later) have approximately opposite potentials, with very few exceptions (e.g. subject 8 at time instants 875 and 1875 ms).



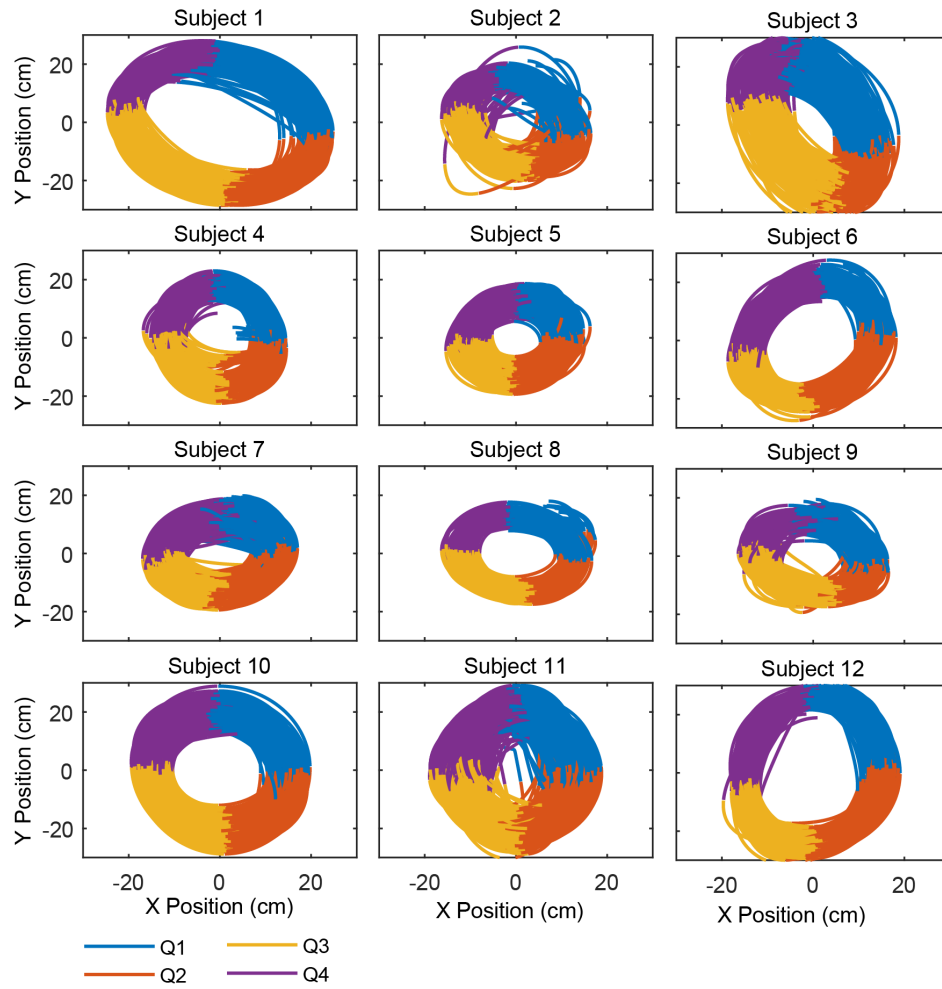


FIGURE 4.1: Subjects' right-hand X and Y coordinates (in cm) during cycles, divided into quarter sections according to the maximums and minimums in these coordinates.

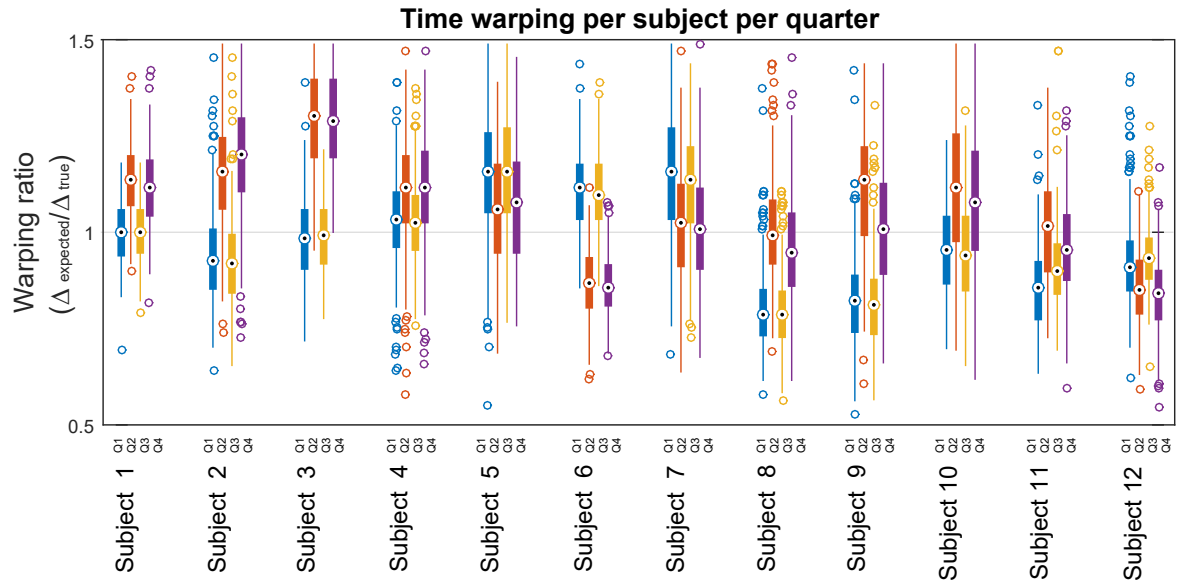


FIGURE 4.2: Boxplots of the level of time warping the quarters suffered per subject (after data processing).

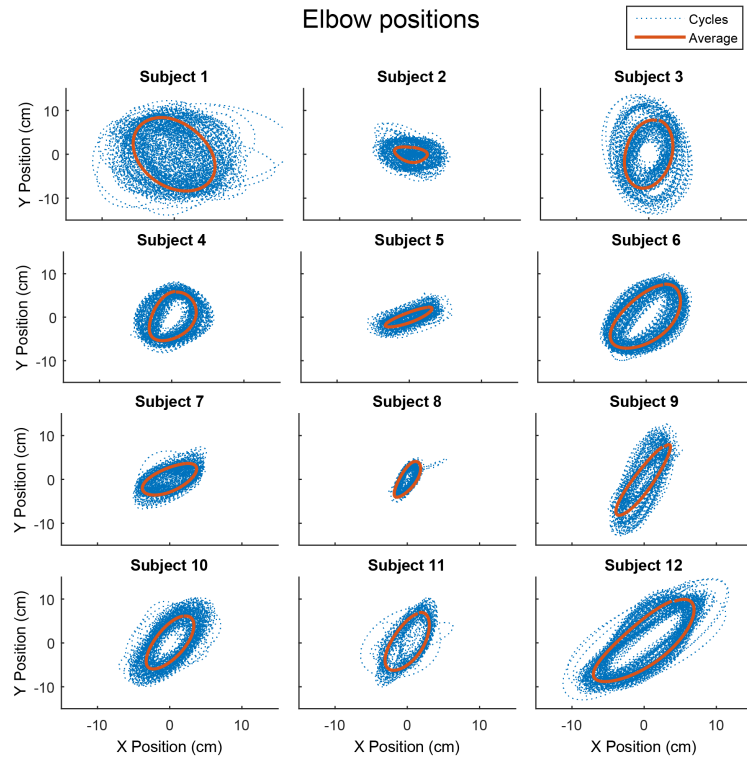


FIGURE 4.3: Subjects' right-elbow X and Y coordinates (in cm) during cycles (dotted blue line) and averaged-cycles (orange thick line).

The rotation patterns vary among subjects. Some subjects show very similar potential changes over cycle, but with delay among each other. This is the case for subjects 4 and 6 whose scalp potentials would look very similar if we delay subject 4's potentials for 250 ms.

An average of all subjects is displayed in Figure 4.5. In this figure we can still see the mentioned rotational pattern. Figure 4.5a displays the scalp distribution in time windows 250 ms apart (much like in Figure 4.4). Figure 4.5b displays the same information in a more continuous format. The channel order is in Figure 4.5c. In this figure we see how the average cycle potentials changes smoothly in all channels and how the end of the average cycle is continuous with its beginning.

### 4.2.1 Rotating dipoles

Scalp maps are not the best way of observing rotation. We questioned whether these patterns could be described by a rotating dipole (as mentioned in section 3.3.1).

Figure 4.6 depicts the dipole projections of the all-subject grand averaged data used in Figure 4.5. On the left we see the results using one single moving dipole (position of the dipole changes over time) and on the right one single regional dipole (fixed position, only direction changes). The color encodes time from blue (beginning of the cycle) until red (end of the cycle). The origin of the dipoles is not considered the source of activity but rather the average source of all brain activity and is, therefore, not our main focus.

We can see how the regional dipole satisfactorily projects the direction of the moving dipole, while keeping the figure neater. Since the origin of the dipole is not our main focus, we used regional dipoles to describe the rotational patterns in the scalp throughout the project.

Still in Figure 4.6, we see how the dipole direction changes uniformly from the beginning to the end of the cycle. If we consider the right-hand grip rule, the dipole rotation can be described by a rotation vector pointing to the front left bottom of the brain.

Single subject results can be found in Figures 4.7 and 4.8. The centers of each subjects' dipoles are pictured in Figure 4.9. The origins of the single subjects' dipoles are all placed in the center of the brain, as expected.

The average-cycle dipoles of subjects 3, 4, 5, 6 and 9 rotate the most uniformly. The other subjects' dipoles either overlap or have a gap at some point of the cycle. Either way, all subjects' dipoles rotate over time. Again using the right-hand grip rule, we see most subjects' dipole rotation vectors point to the front-left part of the brain, the same as their grand-average. The exceptions are the dipoles from subjects 1, 7 and 10 whose rotation vector would point to the front-right and subjects 3 and 8 whose rotation vector would point to the back of the brain, meaning the dipole rotates in the opposite direction.

Regarding the timing of the rotation we can observe that the rotation starts at different directions for each subject. Most of the subjects (1, 2, 4, 5, 7, 9, 11 and 12) have the dipole's first direction pointing

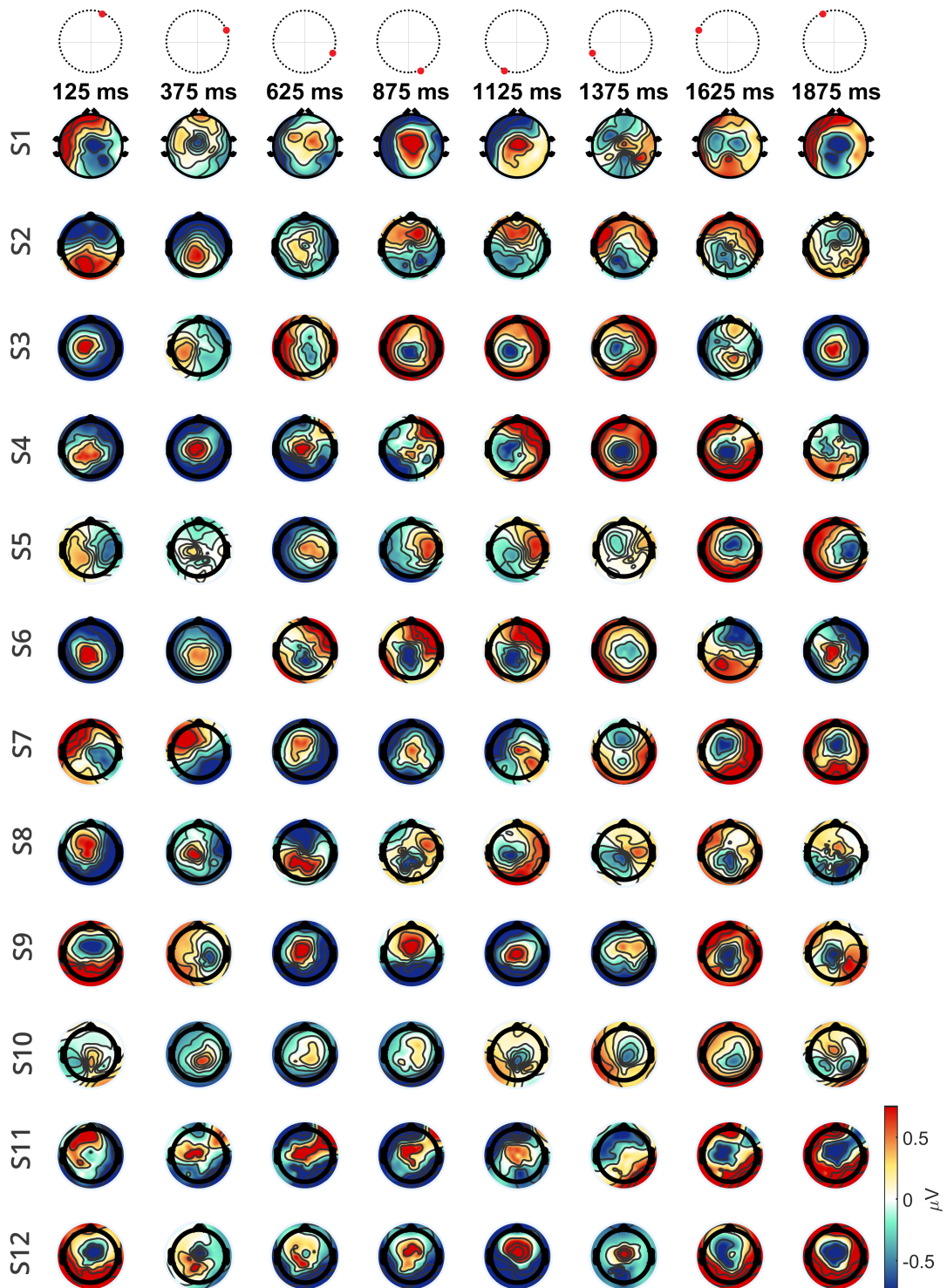
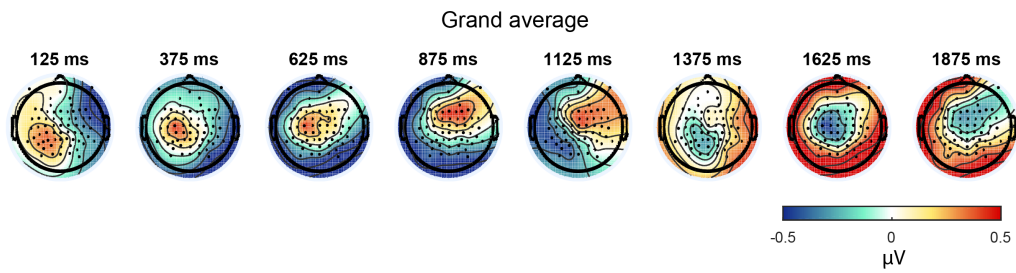
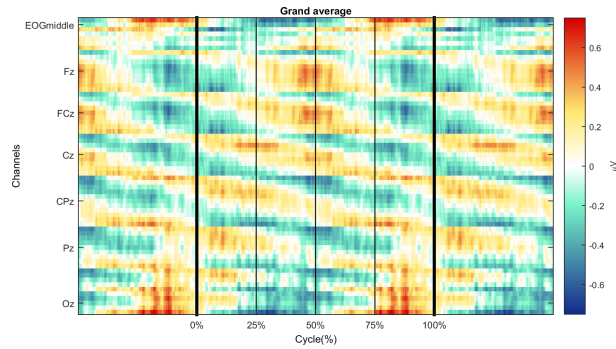


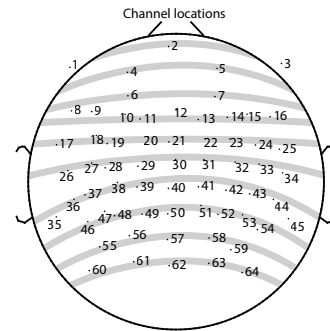
FIGURE 4.4: Single subject potential distribution in 8 time instants of the averaged arm cycle data, separated by 250 ms.



(A) Scalp projections



(B) Channels vs. time graph



(C) Channel order

FIGURE 4.5: Grand average of all subjects' potential distribution during arm cycles. In (A) the scalp projections in the same time instants as in Figure 4.4, in (B) a continuous graph of channels' potential change before, during and after each average cycle, in (C) the channel order to more easily interpret (B) - the channels are ordered from left to right and from front to back.

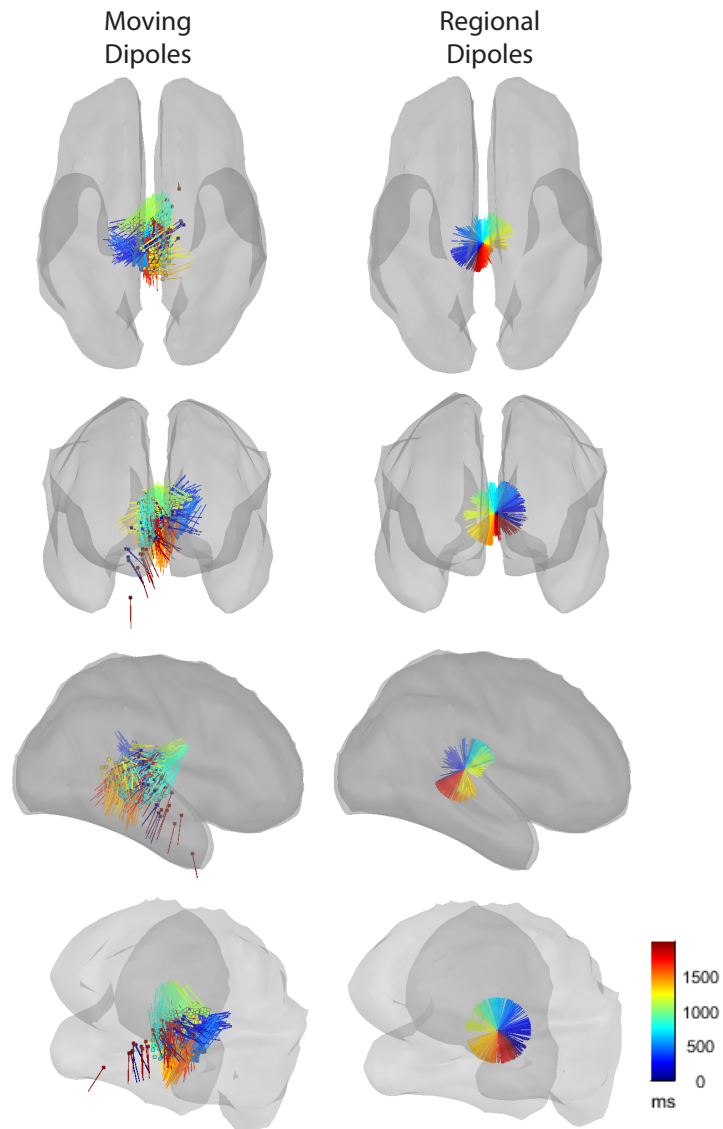


FIGURE 4.6: Dipole of the grand-average cycles from all subjects. On the left we used a moving dipole method, on the right a regional dipole. Color encodes time from the beginning (blue) to the end (red) of the cycle.

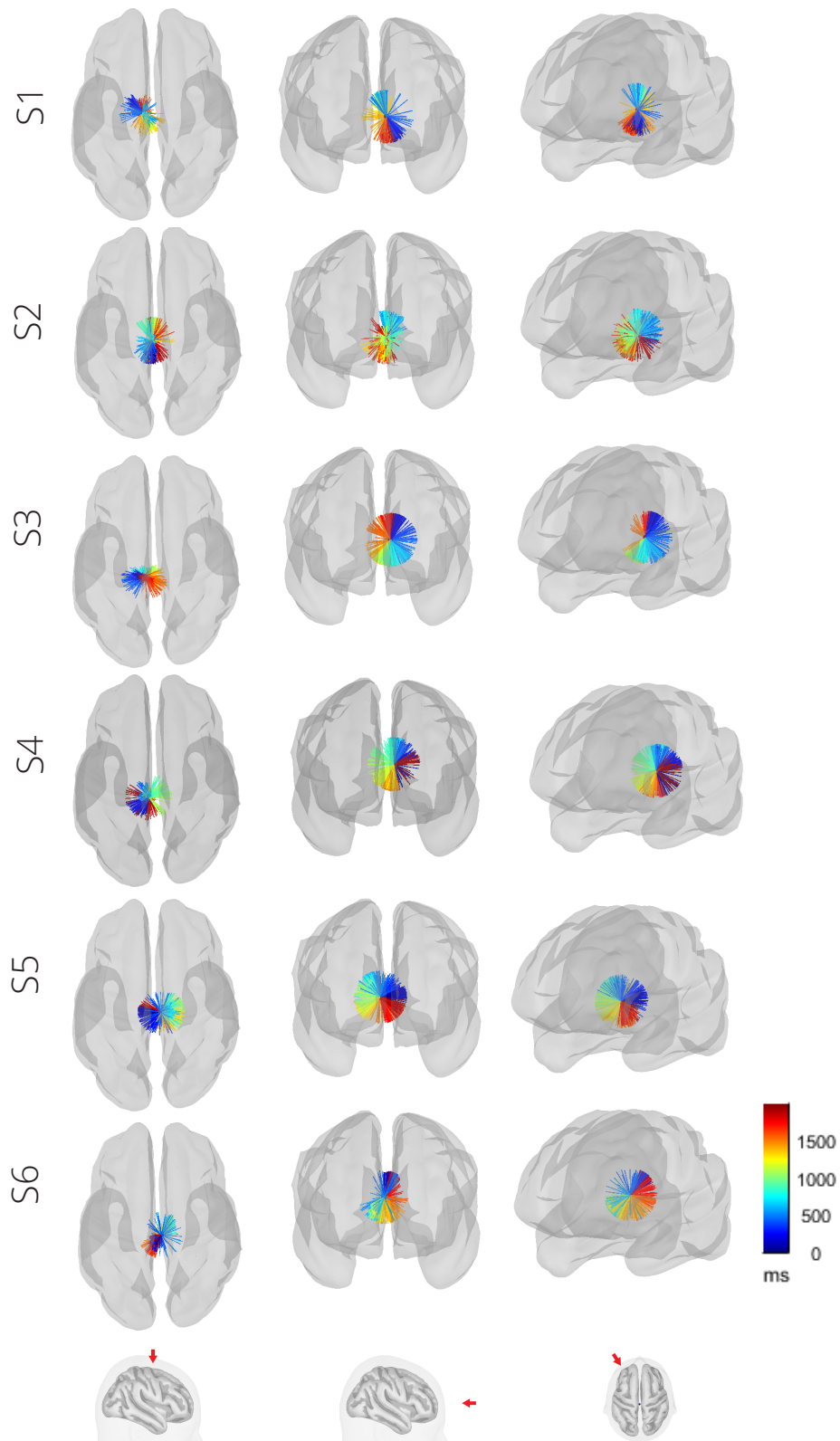


FIGURE 4.7: Single subject dipoles of the average cycles viewed from the top, front and front-right - subjects 1 to 6.



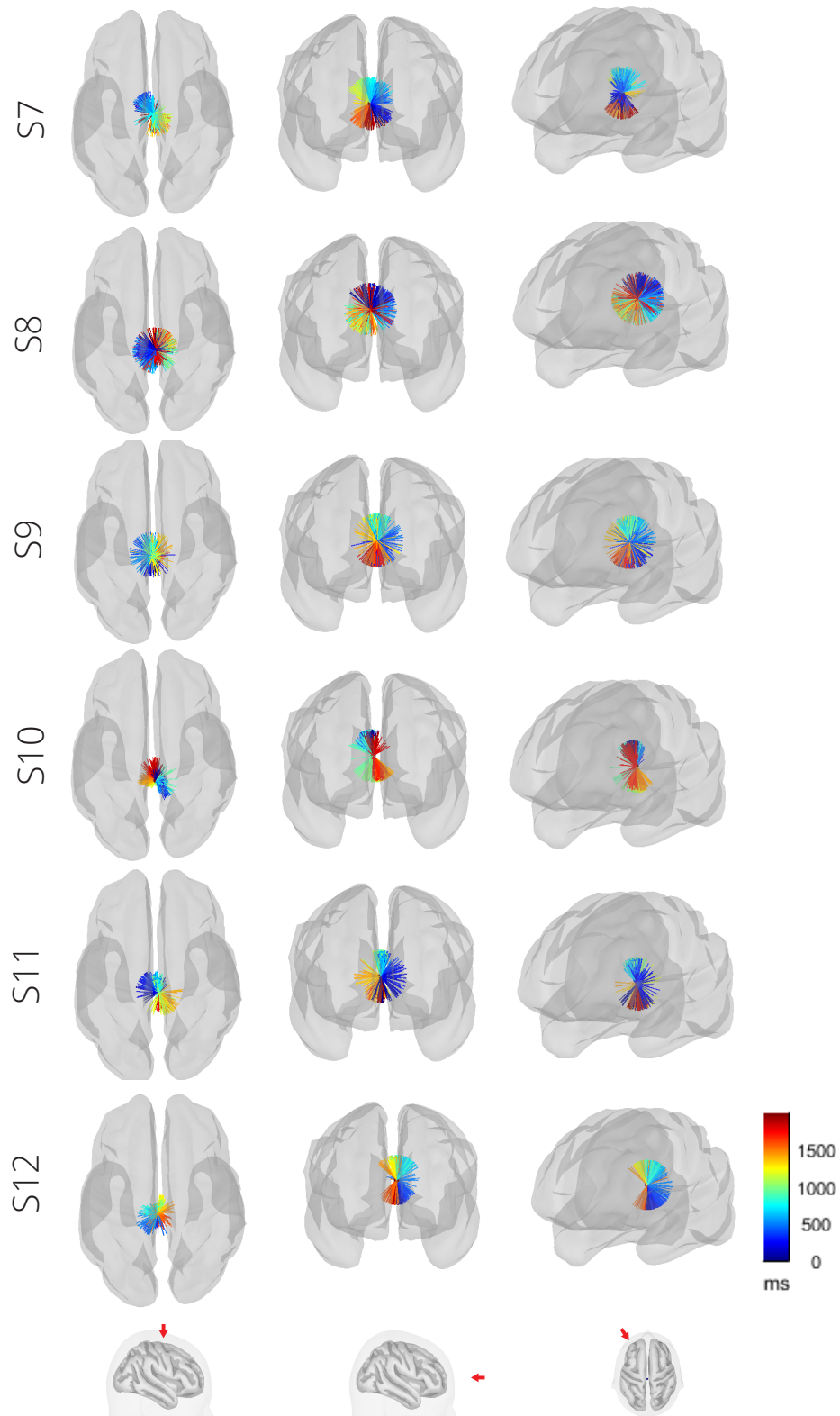


FIGURE 4.8: Single subject dipoles of the average cycles viewed from the top, front and front-left - subjects 7 to 12.



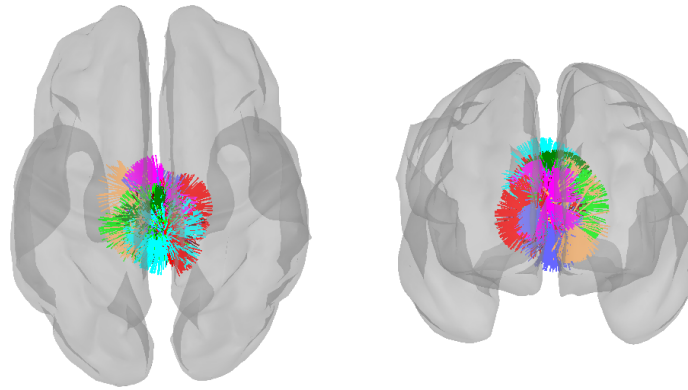


FIGURE 4.9: Centers of the brain estimated dipoles during arm cycles. Each color encodes one subject. All centers are placed in the center region of the brain.

down-left, while subjects 6 and 10 start up-left. Subjects 3 and 8 have the opposite rotation, starting at direction up.

We took the cycle data from subject 1, and shuffled the quarters within the cycles. In Figure 4.10 we can compare the average cycle dipoles with an averaged cycle with shuffled quarters dipoles and the average rest data (epoched in 2-second periods). Only the true average cycle creates a uniform and coherent rotating dipole. Both Rest and shuffled-quarter data created disperse dipoles with an apparent random order as expected.

## 4.3 Frequency domain

We computed the frequency spectra for each subject for both Move and Rest trial conditions. In Figure 4.11a we see the all-subject grand average power difference between move and rest condition for several frequency bands (0.25-4, 4-10, 10-13, 13-20, 20-24, 24-30, 30-45, 45-60, 60-80 Hz). This same information can be seen in Figure 4.11b in a more continuous format. The vertical axis of Figure 4.11b follows the same order as in Figure 4.5c.

Between 4 and 30 Hz there is a power decrease in the left motor area during the movement task, when comparing to the Rest trials. This difference is more pronounced in the 10-13 Hz ( $\mu$ ) and 20-24 Hz (mid- $\beta$ ) frequency bands. This is to be expected as stated in section 1.3.1. We can also see an increase of power in the right peripheral head area, maybe due to muscle activity of the neck while the shoulder moved (muscle activity has a frequency of 20-300 Hz, but posterior head muscles' activity is usually around 100 Hz [102]).

Results of frequency changes for single subject can be seen in section B, Figure B.1. Subjects 3 and 8 had a large power increase in the  $\gamma$  activity (frequencies  $>30$  Hz) when they moved when comparing to the rest state. This power increase was largest at peripheral channels, which indicates they were due to

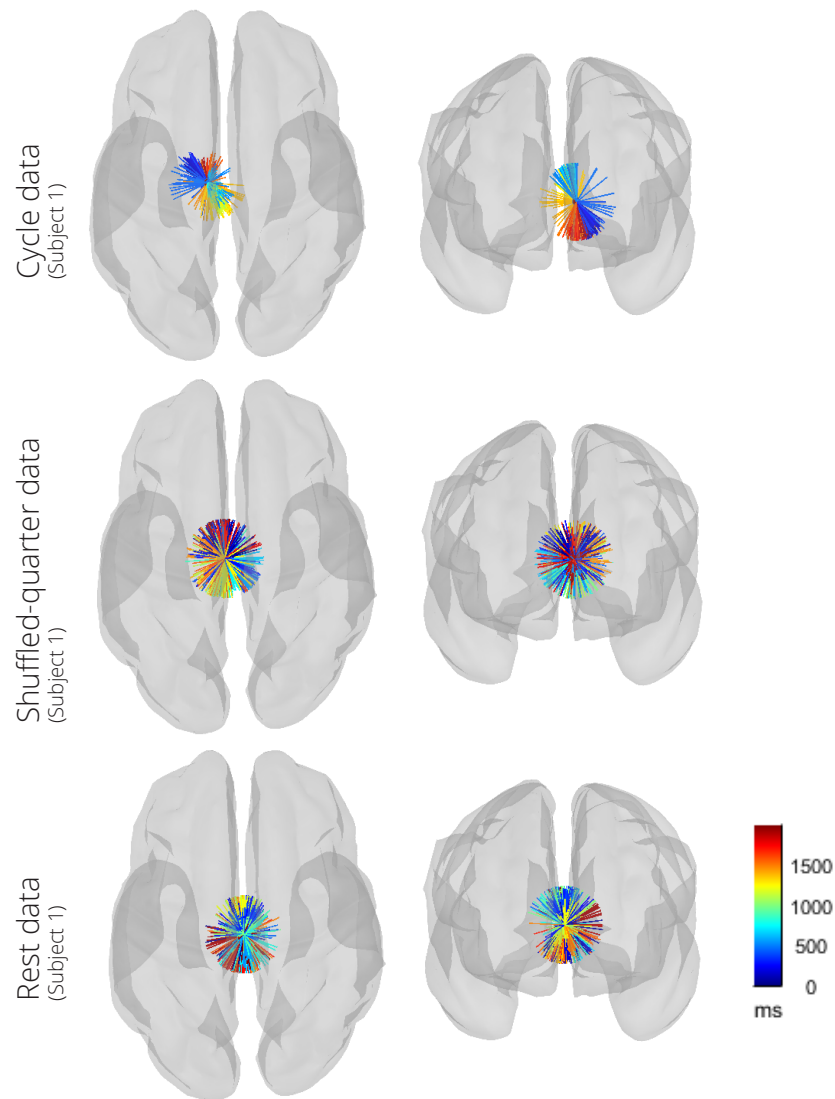
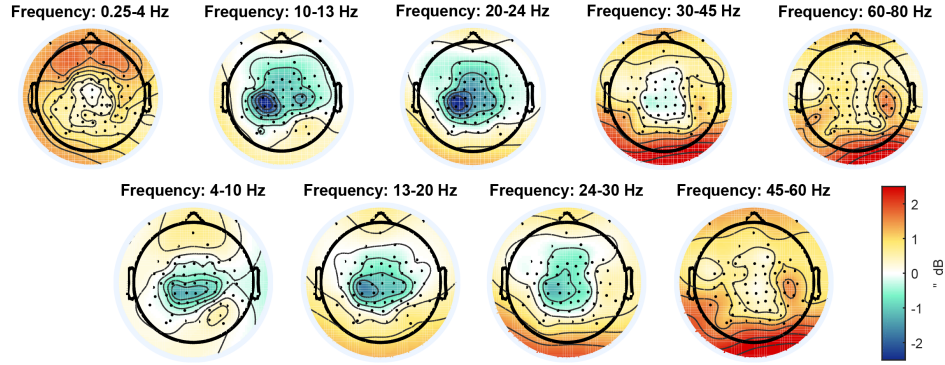
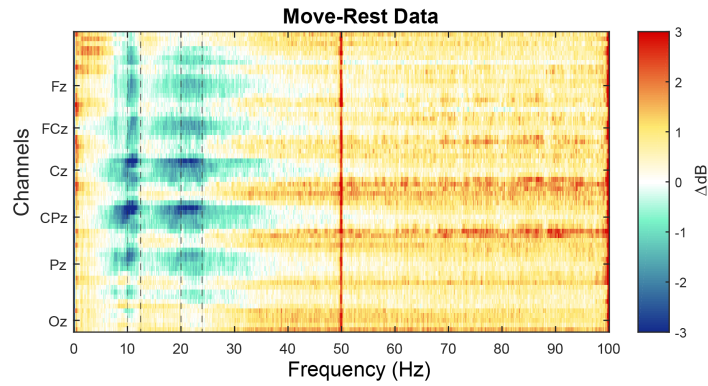


FIGURE 4.10: Estimated dipole over time from the average cycle data (top), of the average cycle data with shuffled quarters (mid) and from the average 2-second epoched rest data (bottom) from data of subject 1. The change in color encodes the change in time from the start of a cycle (dark blue) to the end of the cycle (red).

### 4.3. Frequency domain



(A) Scalp projections



(B) Graph

FIGURE 4.11: Difference between Move and Rest spectra: Grand-average from all subjects. See Figure 4.5c for channel reference.

muscle activity (these frequency plots were computed with the data of the Move and Rest trials before artifact rejection - see Figure 3.6).

#### 4.3.1 SPoC

To further explore the data in the frequency domain we used the SPoC algorithm described before (section 3.3.2).

We computed SPoC for the frequency bands 10-13 Hz ( $\mu$ ), 13-20 Hz (low- $\beta$ ), 20-24 Hz (mid- $\beta$ ) and 24-30 Hz (high- $\beta$ ), which resulted in one component per direction (D1 and D2), per subject and per frequency band. Figure 4.12 shows the results obtained for D1 (above) and D2 (below) in the frequency band 20-24 Hz. The results for other frequency bands are presented in section B, in Figures B.2, B.3 and B.4, for the frequency bands 10-13 Hz, 13-20 Hz, and 24-30 Hz respectively. For each component we display its activation pattern in a scalp plot (top), the instantaneous power of the component's source activity for each cycle (mid), and the average Hilbert power activity for all cycles (blue line) which is suppose to correlate with the target variable (orange line - bottom).

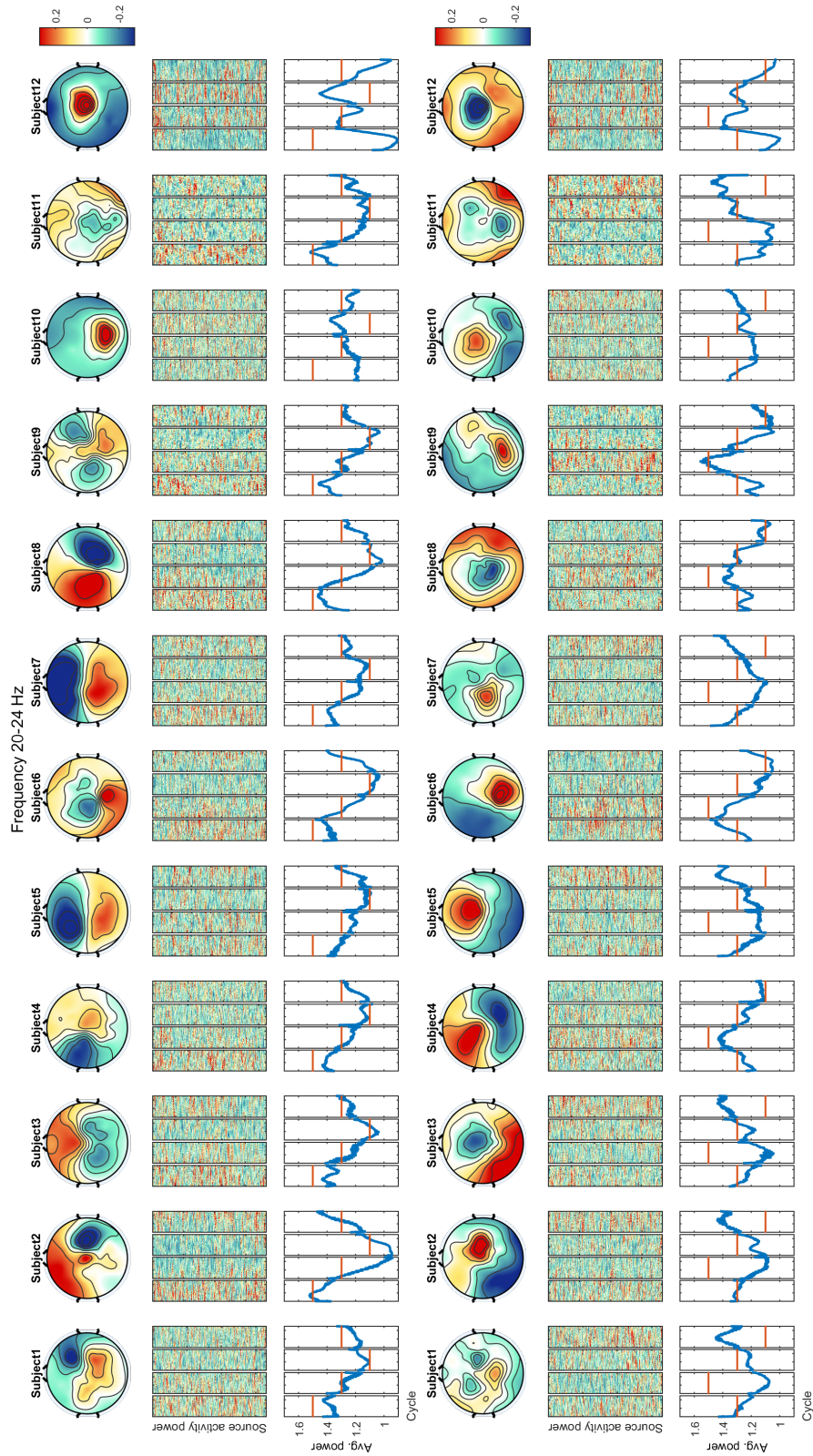


FIGURE 4.12: SPoC algorithm outputs for frequency band 20-24 Hz, for direction D1 (top) and direction D2 (bottom). For each components we display one scalp plot of the components's activity pattern, the Hilbert power of the activity of each cycle, and the average Hilbert power activity for all cycles (blue line) which is suppose to correlate with the target variable (orange line).

### 4.3. Frequency domain

---

Compared with the different frequency bands, we notice how the band 20-24 Hz creates components with smoother power changes and with relevant activation patterns. Frequency band 10-13 Hz creates both very noisy activation patterns and power changes; frequency bands 13-20 Hz and 24-30 Hz create relevant activation patterns, but noisier power changes. In the end we chose to further explore frequency 20-24 Hz.

Regarding the results for the frequency band 20-24 Hz (Figure 4.12), there does not seem to be a straightforward pattern common for all subjects, but most components' source activity power seems to correlate/anti-correlate with the target variables. Regarding D1, we can highlight subjects 10 and 12 whose average activity power has negative correlation with the target, as opposing to the rest of the subjects who have positive correlation. SPoC maximizes squared correlation which means it only takes into consideration the correlation's norm. We can point out the same in D2 results for subjects 1, 2, 3, 5, 7, 10 and 11 (7 out of 12).

We can visually cluster some of the components according to their activity patterns. For D1 we can cluster the components from subjects 1, 5, 6, 7, 9 and 10 whose pattern consists on positive patterns in the back of the scalp and negative in the front. Subjects 3 and 11 have the exact opposite patterns. We should note that subject 10's activity power anti-correlates with the target, unlike the rest of the subject whose correlation is positive. Still in D1, we can cluster the components from subjects 2 and 8 - positivity in the front/left area of the scalp and negativity in the back right area of the scalp.

Regarding the results for D2, we can group subjects 3 and 12 whose component's both show a negativity in the center front of the scalp. Subjects 4, 5 and 10 have the opposite activity patterns from subjects 3 and 12. We can also group subjects 1, 6 and 9 (positivity in the center-back of the scalp), and subject 11 with the opposite patterns (negativity in the center-back of the scalp). All these D2 groups have component's with high positive and high negative correlation among themselves.

By applying the component's unmixing matrices to the non-filtered data, we can check how well the power modulations remain. For that, we subtracted each subject's average Rest data from the data power modulations (calculated by applying the unmixing matrixes to the rest data and averaging all data over time to get a baseline value per channel). Figures 4.13 and 4.14 show the results for direction D1 and D2 respectively. The dark dotted line represents the average power in the 20-24 Hz spectra. We can see the correlations between the modulations and the movement kinematics above the graphs, and later summarized in Table 4.2. The movement kinematics we used for correlation were the inner product between directions D1 and D2 and the average movement direction.

The spectrograms in Figures 4.13 and 4.14 were computed on the non-time-warped data. The spectrograms itself were then time warped and the artefactual epochs that were removed in the processing of the data were removed. Note that the color scales vary from subject to subject.

We can group together some of the subjects frequency spectra. For D1 we can highlight subjects 3, 7 and 9, whose spectra and activation patterns have resemblances. Still in D1, we can see similarities among subjects 1, 2, 4 and 6. In D2 we can create a group with subjects 1, 2, 5 and 7, and another with subjects 4, 8 and 9.

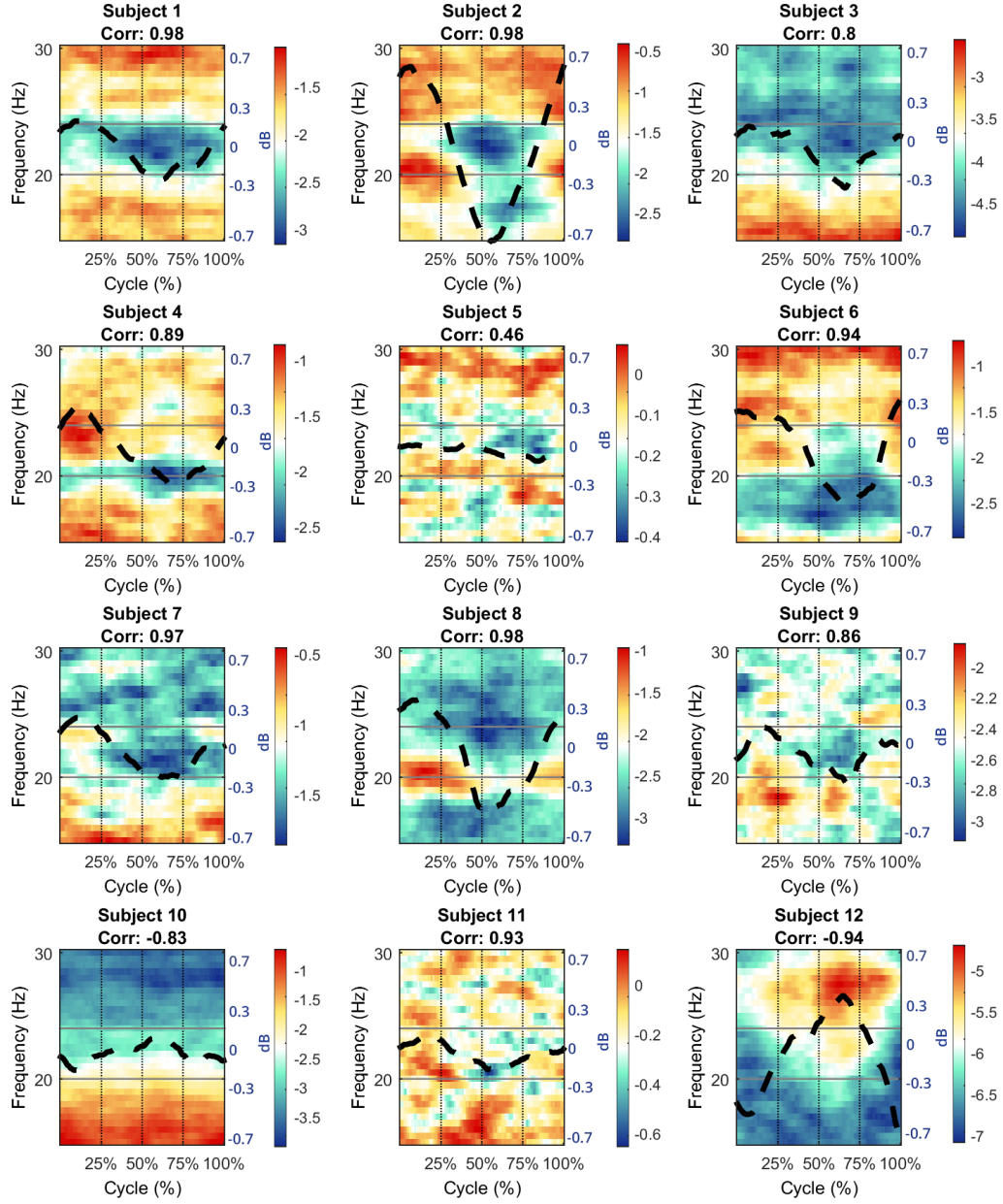


FIGURE 4.13: Frequency modulations of the data with the SPoC components' weights applied - Direction D1. The color scales vary from subject to subject.



### 4.3. Frequency domain

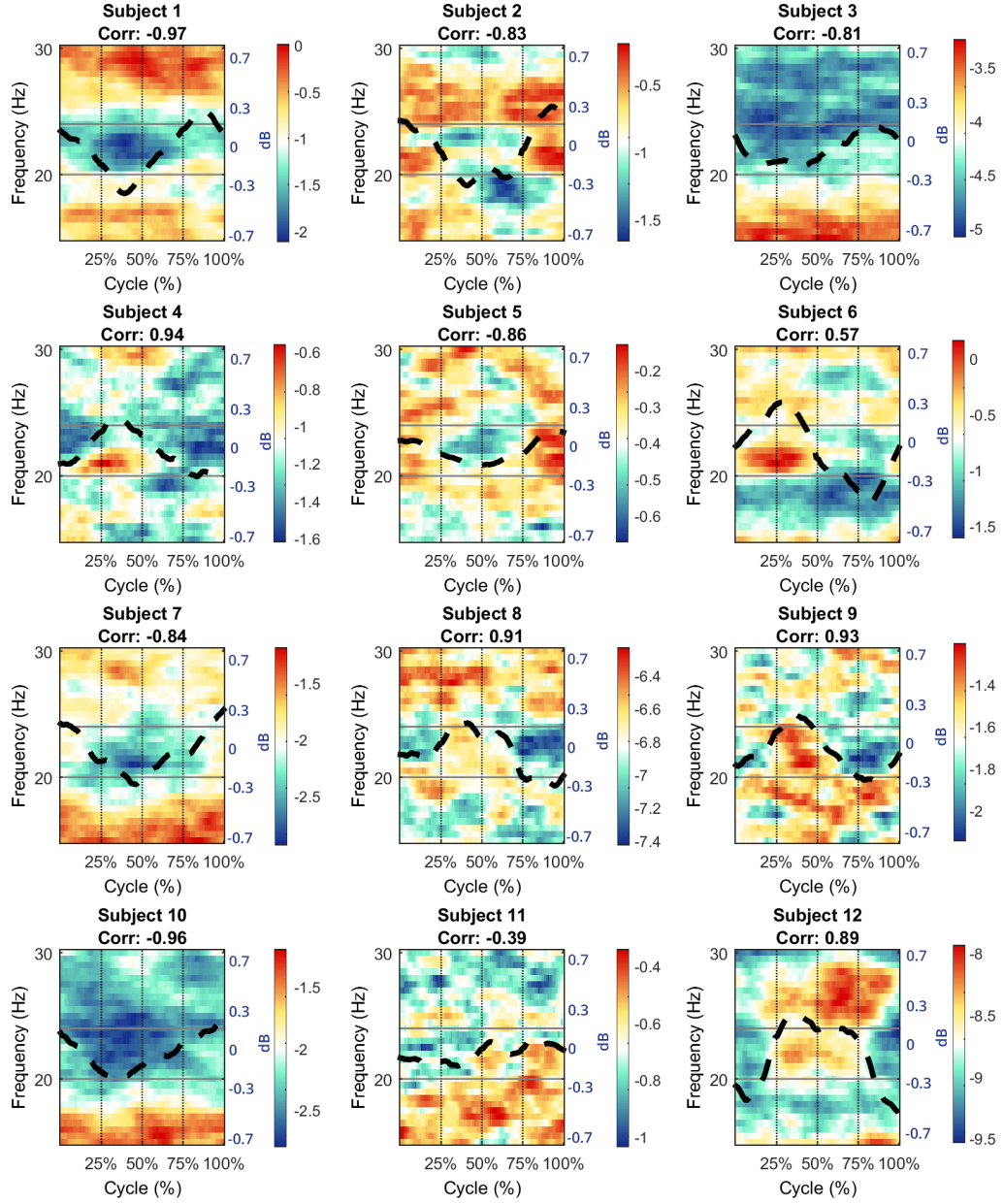


FIGURE 4.14: Frequency modulations of the data with the SPoC components' weights applied - Direction D2. The color scales vary from subject to subject.

TABLE 4.2: Correlations of SPoC's components 20-24 Hz frequency modulations applied to the unfiltered data. In green the values higher than 80% and in blue the values lower than -80%.

	Direction 1	Direction 2	Average $ x $
<b>Subject 1</b>	0.98	-0.97	<b>0.98</b>
<b>Subject 2</b>	0.98	-0.83	<b>0.91</b>
<b>Subject 3</b>	0.8	-0.81	<b>0.8</b>
<b>Subject 4</b>	0.89	0.94	<b>0.92</b>
<b>Subject 5</b>	0.46	-0.86	<b>0.66</b>
<b>Subject 6</b>	0.94	0.57	<b>0.76</b>
<b>Subject 7</b>	0.97	-0.84	<b>0.9</b>
<b>Subject 8</b>	0.98	0.91	<b>0.94</b>
<b>Subject 9</b>	0.86	0.93	<b>0.9</b>
<b>Subject 10</b>	-0.83	-0.96	<b>0.9</b>
<b>Subject 11</b>	0.93	-0.39	<b>0.66</b>
<b>Subject 12</b>	-0.94	0.89	<b>0.91</b>
<b>Average <math> x </math></b>	<b>0.88</b>	<b>0.83</b>	<b>0.85</b>

SPoC successfully estimated components whose power correlated with the movement. For direction D1, the components' power modulations from most subjects highly correlate ( $>80\%$ ) with the subject's average movement direction, with exception for subjects 10 and 12 where the correlation is  $<-80\%$  (high anti-correlation) and subject 5 whose correlation was 46%. The results from direction D2 were not as satisfactory. Six out of the 12 subjects had modulations anti-correlating ( $<-80\%$ ) with the movement. Regarding the rest of the subjects, four were highly correlated (subjects 4, 8, 9 and 12).

The average absolute correlation for direction D1 and D2 were of 88% and 83%. Even though some components show negative correlations with the movement, most are still very high in absolute value.



# 5 Discussion

## 5.1 Behavioral analysis

We rejected an average of 38% of the cycle data per subject (Table 4.1). The subjects were not restrained during the experiment and so the data was prone to muscle artifacts. Continuously staring at the screen for long periods of time also made the subjects tired, so eye blinks and saccades had to be removed from the data. The subjects with the most data rejected (over 50%) had either very noisy channels (subject 3, see Figure 4.11b) or bad kinematic data quality (see section 2.2.3).

Regarding quarter speed variability, several subjects struggled with the uniformity of the movement. In Figure 4.2, we can observe that all subjects show a clear difference in quarter speed between groups of opposite quarters of the cycle - Q1 and Q3 vs. Q2 and Q4. Subjects 5, 6, 7 and 12 performed the cycle with quarters Q1 and Q3 faster than the Q2 and Q4, unlike the rest of the subjects who performed quarters Q2 and Q4 faster. Some possible explanations for these constant differences between opposing quarters are the following:

1. When changing the direction in the vertical axis, gravity might influence how we perform the movement;
2. The movements were at times performed in depth. We used PCA to get 2 main coordinates from the trial data when separating the data into quarters. But the plane of rotation is never perfectly constant over one 20-second trial. Therefore, the slight changes of the movement plane might cause the two opposing quarters to be smaller than the other two, and therefore appear faster;

Whether the reason is one or all of the above, we believe time-warping should not negatively affect the data. This method allowed us to average the cycle data which was necessary for all methods we used to explore the data. Although some quarters were time warped  $\pm 50\%$ , the mean of the absolute values of time warping percentage for all subjects was around  $14\% \pm 10\%$ , and we should keep in mind that the performance of a non-guided uniform movement is very difficult for any person.

In Figures 4.1, 4.2 and 4.3 we can observe that each subject performed the movement in his own way with different speed, broadness and different joint rotation. Our goal was to study the direction of the movement, and not other parameters. We could not find a direct link between these other movement spatial parameters and the rest of our results, which would be expected according to Caminiti *et al.* [45]. They state that while performing the movement in different spatial conditions, the projection of the direction of the movement in the brain does not relevantly change.

## 5.2 Time domain analysis

The average activity during arm cycles shows a rotational pattern for all subjects (Figure 4.4). We can state the same from the dipole Figures 4.7 and 4.8. In both we can observe that most subjects display a similar rotation pattern, with a few exceptions. Some exceptions are subjects 3 and 8 whose dipoles rotate in an opposite direction from the others. These were also the subjects whose number of noisy channels was higher (see Figure B.1). The plane of rotation was more or less constant among the remaining subjects, except for subjects 1, 7 and 10 whose plane was slightly different.

The similarities between subjects' dipole rotation look as if each had a different time delay between the arm and the dipole rotation. To illustrate this problem let us delay the cycles of the subjects to align the rotation (see Figure 5.1, which corresponds to the data in Figure 4.4 with added delays on the cycles). The patterns look more similar among subjects with the added delay. A possible reason for this apparent delay might be single subject physiology. The delay would be of around  $\pm 250$  ms, which is a long time interval in the neurons' time scale. Another possible reason is the different ways the subjects performed the movement (different elbow/shoulder rotation, broader movement, faster...). Joint rotation should not influence the results for direction decoding, but it could have influence in the timing of rotation. We also need to take into consideration the possibility that the rotational patterns do not have origin in brain signals but rather neck and shoulder muscles. In this case, the way in which one performed the movement would bring different results. This does not seem to be the case since there is no relation between the kinematics and dipole rotation timing in subject's with similar results. Finally, this could also be explained by the quarter division and time warping. The problems of time warping described in the previous section could induce this apparent single subject delay. The time warping can also explain the non-uniformity of the dipole rotation in some subjects.

The grand-averages of all subjects show very continuous patterns (Figure 4.5) and the dipole we fit to represent the rotation patterns rotates uniformly (Figure 4.6). The dipole does not point in the direction of movement as Georgopoulos' population vector does, but it rotates in a similar plane as the movement and in the same direction (see Figure 5.2). The different phase can simply be explained by a difference in the brain referential space, and also partially due to the reaction time of the subjects (from the thought and planning of the movement until the execution).

Results from Figure 4.10 show that the rotation of the subjects' dipoles are not random, *i.e.*, that the circular patterns are due to the circular task. The source of the patterns and their physiological reason are not entirely known. As far as we know, the source is in the brain and not due to eye or muscle movements, but we should not discard any option. The scalp projections in Figure 4.4 indicate that the patterns are distributed all over the scalp. This can either be due to several areas of the brain working together to create these kind of patterns, or due to one more specific area whose potentials are dispersed over the scalp. Because we could only fit one dipole per time stamp, we could not find the exact explanation for this matter.

Regarding the methods used, the dipole projections were a good representation of how the overall scalp potentials "rotated". One dipole per time stamp is not ideal if we are searching for the source

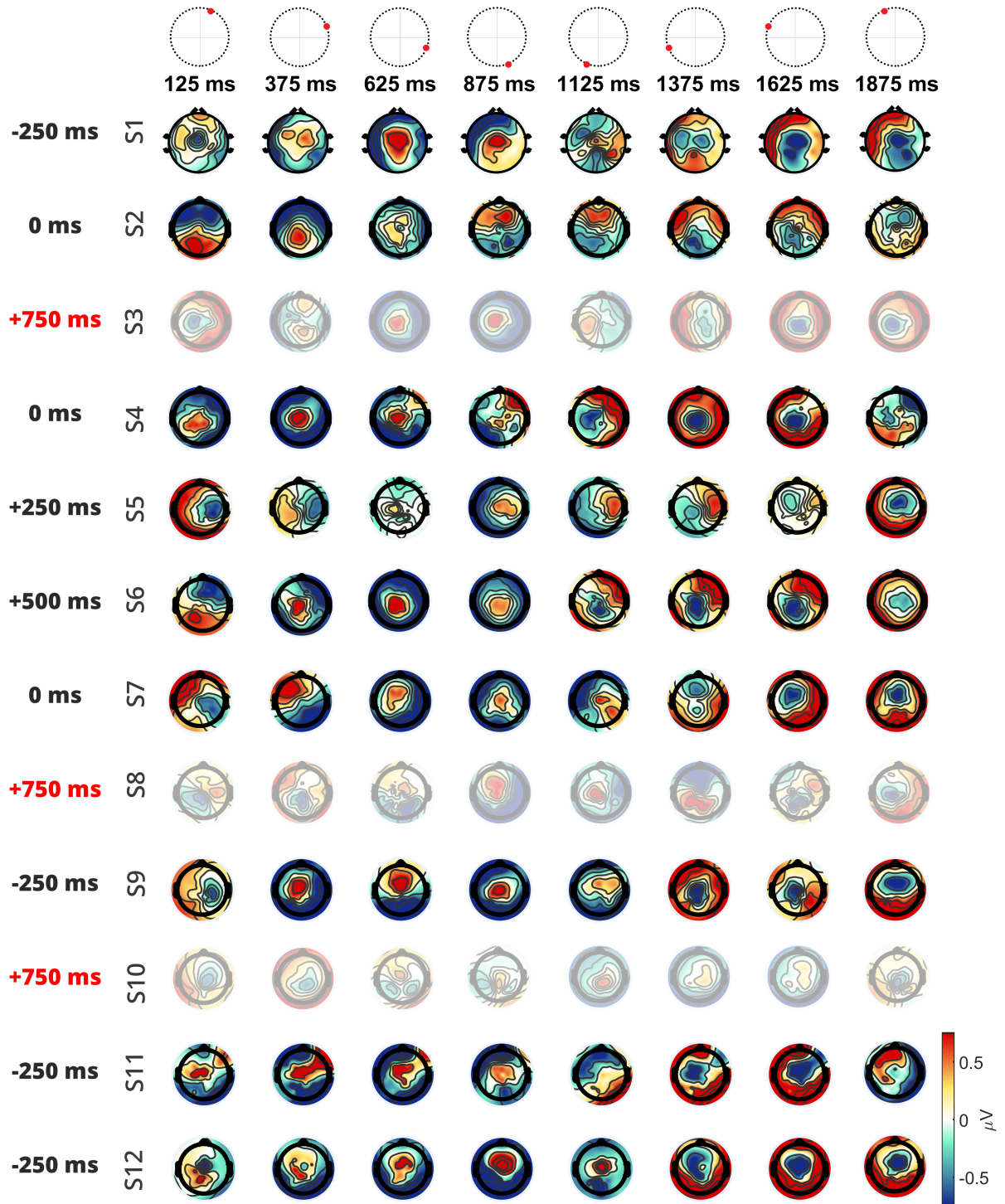


FIGURE 5.1: Single subject average cycle in 8 distinct time windows equally spaced (250 ms). These correspond to the same single subject average as in Figure 4.4, but with added time delay according to the dipole rotation timing.

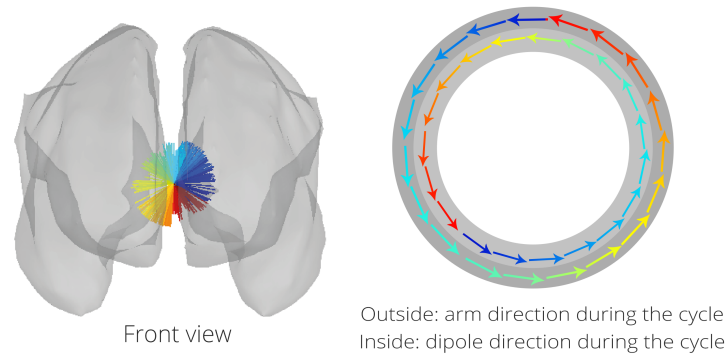


FIGURE 5.2: Diagram of the grand-average dipole rotation with arm rotation.

of activity, but functions well as a representation of how overall polarity changes in the average cycle. Furthermore, the regional dipole method transposed well the moving dipole's direction (Figure 4.6), while keeping the figure neater. Even though we lose the information of the origin of the dipole, the direction information remains, which is our goal.

Overall, in the time domain analysis we found what we think is activity in the brain (with one or several sources) that shows a rotational pattern when the arm does a circular motion, and that can be described by a dipole per time stamp. There is variability between subjects that we cannot explain, and overall we do not know the origin of the rotational pattern yet. In the end, we found a dipole that rotates with the arm cycle, but was estimated in the average data from several cycles per subject. To be used for arm directional decoding we would need to explore the single trial data further.

### 5.3 Frequency domain analysis

We explored several frequency bands of the data. According to Figure 4.11, the bands 10-13 Hz and 20-24 Hz had the biggest decrease in power in the right-arm area motor cortex during the movement, as expected. Arm movement is also associated with the increase of power in high frequencies (>30 Hz). In this case, we can see an increase of power in high frequencies in the periphery, on right side of the head close to the moving shoulder. According to Muthukumaraswamy *et al.* [102], muscle activity frequency ranges from 20-300 Hz, with posterior muscles peaking at around 100 Hz. The origin and frequency band indicate that this increase was probably due to muscle movement. These plots were computed in the data before artifact rejection and therefore it is expected that muscle artifacts are still present in the data.

SPoC succeeded in finding components whose frequency modulations in the mid- $\beta$  band (20-24 Hz) correlated with the target variable - the movement kinematics (Figures 4.12, 4.13 and 4.14). SPoC searched for the component that most correlates with the target, but nothing assures us that there aren't several sources of power modulations in the brain signals. Subject variability is, therefore, to be expected.

The fact that we can find similar components between subjects suggests there might be a few power-correlating components that may be present in the other subjects as well, but whose activity power correlated to a lesser extent.

Most subjects show high correlation between the cycle's frequency modulations and the target variable. A few components show frequency modulations that anti-correlate with the target (two out of 12 for the first direction (D1) and seven out of 12 for the second (D2)). SPoC maximizes the absolute correlation, so this is to be expected. We should note that regarding the component's activation patterns (seen in the scalp plots of Figure 4.12), their signals are irrelevant since both the pattern and its opposite will give the same frequency spectrum (for example subjects 3 and 5 for D1 in Figure 4.12). The anti-correlation of the frequency of some components is more relevant than the signal of the scalp projection of the component.

The visual clustering of subjects according to their SPoC components was more interesting for direction D1 than for D2. D1 showed more coherent results for both activation patterns and activity power correlation with the target. We can highlight the activation pattern with high activity in the central parietal area (subjects 1, 3, 5, 7, 9, and to a lesser extent 6 and 11) whose power activity positively and highly correlate with the kinematic target. The parietal area is associated with sensory information and proprioception, which is closely related to how we perform a movement.

The modulations and correlations in the unfiltered data points (Figures 4.13 and 4.14 and Table 4.2) corroborate the usefulness of SPoC. SPoC did find components whose power highly correlated with the kinematics, most of them above 80% (or below -80%). We applied the activation patterns on the unfiltered data with the artefactual ICs and epochs removed, so we would expect that the results would highly correlate, as SPoC searched for the highest correlations.

Regarding other frequency bands, SPoC got some correlating components. We decided to explore the band 20-24 Hz because the results showed components more coherent with the task in hand, the frequency band 18-24 Hz was mentioned in Seeber *et al.* [84], Korik *et al.* mentioned there should be modulations in the  $\alpha$  and  $\beta$  frequency bands as opposing to what other researchers had mentioned before [78], and the band 20-24 Hz had an accentuated decrease in frequency during the movement. The frequency band of 10-13 Hz (Figure B.2) showed very noisy activation patterns, inconsistent between subjects. The power modulations seemed to correlate nicely with the target, but were also very noisy. The frequency band of 13-20 Hz (Figure B.3) resulted in a few interesting components (for example, for D2 subjects 1, 2 and 9 with similar activation patterns and good correlation with the target). However, the instantaneous power of the components was noisy and several had low correlation. On the other hand, the Hilbert power of the component's activity for frequency band 24-30 Hz (Figure B.4) were smooth, but their activation patterns were rather noisy.

Overall, the SPoC algorithm found relevant components whose power did correlate with the movement, with direction D1 acquiring more interesting results than D2. In the end, the sources we found in SPoC were not explored enough to relate it to the vector that points in the direction of movement (as the

population vector would). Time was a limiting factor against this ultimate goal, and it should be further explored in future work.

## 5.4 Limitations of the study

One of the biggest limitation of any study on the decoding of movement from brain activity is whether the movement (muscular) has an influence (either positive or negative) in the results. In our case, the subjects are moving the right arm at a rhythmic pace. One can argue that shoulder movements influence the results, or that the hand may distort the electric field around the head. It is challenging to make sure that this activity is, in fact, originated in the brain motor areas. Several efforts have been done to restrain the data to brain activity. Some preprocessing methods such as ICA were also used to remove influence from some channels that we suspected could be due to muscle or eye movements.

One dipole in time domain is not enough to precisely describe the brain potential distribution during the movement – here the dipole we fit is a mere representation of the scalp patterns rotation. It would be interesting to fit more dipoles per time stamp.

We used standard head models for dipole fitting in both EEGLAB and Brainstorm. In EEGLAB we used a BEM model composed of three surfaces (the brain used is referred to as Colin27). In Brainstorm we used a 3-sphere head model, which is not the most reliable head model for source analysis. Since our goal was not exactly to search for sources but rather describe the scalp's potential distribution, we think this model was reliable enough for this function.

Another limitation of this study is whether the results can be transferred to movement imagery. Although decoding movement is interesting, the goal would be to decode imagery, and we do not know for sure if the same concepts studied here would apply. Several studies indicate they should (see section 1.4.3), but further research is needed to understand this fully.

Finally, time was also a limitation for this project. During the course of 7 months, most of the time was spent exploring different methods for data cleaning and data analysis. The end of my thesis project described here should be seen as a first step in the whole project's context.

## 5.5 Future Work

Regarding time domain results, there is still an unanswered question of what is the physiological explanation for the rotational patterns. We can also question whether there is a single subject delay that could better explain the difference between different subject results, and if so, how does it influences the frequency domain results. Also, would the patterns look similar for left arm movement? These are questions we can only answer with further research.

To search for the possible sources of activity in the time domain analysis we could fit more than one dipole per time stamp. The single dipole we fit now is enough to describe the scalps' potential distribution, but should not be regarded as a source of activity. By fitting more dipoles, we would search for source locations and could maybe see how they changed over time, possibly finding interesting sources that would enable single trial decoding. For a more accurate source activity search, we could also consider using boundary element head models (instead of the 3-sphere approximation model used in this project) and distributed source estimation algorithms.

Regarding frequency domain results, the components and their application to the unfiltered data needs to be further explored. More components may enable more similarities between subjects. It would be interesting to find one or more sources that are associated with the movement and are present in several subjects.

In both time and frequency domain analysis, statistical analysis is still missing to corroborate results. Furthermore, we only studied the averaged cycle signals in all analysis. One important analysis for the future would involve single trial analysis.

## 5.6 Relevance of the study

In the time domain analysis we managed to find a dipole that rotates with the arm movement. This was explored in the average cycle data, and for it to be useful for online decoding of arm direction we need to further explore single trial data.

In the frequency domain we found source components whose power correlated with movement kinematics in the 20-24 Hz frequency band. The frequency band we found most related to the arm movement was mentioned in works of Korik *et al.* [78] who argued that power pattern of  $\mu$  and  $\beta$  frequency bands hold significant information regarding movement parameters, and Seeber *et al.* [84] who explored the frequency 18-24 Hz in finger movements.

This project indicates the possibility of a dipole estimated from noninvasive brain signals being able to point in the direction of movement with further research.





## 6 Conclusion

The results obtained in both time and frequency domain varied considerably across subjects, but there seems to be a pattern present in most subjects that correlates with the movement executed.

We found a rotational dipole in the time domain. Each subject's dipole rotated with slightly different phases and in some subjects rotated in different planes. Still, we managed to find a coherent result for most of the subjects (7 out of 12). This rotating dipole comes from the average activity of several arm cycles (296 per subject, on average). Single cycle identification of the direction of the arm would be necessary for the results to be used for control of arm prosthesis, but this was not addressed in this project and should be regarded as future work.

Regarding the frequency domain analysis, some subjects showed interesting activation patterns whose power of the source activity correlated with the arm movement. The average of the absolute values were 88% and 83% for directions D1 and D2. These average values are taking into consideration high anti-correlation values. Although these were not our goal, they are still of interest, since they are still sources related to movement parameters.

The physiological reasons for both time and frequency-domain results are still to be better understood, and further research is necessary. Regarding the noninvasive analogous of Georgopoulos' population vector, there is still work to be done. In the time domain we might have found an interesting behavior of the scalp potentials distribution, which might be related to a source which we did not yet discover. If this hypothetical source would behave as the average cycle data, it would maybe enable us to decode movement direction in single trial basis. We hope this work can be a first step in that direction.



# Bibliography

- [1] R. S. Snell, *Clinical neuroanatomy*, 7th ed. Philadelphia: Wolters Kluwer Health/Lippincott Williams & Wilkins, 2010, ISBN: 978-0-7817-9427-5.
- [2] G. J. Mogenson, D. L. Jones, and C. Y. Yim, "From motivation to action: Functional interface between the limbic system and the motor system", *Progress in Neurobiology*, vol. 14, no. 2–3, pp. 69–97, 1980, ISSN: 0301-0082.
- [3] T. Ball, A. Schreiber, B. Feige, M. Wagner, C. H. Lücking, and R. Kristeva-Feige, "The Role of Higher-Order Motor Areas in Voluntary Movement as Revealed by High-Resolution EEG and fMRI", *NeuroImage*, vol. 10, no. 6, pp. 682–694, Dec. 1999, ISSN: 1053-8119.
- [4] W. Penfield and E. Boldrey, "Somatic Motor and Sensory Representation in the Cerebral Cortex of Man as Studied by Electrical Stimulation", *Brain*, vol. 60, no. 4, pp. 389–443, Dec. 1937, ISSN: 0006-8950.
- [5] R. F. Becker, "The cerebral cortex of man. By Wilder Penfield and Theodore Rasmussen. The Macmillan Company, New York, N.Y. 1950. 248 pp", en, *American Journal of Physical Anthropology*, vol. 11, no. 3, pp. 441–444, Sep. 1953, ISSN: 1096-8644.
- [6] S. Schaal, D. Sternad, R. Osu, and M. Kawato, "Rhythmic arm movement is not discrete", en, *Nature Neuroscience*, vol. 7, no. 10, pp. 1136–1143, Oct. 2004, ISSN: 1097-6256.
- [7] P. A. Lewis and R. C. Miall, "Distinct systems for automatic and cognitively controlled time measurement: Evidence from neuroimaging", en, *Current Opinion in Neurobiology*, vol. 13, no. 2, pp. 250–255, Apr. 2003, ISSN: 09594388.
- [8] J. R. Wolpaw, N. Birbaumer, D. J. McFarland, G. Pfurtscheller, and T. M. Vaughan, "Brain–computer interfaces for communication and control", *Clinical Neurophysiology*, vol. 113, no. 6, pp. 767–791, Jun. 2002, ISSN: 1388-2457.
- [9] B. T. Smith, M. J. Mulcahey, and R. R. Betz, "Development of an upper extremity FES system for individuals with C4 tetraplegia", *IEEE Transactions on Rehabilitation Engineering*, vol. 4, no. 4, pp. 264–270, 1996.
- [10] P. Thoumie, J. R. Charlier, M. Alecki, D. D’Erceville, A. Heurtin, J. F. Mathe, G. Nadeau, and L. Wiart, "Clinical and functional evaluation of a gaze controlled system for the severely handicapped", eng, *Spinal Cord*, vol. 36, no. 2, pp. 104–109, Feb. 1998, ISSN: 1362-4393.
- [11] J. J. Tecce, J. Gips, C. P. Olivieri, L. J. Pok, and M. R. Consiglio, "Eye movement control of computer functions", *International Journal of Psychophysiology*, vol. 29, no. 3, pp. 319–325, Aug. 1998, ISSN: 0167-8760.
- [12] R. C. Simpson and S. P. Levine, "Voice control of a powered wheelchair", *IEEE Transactions on Neural Systems and Rehabilitation Engineering*, vol. 10, no. 2, pp. 122–125, 2002.

- 
- [13] World Health Organization and International Spinal Cord Society, *International Perspectives on Spinal Cord Injury*, en. World Health Organization, 2013, ISBN: 978-92-4-156466-3.
- [14] F. Galán, M. Nuttin, E. Lew, P. W. Ferrez, G. Vanacker, J. Philips, and J. d. R. Millán, “A brain-actuated wheelchair: Asynchronous and non-invasive Brain–computer interfaces for continuous control of robots”, *Clinical Neurophysiology*, vol. 119, no. 9, pp. 2159–2169, Sep. 2008, ISSN: 1388-2457.
- [15] R. Leeb, D. Friedman, G. R. Müller-Putz, R. Scherer, M. Slater, and G. Pfurtscheller, “Self-Paced (Asynchronous) BCI Control of a Wheelchair in Virtual Environments: A Case Study with a Tetraplegic”, en, *Computational Intelligence and Neuroscience*, vol. 2007, pp. 1–8, 2007, ISSN: 1687-5265, 1687-5273.
- [16] G. Pfurtscheller, G. R. Müller, J. Pfurtscheller, H. J. Gerner, and R. Rupp, “‘Thought’ – control of functional electrical stimulation to restore hand grasp in a patient with tetraplegia”, *Neuroscience Letters*, vol. 351, no. 1, pp. 33–36, Nov. 2003, ISSN: 0304-3940.
- [17] G. R. Müller-Putz, R. Scherer, G. Pfurtscheller, and R. Rupp, “EEG-based neuroprosthesis control: A step towards clinical practice”, *Neuroscience Letters*, vol. 382, no. 1–2, pp. 169–174, Jul. 2005, ISSN: 0304-3940.
- [18] B. S. Baxter, A. Decker, and B. He, “Noninvasive control of a robotic arm in multiple dimensions using scalp electroencephalogram”, in *2013 6th International IEEE/EMBS Conference on Neural Engineering (NER)*, Nov. 2013, pp. 45–47.
- [19] M. Rohm, M. Schneiders, C. Müller, A. Kreilinger, V. Kaiser, G. R. Müller-Putz, and R. Rupp, “Hybrid brain–computer interfaces and hybrid neuroprostheses for restoration of upper limb functions in individuals with high-level spinal cord injury”, *Artificial Intelligence in Medicine*, Special Issue: Brain-computer interfacing, vol. 59, no. 2, pp. 133–142, Oct. 2013, ISSN: 0933-3657.
- [20] R. Rupp, M. Rohm, M. Schneiders, A. Kreilinger, and G. R. Müller-Putz, “Functional Rehabilitation of the Paralyzed Upper Extremity After Spinal Cord Injury by Noninvasive Hybrid Neuroprostheses”, *Proceedings of the IEEE*, vol. 103, no. 6, pp. 954–968, Jun. 2015, ISSN: 0018-9219.
- [21] L. A. Farwell and E. Donchin, “Talking off the top of your head: Toward a mental prosthesis utilizing event-related brain potentials”, eng, *Electroencephalography and Clinical Neurophysiology*, vol. 70, no. 6, pp. 510–523, Dec. 1988, ISSN: 0013-4694.
- [22] B. Blankertz, G. Dornhege, M. Krauledat, M. Schröder, J. Williamson, R. Murray-Smith, and K.-R. Müller, “The Berlin Brain-Computer Interface presents the novel mental typewriter Hex-o-Spell.”, 2006.
- [23] F. Nijboer, E. W. Sellers, J. Mellinger, M. A. Jordan, T. Matuz, A. Furdea, S. Halder, U. Mochty, D. J. Krusienski, T. M. Vaughan, J. R. Wolpaw, N. Birbaumer, and A. Kübler, “A P300-based brain–computer interface for people with amyotrophic lateral sclerosis”, *Clinical Neurophysiology*, vol. 119, no. 8, pp. 1909–1916, Aug. 2008, ISSN: 1388-2457.
- [24] S. Halder, A. Pinegger, I. Käthner, S. C. Wriessnegger, J. Faller, J. B. Pires Antunes, G. R. Müller-Putz, and A. Kübler, “Brain-controlled applications using dynamic P300 speller matrices”, *Artificial Intelligence in Medicine*, vol. 63, no. 1, pp. 7–17, Jan. 2015, ISSN: 0933-3657.

- [25] G. Pfurtscheller and A. Aranibar, “Event-related cortical desynchronization detected by power measurements of scalp EEG”, *Electroencephalography and Clinical Neurophysiology*, vol. 42, no. 6, pp. 817–826, Jun. 1977, ISSN: 0013-4694.
- [26] G. Pfurtscheller, C. Neuper, D. Flotzinger, and M. Pregenzer, “EEG-based discrimination between imagination of right and left hand movement”, *Electroencephalography and Clinical Neurophysiology*, vol. 103, no. 6, pp. 642–651, Dec. 1997, ISSN: 0013-4694.
- [27] A. Vučković and F. Sepulveda, “A two-stage four-class BCI based on imaginary movements of the left and the right wrist”, *Medical Engineering & Physics*, vol. 34, no. 7, pp. 964–971, Sep. 2012, ISSN: 1350-4533.
- [28] Y. Hashimoto and J. Ushiba, “EEG-based classification of imaginary left and right foot movements using beta rebound”, *Clinical Neurophysiology*, vol. 124, no. 11, pp. 2153–2160, Nov. 2013, ISSN: 1388-2457.
- [29] G. Pfurtscheller, C. Brunner, A. Schlögl, and F. H. Lopes da Silva, “Mu rhythm (de)synchronization and EEG single-trial classification of different motor imagery tasks”, *NeuroImage*, vol. 31, no. 1, pp. 153–159, May 2006, ISSN: 1053-8119.
- [30] X. Yong and C. Menon, “EEG Classification of Different Imaginary Movements within the Same Limb”, *PLOS ONE*, vol. 10, no. 4, e0121896, Apr. 2015, ISSN: 1932-6203.
- [31] E. C. Leuthardt, G. Schalk, J. R. Wolpaw, J. G. Ojemann, and D. W. Moran, “A brain–computer interface using electrocorticographic signals in humans”, en, *Journal of Neural Engineering*, vol. 1, no. 2, p. 63, 2004, ISSN: 1741-2552.
- [32] E. M. Holz, L. Botrel, T. Kaufmann, and A. Kübler, “Long-Term Independent Brain-Computer Interface Home Use Improves Quality of Life of a Patient in the Locked-In State: A Case Study”, en, *Archives of Physical Medicine and Rehabilitation*, vol. 96, no. 3, S16–S26, Mar. 2015, ISSN: 00039993.
- [33] E. M. Holz, L. Botrel, and A. Kübler, “Independent home use of Brain Painting improves quality of life of two artists in the locked-in state diagnosed with amyotrophic lateral sclerosis”, en, *Brain-Computer Interfaces*, vol. 2, no. 2-3, pp. 117–134, Apr. 2015, ISSN: 2326-263X, 2326-2621.
- [34] G. R. Müller-Putz, A. Schwarz, J. Pereira, and P. Ofner, “Chapter 2 - From classic motor imagery to complex movement intention decoding: The noninvasive Graz-BCI approach”, in *Progress in Brain Research*, ser. Brain-Computer Interfaces: Lab Experiments to Real-World Applications, D. Coyle, Ed., vol. 228, DOI: 10.1016/bs.pbr.2016.04.017, Elsevier, 2016, pp. 39–70.
- [35] S. Waldert, H. Preissl, E. Demandt, C. Braun, N. Birbaumer, A. Aertsen, and C. Mehring, “Hand Movement Direction Decoded from MEG and EEG”, en, *Journal of Neuroscience*, vol. 28, no. 4, pp. 1000–1008, Jan. 2008, ISSN: 0270-6474, 1529-2401.
- [36] C. H. Blabe, V. Gilja, C. A. Chestek, K. V. Shenoy, K. D. Anderson, and J. M. Henderson, “Assessment of brain–machine interfaces from the perspective of people with paralysis”, en, *Journal of Neural Engineering*, vol. 12, no. 4, p. 043 002, 2015, ISSN: 1741-2552.
- [37] M. Teplan, “Fundamentals of EEG measurement”, *Measurement science review*, vol. 2, no. 2, pp. 1–11, 2002.

- 
- [38] T. Kirschstein and R. Köhling, “What is the Source of the EEG?”, *Clinical EEG and neuroscience*, vol. 40, no. 3, pp. 146–149, 2009.
  - [39] D. Steyrl, R. J. Kobler, and G. R. Müller-Putz, “On Similarities and Differences of Invasive and Non-Invasive Electrical Brain Signals in Brain-Computer Interfacing”, en, *Journal of Biomedical Science and Engineering*, vol. 09, no. 08, p. 393, Jun. 2016.
  - [40] G. Pfurtscheller and F. L. Da Silva, “Event-related EEG/MEG synchronization and desynchronization: Basic principles”, *Clinical neurophysiology*, vol. 110, no. 11, pp. 1842–1857, 1999.
  - [41] A. P. Georgopoulos, J. F. Kalaska, R. Caminiti, and J. T. Massey, “On the relations between the direction of two-dimensional arm movements and cell discharge in primate motor cortex”, *Journal of Neuroscience*, vol. 2, no. 11, pp. 1527–1537, 1982.
  - [42] A. P. Georgopoulos, “Spatial Coding of Movement: A Hypothesis Concerning the Coding of Movement Direction by Motor Cortical Populations”, *ResearchGate*, 1983.
  - [43] A. Georgopoulos, A. Schwartz, and R. Kettner, “Neuronal population coding of movement direction”, en, *Science*, vol. 233, no. 4771, pp. 1416–1419, Sep. 1986, ISSN: 0036-8075, 1095-9203.
  - [44] A. P. Georgopoulos, R. E. Kettner, and A. B. Schwartz, “Primate motor cortex and free arm movements to visual targets in three-dimensional space. II. Coding of the direction of movement by a neuronal population”, *Journal of Neuroscience*, vol. 8, no. 8, pp. 2928–2937, 1988.
  - [45] R. Caminiti, P. B. Johnson, and A. Urbano, “Making arm movements within different parts of space: Dynamic aspects in the primate motor cortex”, *Journal of Neuroscience*, vol. 10, no. 7, pp. 2039–2058, 1990.
  - [46] K. Kurata, “Premotor cortex of monkeys: Set- and movement-related activity reflecting amplitude and direction of wrist movements”, en, *Journal of Neurophysiology*, vol. 69, no. 1, pp. 187–200, Jan. 1993, ISSN: 0022-3077, 1522-1598.
  - [47] Y. Koike, H. Hirose, Y. Sakurai, and T. Iijima, “Prediction of arm trajectory from a small number of neuron activities in the primary motor cortex”, en, *Neuroscience Research*, vol. 55, no. 2, pp. 146–153, Jun. 2006, ISSN: 01680102.
  - [48] Q. G. Fu, J. I. Suarez, and T. J. Ebner, “Neuronal specification of direction and distance during reaching movements in the superior precentral premotor area and primary motor cortex of monkeys”, en, *Journal of Neurophysiology*, vol. 70, no. 5, pp. 2097–2116, Nov. 1993, ISSN: 0022-3077, 1522-1598.
  - [49] G. H. Mulliken, S. Musallam, and R. A. Andersen, “Decoding Trajectories from Posterior Parietal Cortex Ensembles”, en, *Journal of Neuroscience*, vol. 28, no. 48, pp. 12 913–12 926, Nov. 2008, ISSN: 0270-6474, 1529-2401.
  - [50] D. M. Taylor, S. I. H. Tillery, and A. B. Schwartz, “Direct Cortical Control of 3d Neuroprosthetic Devices”, en, *Science*, vol. 296, no. 5574, pp. 1829–1832, Jun. 2002, ISSN: 0036-8075, 1095-9203.
  - [51] L. R. Hochberg, M. D. Serruya, G. M. Friehs, J. A. Mukand, M. Saleh, A. H. Caplan, A. Branner, D. Chen, R. D. Penn, and J. P. Donoghue, “Neuronal ensemble control of prosthetic devices by a human with tetraplegia”, *Nature*, vol. 442, no. 7099, pp. 164–171, Jul. 2006, ISSN: 0028-0836, 1476-4687.

- [52] W. Truccolo, G. M. Friehs, J. P. Donoghue, and L. R. Hochberg, “Primary Motor Cortex Tuning to Intended Movement Kinematics in Humans with Tetraplegia”, en, *Journal of Neuroscience*, vol. 28, no. 5, pp. 1163–1178, Jan. 2008, ISSN: 0270-6474, 1529-2401.
- [53] S.-P. Kim, J. D. Simeral, L. R. Hochberg, J. P. Donoghue, and M. J. Black, “Neural control of computer cursor velocity by decoding motor cortical spiking activity in humans with tetraplegia”, *Journal of Neural Engineering*, vol. 5, no. 4, pp. 455–476, Dec. 2008, ISSN: 1741-2560, 1741-2552.
- [54] E. K. Chadwick, D. Blana, J. D. Simeral, J. Lambrecht, S. P. Kim, A. S. Cornwell, D. M. Taylor, L. R. Hochberg, J. P. Donoghue, and R. F. Kirsch, “Continuous neuronal ensemble control of simulated arm reaching by a human with tetraplegia”, *Journal of Neural Engineering*, vol. 8, no. 3, p. 034 003, Jun. 2011, ISSN: 1741-2560, 1741-2552.
- [55] C. Mehring, J. Rickert, E. Vaadia, S. C. de Oliveira, A. Aertsen, and S. Rotter, “Inference of hand movements from local field potentials in monkey motor cortex”, en, *Nature Neuroscience*, vol. 6, no. 12, pp. 1253–1254, Dec. 2003, ISSN: 1097-6256.
- [56] J. Rickert, S. C. d. Oliveira, E. Vaadia, A. Aertsen, S. Rotter, and C. Mehring, “Encoding of Movement Direction in Different Frequency Ranges of Motor Cortical Local Field Potentials”, en, *Journal of Neuroscience*, vol. 25, no. 39, pp. 8815–8824, Sep. 2005, ISSN: 0270-6474, 1529-2401.
- [57] C. Toro, C. Cox, G. Friehs, C. Ojakangas, R. Maxwell, J. R. Gates, R. J. Gumnit, and T. J. Ebner, “8-12 Hz rhythmic oscillations in human motor cortex during two-dimensional arm movements: Evidence for representation of kinematic parameters”, eng, *Electroencephalography and Clinical Neurophysiology*, vol. 93, no. 5, pp. 390–403, Oct. 1994, ISSN: 0013-4694.
- [58] T. Ball, A. Schulze-Bonhage, A. Aertsen, and C. Mehring, “Differential representation of arm movement direction in relation to cortical anatomy and function”, en, *Journal of Neural Engineering*, vol. 6, no. 1, p. 016 006, 2009, ISSN: 1741-2552.
- [59] Y. Nakanishi, T. Yanagisawa, D. Shin, R. Fukuma, C. Chen, H. Kambara, N. Yoshimura, M. Hirata, T. Yoshimine, and Y. Koike, “Prediction of Three-Dimensional Arm Trajectories Based on ECoG Signals Recorded from Human Sensorimotor Cortex”, *PLOS ONE*, vol. 8, no. 8, e72085, Aug. 2013, ISSN: 1932-6203.
- [60] G. Schalk, J. Kubánek, K. J. Miller, N. R. Anderson, E. C. Leuthardt, J. G. Ojemann, D. Limbrick, D. Moran, L. A. Gerhardt, and J. R. Wolpaw, “Decoding two-dimensional movement trajectories using electrocorticographic signals in humans”, *Journal of Neural Engineering*, vol. 4, no. 3, pp. 264–275, Sep. 2007, ISSN: 1741-2560, 1741-2552.
- [61] T. Pistohl, T. Ball, A. Schulze-Bonhage, A. Aertsen, and C. Mehring, “Prediction of arm movement trajectories from ECoG-recordings in humans”, en, *Journal of Neuroscience Methods*, vol. 167, no. 1, pp. 105–114, Jan. 2008, ISSN: 01650270.
- [62] M. Spüler, A. Walter, A. Ramos-Murguialday, G. Naros, N. Birbaumer, A. Gharabaghi, W. Rosenstiel, and M. Bogdan, “Decoding of motor intentions from epidural ECoG recordings in severely paralyzed chronic stroke patients”, en, *Journal of Neural Engineering*, vol. 11, no. 6, p. 066 008, 2014, ISSN: 1741-2552.

- [63] T. Yanagisawa, M. Hirata, Y. Saitoh, T. Goto, H. Kishima, R. Fukuma, H. Yokoi, Y. Kamitani, and T. Yoshimine, “Real-time control of a prosthetic hand using human electrocorticography signals”, *Journal of neurosurgery*, vol. 114, no. 6, pp. 1715–1722, 2011.
- [64] A. P. Georgopoulos, F. J. P. Langheim, A. C. Leuthold, and A. N. Merkle, “Magnetoencephalographic signals predict movement trajectory in space”, en, *Experimental Brain Research*, vol. 167, no. 1, pp. 132–135, Nov. 2005, ISSN: 0014-4819, 1432-1106.
- [65] T. J. Bradberry, J. L. Contreras-Vidal, and F. Rong, “Decoding hand and cursor kinematics from magnetoencephalographic signals during tool use”, in *2008 30th Annual International Conference of the IEEE Engineering in Medicine and Biology Society*, Aug. 2008, pp. 5306–5309.
- [66] T. J. Bradberry, F. Rong, and J. L. Contreras-Vidal, “Decoding center-out hand velocity from MEG signals during visuomotor adaptation”, *NeuroImage*, vol. 47, no. 4, pp. 1691–1700, Oct. 2009, ISSN: 1053-8119.
- [67] T. J. Bradberry, R. J. Gentili, and J. L. Contreras-Vidal, “Decoding three-dimensional hand kinematics from electroencephalographic signals”, in *2009 Annual International Conference of the IEEE Engineering in Medicine and Biology Society*, Sep. 2009, pp. 5010–5013.
- [68] T. J. Bradberry, R. J. Gentili, and J. L. Contreras-Vidal, “Reconstructing Three-Dimensional Hand Movements from Noninvasive Electroencephalographic Signals”, en, *Journal of Neuroscience*, vol. 30, no. 9, pp. 3432–3437, Mar. 2010, ISSN: 0270-6474, 1529-2401.
- [69] P. Ofner and G. R. Müller-Putz, “Decoding of velocities and positions of 3d arm movement from EEG”, in *Engineering in Medicine and Biology Society (EMBC), 2012 Annual International Conference of the IEEE, IEEE*, 2012, pp. 6406–6409.
- [70] P. S. Hammon, S. Makeig, H. Poizner, E. Todorov, and V. R. D. Sa, “Predicting Reaching Targets from Human EEG”, *IEEE Signal Processing Magazine*, vol. 25, no. 1, pp. 69–77, 2008, ISSN: 1053-5888.
- [71] H. G. Yeom, J. S. Kim, and C. K. Chung, “Estimation of the velocity and trajectory of three-dimensional reaching movements from non-invasive magnetoencephalography signals”, *Journal of Neural Engineering*, vol. 10, no. 2, p. 026 006, Apr. 2013, ISSN: 1741-2560, 1741-2552.
- [72] D. J. McFarland, W. A. Sarnacki, and J. R. Wolpaw, “Electroencephalographic (EEG) control of three-dimensional movement”, *Journal of Neural Engineering*, vol. 7, no. 3, p. 036 007, Jun. 2010, ISSN: 1741-2560, 1741-2552.
- [73] K. Choi, “Reconstructing for joint angles on the shoulder and elbow from non-invasive electroencephalographic signals through electromyography”, English, *Frontiers in Neuroscience*, vol. 7, 2013, ISSN: 1662-453X.
- [74] J. Lv and Y. Li, “Decoding hand movement velocities from EEG signals during a continuous drawing task”, in *2010 Seventh International Conference on Fuzzy Systems and Knowledge Discovery*, vol. 5, Aug. 2010, pp. 2186–2189.
- [75] N. Robinson, C. Guan, A. P. Vinod, K. K. Ang, and K. P. Tee, “Multi-class EEG classification of voluntary hand movement directions”, en, *Journal of Neural Engineering*, vol. 10, no. 5, p. 056 018, 2013, ISSN: 1741-2552.



- [76] J. H. Kim, R. Chavarriaga, J. d. R. Millán, and S. W. Lee, “Three-dimensional upper limb movement decoding from EEG signals”, in *2013 International Winter Workshop on Brain-Computer Interface (BCI)*, Feb. 2013, pp. 109–111.
- [77] J. M. Antelis, L. Montesano, A. Ramos-Murguialday, N. Birbaumer, and J. Minguez, “On the Usage of Linear Regression Models to Reconstruct Limb Kinematics from Low Frequency EEG Signals”, *PLOS ONE*, vol. 8, no. 4, e61976, Apr. 2013, ISSN: 1932-6203.
- [78] A. Korik, R. Sosnik, N. Siddique, and D. Coyle, “Chapter 3 - 3d hand motion trajectory prediction from EEG mu and beta bandpower”, *Brain-Computer Interfaces: Lab Experiments to Real-World Applications*, vol. 228, D. Coyle, Ed., pp. 71–105, 2016, DOI: 10.1016/bs.pbr.2016.05.001.
- [79] H. A. Agashe and J. L. Contreras-Vidal, “Reconstructing hand kinematics during reach to grasp movements from electroencephalographic signals”, in *2011 Annual International Conference of the IEEE Engineering in Medicine and Biology Society*, Aug. 2011, pp. 5444–5447.
- [80] A. Y. Paek, H. Agashe, and J. L. Contreras-Vidal, “Decoding repetitive finger movements with brain activity acquired via non-invasive electroencephalography”, English, *Frontiers in Neuro-engineering*, vol. 7, 2014, ISSN: 1662-6443.
- [81] K. Liao, R. Xiao, J. Gonzalez, and L. Ding, “Decoding Individual Finger Movements from One Hand Using Human EEG Signals”, *PLOS ONE*, vol. 9, no. 1, e85192, Jan. 2014, ISSN: 1932-6203.
- [82] W. Wang, G. P. Sudre, Y. Xu, R. E. Kass, J. L. Collinger, A. D. Degenhart, A. I. Bagic, and D. J. Weber, “Decoding and Cortical Source Localization for Intended Movement Direction With MEG”, en, *Journal of Neurophysiology*, vol. 104, no. 5, pp. 2451–2461, Nov. 2010, ISSN: 0022-3077, 1522-1598.
- [83] A. Toda, H. Imamizu, M. Kawato, and M.-a. Sato, “Reconstruction of two-dimensional movement trajectories from selected magnetoencephalography cortical currents by combined sparse Bayesian methods”, *NeuroImage*, vol. 54, no. 2, pp. 892–905, Jan. 2011, ISSN: 1053-8119.
- [84] M. Seeber, R. Scherer, and G. R. Müller-Putz, “EEG Oscillations Are Modulated in Different Behavior-Related Networks during Rhythmic Finger Movements”, en, *Journal of Neuroscience*, vol. 36, no. 46, pp. 11 671–11 681, Nov. 2016, ISSN: 0270-6474, 1529-2401.
- [85] K. Jerbi, J. Vidal, J. Mattout, E. Maby, F. Lecaigard, T. Ossandon, C. Hamamé, S. Dalal, R. Bouet, J.-P. Lachaux, R. Leahy, S. Baillet, L. Garnero, C. Delpuech, and O. Bertrand, “Inferring hand movement kinematics from MEG, EEG and intracranial EEG: From brain-machine interfaces to motor rehabilitation”, en, *IRBM*, vol. 32, no. 1, pp. 8–18, Feb. 2011, ISSN: 19590318.
- [86] A. Vučković and F. Sepulveda, “Delta band contribution in cue based single trial classification of real and imaginary wrist movements”, en, *Medical & Biological Engineering & Computing*, vol. 46, no. 6, pp. 529–539, Jun. 2008, ISSN: 0140-0118, 1741-0444.
- [87] Y. Gu, D. Farina, A. R. Murguialday, K. Dremstrup, P. Montoya, and N. Birbaumer, “Offline Identification of Imagined Speed of Wrist Movements in Paralyzed ALS Patients from Single-Trial EEG”, *Frontiers in Neuroscience*, vol. 3, Aug. 2009, ISSN: 1662-4548.

- 
- [88] T. J. Bradberry, R. J. Gentili, and J. L. Contreras-Vidal, “Fast attainment of computer cursor control with noninvasively acquired brain signals”, en, *Journal of Neural Engineering*, vol. 8, no. 3, p. 036 010, 2011, ISSN: 1741-2552.
  - [89] R. Poli and M. Salvaris, “Comment on ‘Fast attainment of computer cursor control with noninvasively acquired brain signals’”, en, *Journal of Neural Engineering*, vol. 8, no. 5, p. 058 001, 2011, ISSN: 1741-2552.
  - [90] T. J. Bradberry, R. J. Gentili, and J. L. Contreras-Vidal, “Reply to comment on ‘Fast attainment of computer cursor control with noninvasively acquired brain signals’”, en, *Journal of Neural Engineering*, vol. 8, no. 5, p. 058 002, 2011, ISSN: 1741-2552.
  - [91] P. Ofner and G. R. Müller-Putz, “Movement target decoding from EEG and the corresponding discriminative sources: A preliminary study”, in *2015 37th Annual International Conference of the IEEE Engineering in Medicine and Biology Society (EMBC)*, Aug. 2015, pp. 1468–1471.
  - [92] A. P. Georgopoulos, “Neurophysiology of reaching”, *ResearchGate*, 1990.
  - [93] A. P. Georgopoulos, “On the translation of directional motor cortical commands to activation of muscles via spinal interneuronal systems”, *Cognitive Brain Research*, Mental representations of motor acts, vol. 3, no. 2, pp. 151–155, Mar. 1996, ISSN: 0926-6410.
  - [94] A. Delorme and S. Makeig, “EEGLAB: An open source toolbox for analysis of single-trial EEG dynamics including independent component analysis”, en, *Journal of Neuroscience Methods*, vol. 134, no. 1, pp. 9–21, Mar. 2004, ISSN: 01650270.
  - [95] S. Makeig, A. J. Bell, T.-P. Jung, T. J. Sejnowski, and others, “Independent component analysis of electroencephalographic data”, *Advances in neural information processing systems*, pp. 145–151, 1996.
  - [96] P. H. Westfall, “Kurtosis as Peakedness, 1905 – 2014. R.I.P.”, *The American statistician*, vol. 68, no. 3, pp. 191–195, 2014, ISSN: 0003-1305.
  - [97] A. J. Bell and T. J. Sejnowski, “An information-maximization approach to blind separation and blind deconvolution”, *Neural computation*, vol. 7, no. 6, pp. 1129–1159, 1995.
  - [98] I. Winkler, S. Haufe, and M. Tangermann, “Automatic Classification of Artifactual ICA-Components for Artifact Removal in EEG Signals”, *Behavioral and Brain Functions*, vol. 7, p. 30, 2011, ISSN: 1744-9081.
  - [99] R. Oostenveld, P. Fries, E. Maris, and J.-M. Schoffelen, “FieldTrip: Open Source Software for Advanced Analysis of MEG, EEG, and Invasive Electrophysiological Data”, en, *Computational Intelligence and Neuroscience*, 2011.
  - [100] F. Tadel, S. Baillet, J. C. Mosher, D. Pantazis, and R. M. Leahy, “Brainstorm: A User-Friendly Application for MEG/EEG Analysis”, en, *Computational Intelligence and Neuroscience*, 2011.
  - [101] S. Dähne, F. C. Meinecke, S. Haufe, J. Höhne, M. Tangermann, K.-R. Müller, and V. V. Nikulin, “SPoC: A novel framework for relating the amplitude of neuronal oscillations to behaviorally relevant parameters”, *NeuroImage*, vol. 86, pp. 111–122, Feb. 2014, ISSN: 1053-8119.
  - [102] S. D. Muthukumaraswamy, “High-frequency brain activity and muscle artifacts in MEG/EEG: A review and recommendations”, *Frontiers in Human Neuroscience*, vol. 7, Apr. 2013, ISSN: 1662-5161.

# A Study Information Sheet

## Study information sheet

---

### 1 Recorded signals

During this experiment, we will record your brain signals (EEG – Electroencephalogram), your eye movements (EOG – Electrooculogram) and your body movements (Kinect, Microsoft Xbox) while performing specific tasks. The experiment takes around 2 to 3 hours (depending on how the preparation goes, and how long the breaks are).

### 2 Study goal


We want to explore the changes in people's brain activity when people move their arm in a repetitive cycle. We use the recorded data to train models that predict movement parameters (e.g. direction) based on the brain signals.

*Why?* The brain controls people's actions and therefore also arm movements. A person not able to move his arms still has information about an intended arm movement encoded in the brain, therefore we plan to decode that information and use it for controlling a prosthesis with his "thoughts". But first, we need to know more about what movement parameters we can decode from the EEG.

Your contribution to this study will help us to improve our knowledge about the brain activity during repetitive arm movements.

### 3 Experiment schedule

The experiment is divided into the following parts:



Explanation		~45 min
Electrode preparation		
Training		
Experiment	Block 1	~1 h
	Break	
	Block 2	
	Break	
	Block 3	
	Break	
	Block 4	
	Break	
	Block 5	
	Break	
	Block 6	
	Break	
	Block 7	
	Break	
	Block 8	
	Break	
	Block 9	
	Break	
	Block 10	

You will get to know the experiment and the task better. We will mount the EEG electrodes on your head, record their positions and add conducting gel to improve signal quality. After this preparation time, you will have time to practice the task and perform some practice trials, where you will get to know the timings of the experiment. When you feel comfortable enough, we start the actual experiment. The experiment consists of 10 blocks interleaved with breaks. Each run takes around 4 minutes.

## 4 The task

During acquisition time, you will be asked to either perform a **movement** or to stay in a **rest** position.

### 4.1 The movement

The task consists of moving your **right arm** in a **constant circular clockwise** motion, in your **frontal plane** (as if you were drawing a circle on an imaginary board in front of you, slightly to your **lower right side**). An example of the movement will be displayed on video, and you'll have time to practice it. Regarding the movement frequency, you will have the opportunity to practice it before and during the experiment.

While performing the movement:

- Focus your eyes on a fixation cross in the center of the screen.
- You should not see your moving arm (you will have a barrier to occlude the movement).
- Your moving arm should not get too close to your face (perform the movement to your right).
- Try to keep a constant movement speed.
- Keep the rest of your body relaxed and try to move as little as possible.
- Avoid movements not related to the task.
- Keep your hands and fingers relaxed.
- Keep your left arm on your lap.
- Stay focused on the task (this is important!).

### 4.2 The rest position

When you are asked to keep in the rest position you should:

- Keep relaxed and avoid any movement.
- Keep your arms on your lap.
- Keep looking at the fixation cross on the center of the screen
- Stay focused on the task (even though the task is not challenging, it is important that you are not focused on something other than the task).

You will have breaks where you can (and should) actively blink and get yourself comfortable!

## 5 One trial

One trial will take around 30 s.

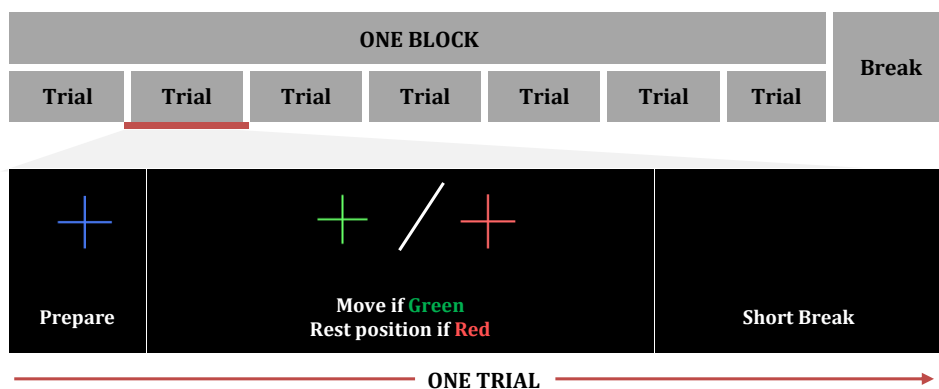
You'll be asked to **perform the movement** mentioned above, when the cross in the center of the screen is **green**, and to stay in **resting position** when the cross turns **red**. Before turning green/red, the cross will be **blue** for a few seconds to announce that the **acquisition** time

(either movement or rest) is about to start. When the screen is all black, you have some seconds of break.

One trial will then consist of the following sequence:

1. A **blue** fixation cross on the center of the screen (**prepare to start**).
2. Cross turns either **green** (**perform movement**) or **red** (stay in **rest position**).
3. Cross disappears (small **break**).

This will be repeated 7 times for each block, and only then you will have a longer break (see diagram below). The order of rest and move trials within one block is randomized.



## 6 During acquisition

Brain signal acquisition is very sensitive to artifacts. For that reason, during acquisition:

- Try to sit comfortable and avoid movements other than the task related.
- Always look at the center of the fixation cross during trials (*this is important to keep you from moving your eyes since that creates non-brain-related electric potentials in your scalp*).
- Relax the muscles of your face, neck, shoulders and lower jaw.
- Avoid clenching your teeth.
- Reduce blinks and swallowing to a minimum during each trial - for those actions you should use the short breaks between the trial.
- Please, focus on the task. Even if the task is not challenging, please keep your focus on the task and not on anything else. In case you feel tired, you can always ask for a longer break after a block.

If you have any question left please ask the conductor now!

**Thank you for your participation!**



## B Frequency domain results - Extra

### B.1 Frequency results for single subjects

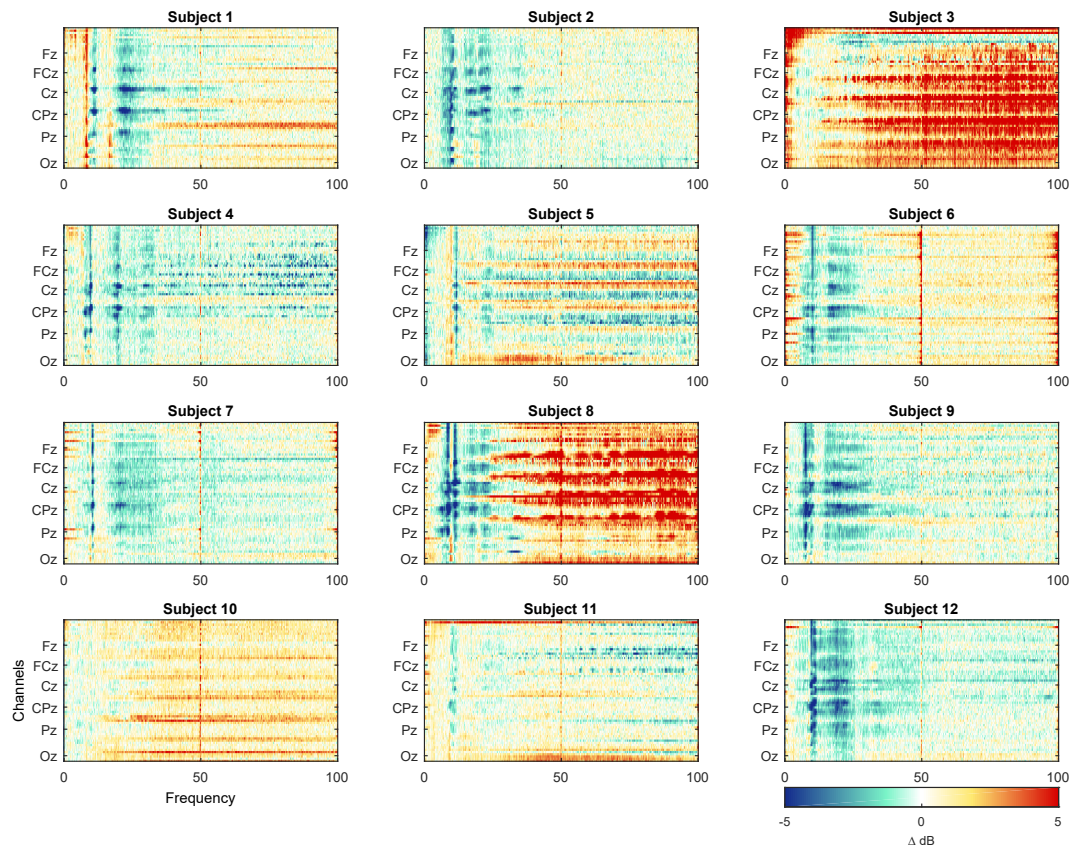


FIGURE B.1: Single subject frequency spectra difference between the Move and Rest data. In the vertical axis we have the EOG and EEG channels, ordered as in figure 4.5c

### B.2 SPOC results for other frequency bands

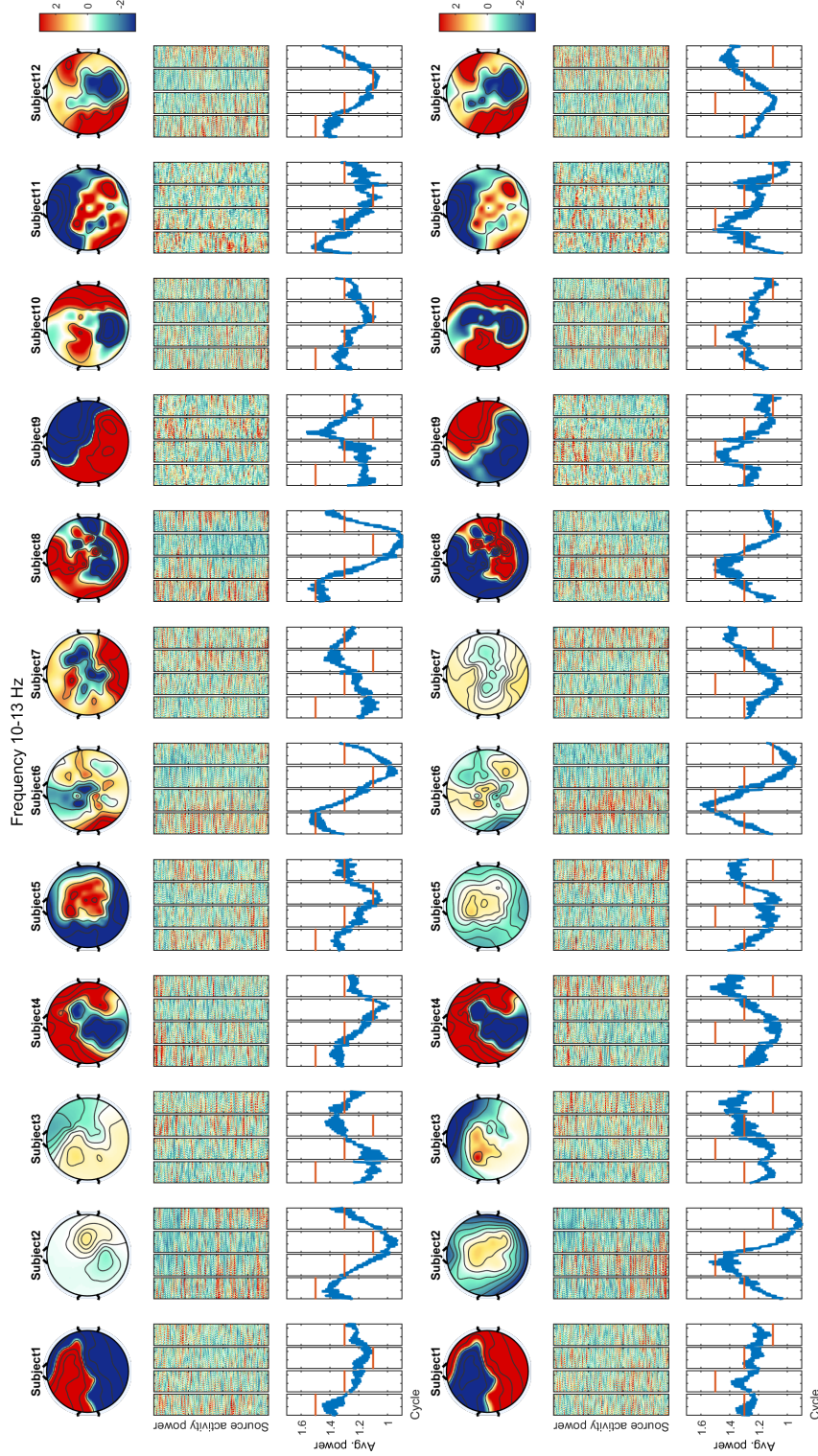


FIGURE B.2: SPoC algorithm outputs for frequency band 10-13 Hz, for direction D1 (top) and D2 (bottom). For each component we display its activity patterns in a scalp plot, the hilbert power of its source activity, the average hilbert power of its source activity and the target variable.



## B.2. SPoC results for other frequency bands

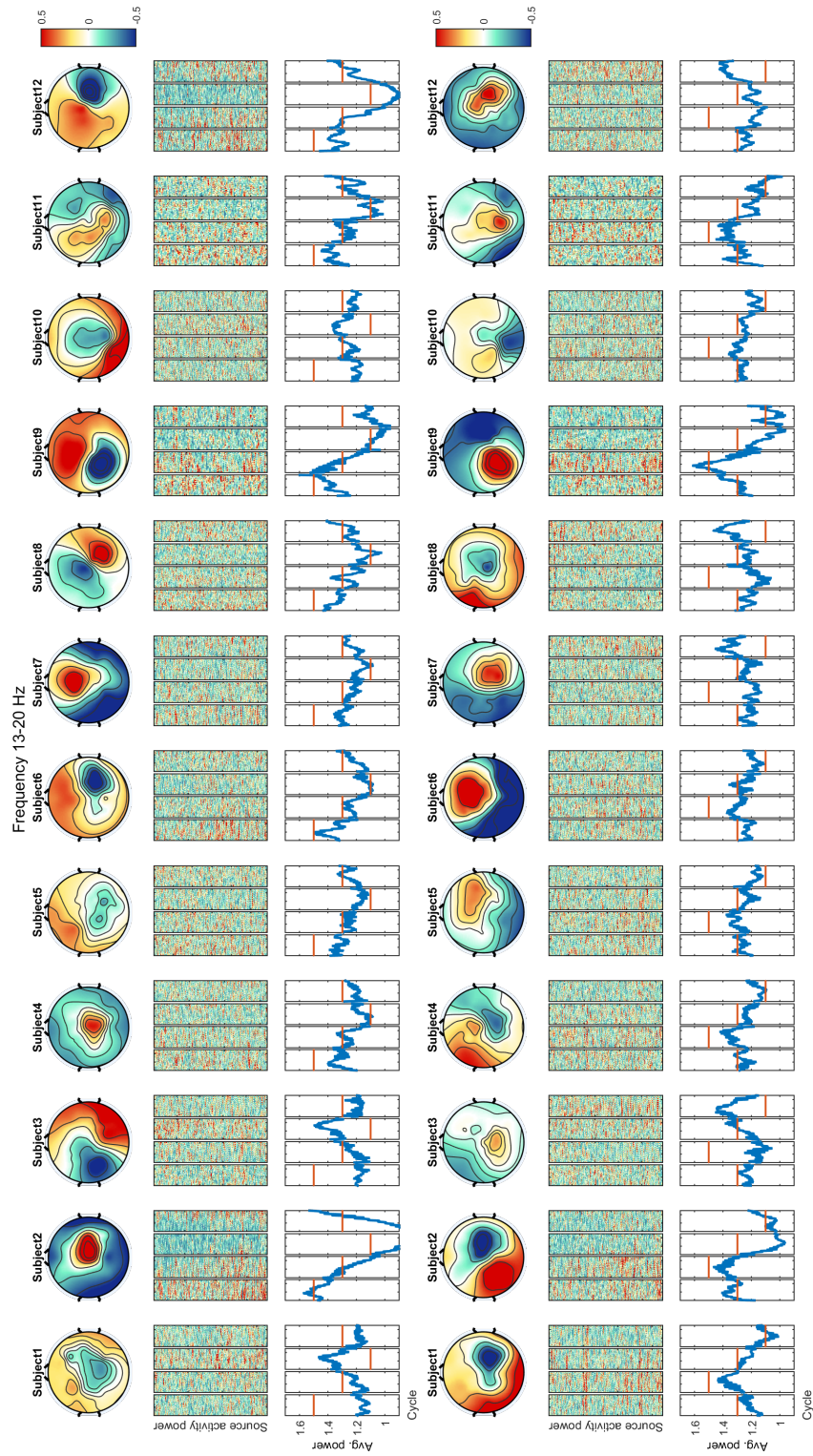


FIGURE B.3: SPoC algorithm outputs for frequency band 13-20 Hz. Same description as for figure B.2.

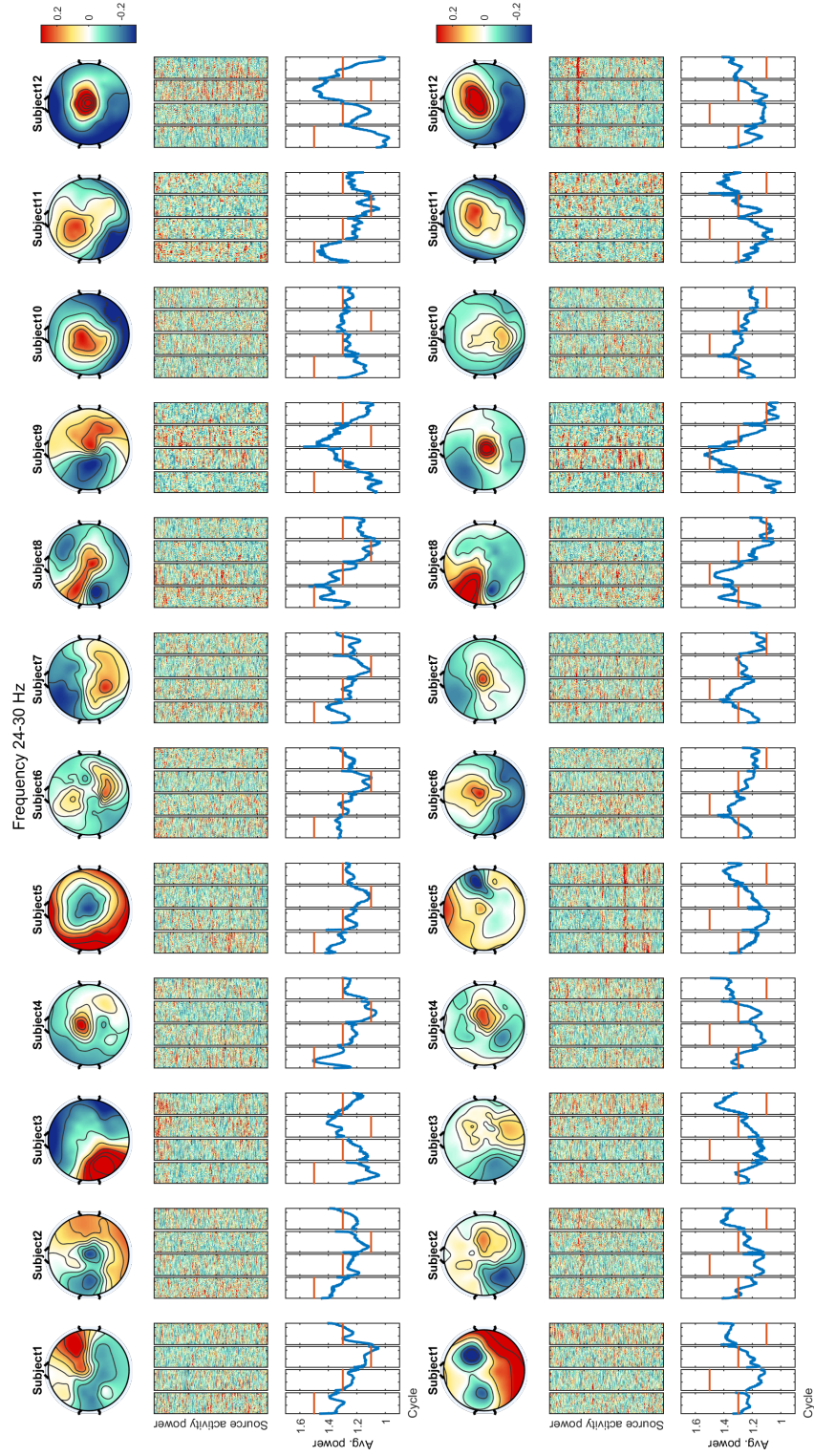


FIGURE B.4: SPoC algorithm outputs for frequency band 24-30 Hz. Same description as for figure B.2.